WHOI-91-25

Woods Hole Oceanographic Institution
Massachusetts Institute of Technology

Joint Program in Oceanography and Oceanographic Engineering

DOCTORAL DISSERTATION

Acoustic Wave Scattering from a Random Ocean Bottom

by

Dajun Tang

June 1991

WHOI-91-25

Acoustic Wave Scattering from a Random Ocean Bottom

by

Dajun Tang

Woods Hole Oceanographic Institution
Woods Hole, Massachusetts 02543

and

The Massachusetts Institute of Technology
Cambridge, Massachusetts 02139

June 1991

DOCTORAL DISSERTATION

Funding was provided by the Office of Naval Research under Contract No. N00014-86-C-0338.

Approved for publication; distribution unlimited.

Approved for Distribution:

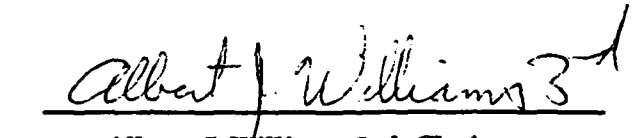

Albert J. Williams 3rd, Chairman
Department of Applied Ocean Physics and Engineering

John W. Farrington
Dean of Graduate Studies

Accesion For	
NTIS CRA&I	☒
DTIC TAB	☐
Unannounced	☐
Justification	
By	
Distribution /	
Availability Codes	
Dist	Avail and / or Special
A-1	

Acoustic Wave Scattering from a Random Ocean Bottom

Dajun Tang
B. S. University of Science and Technology, China (1981)
M. S. Institute of Acoustics, Academia Sinica (1985)

Submitted in Partial Fulfillment of the Requirements for the Degree of

Doctor of Philosophy

at the

Massachusetts Institute of Technology
and the

Woods Hole Oceanographic Institution
June 1991

Signature of Author _____
Department of Ocean Engineering
May 16, 1991

Certified by _____
George V. Frisk
Thesis Supervisor

Accepted by _____
W. Kendall Melville
Chairman, Joint Committee for Oceanographic Engineering,
Massachusetts Institute of Technology - Woods Hole Oceanographic Institution

Acoustic Wave Scattering from a Random Ocean Bottom

Dajun Tang

Abstract

This thesis investigates low frequency acoustic wave scattering from the ocean bottom. It is divided into four parts. The first part models the ocean bottom as a fluid medium where sound speed and density are constants except a layer in which the density is still a constant, but the sound speed is composed of a large constant and superimposed with a small random component. It is assumed that the random sound speed is horizontally well correlated and vertically poorly correlated.

In the second part, an integro-differential equation method is used to calculate the scattering from that random layer. Emphasis is put on the study of the spatial correlation of the scattered field. It is found that the spatial correlation length of the scattered field is related to the correlation length of the scatterer, therefore it is possible to invert the bottom correlation length by measuring the spatial correlation of the scattered field using multiple receivers. Also included in this part are an estimation of energy loss in the coherent field, a discussion on the influence of bottom anisotropy, and a comparison between the integro-differential equation method and the Born approximation.

The third part concerns the influence of the bottom roughness. A small roughness is added to the water/bottom interface and perturbation method is used to calculate the scattering from the roughness. Under the assumption that the roughness and the volume inhomogeneity are uncorrelated, comparisons are made on the scattering strengths between roughness scattering and volume scattering, and the spatial correlation of the total scattered field is evaluated. It is found that at low frequencies, volume scattering cannot be ignored when the seafloor is not very rough, and it is possible to distinguish the two scattering mechanisms by measuring spatial correlations of the scattered field.

In the fourth part, the classical definition of the bottom scattering cross section is questioned, and a new set of parameters, the Scattering Correlation Coefficient, is introduced, which does not have the ambiguities associated with the conventional notion of the scattering cross section.

In memory of mom

Acknowledgments

For the success of this thesis, many people made contributions. First, let me thank George Frisk, my thesis advisor, for his guidance, his encouragement, and his confidence in me. It has been a wonderful five years working with him.

On my thesis committee are Prof. Henrik Schimdt of MIT, from whom I benefited tremendously in numerous consultations; Prof. Arthur Baggeroer of MIT, whose insight and criticism of my research helped me in many ways; and Dr. Subramaniam Rajan of WHOI, whose courage in pursuing science will always be an inspiration for me.

I also thank Dr. Tim Stanton of WHOI who has always been interested in my research, and I value his recommendations to this thesis.

Suggestions by Dr. William Kuperman of the Naval Research Laboratory on several occasions improved this thesis appreciably.

I thank Dr. James Lynch of WHOI for his serving as the thesis defense chairman and his suggestions on my research through the years.

I spent most of the five years in room 5-007 of MIT, and the many discussions and arguments with fellow students were an integral part of my education. In my memory will be Kevin LePage, Dr. Woojae Seong, Dr. Peter Dahl, Dr. Nick Makris, Dr. Chi-Fang Chen, Jim Liu, Chick Corrado, Dan DiPerna, Matt Conti, Dave Ricks, Tarun Kapoor and last, but not least, Ken Rolt to whom I am grateful for his patience in correcting the English of this thesis.

I thank Jake Peirson, Abbie Jackson and the rest of the WHOI Education Office staff for their considerable help in my graduate study.

Love from my family has been an inseparable part in this five years. Mom, who dedicated all her life to the future of her children, passed away the first summer I started my Ph.D. program. Dad and my sister, Liuyan, have been a constant encouragement. Their letters in every stage of my study will always be my treasure. Finally, my lovely wife, Linghong, has been invaluable in sharing all these years with me. Her understanding and trust in me could not have been replaced.

Contents

List of Figures

Chapter 1

INTRODUCTION

Sound scattering is a very important part of underwater acoustics research. Since World War II, considerable effort has been put into understanding the mechanisms that cause scattering of sound waves which propagate in the ocean[1]. The ocean, as an acoustical system, is extremely complicated. Scattering can happen almost everywhere in the ocean and it covers a very wide band of frequencies (from seismic waves of below one Hz up to MHz).

Conventionally, acoustic scattering can be categorized into:

a) Ocean surface scattering: here, scattering is caused by the rough ocean surface and a thin bubble layer immediately below the surface.

b) Volume scattering within the water: here, scattering is due to organic species or temperature and density fluctuations.

c) Bottom scattering: this part of scattering is from the water/bottom rough interface and the inhomogeneities (fluctuations of sound speed and density, isolated rocks, etc.) within the bottom.

Each of these categories is further divided into sub-categories according to the size, nature and/or the position of the scatterers, or the sound frequency being used. In this research, all the efforts will be concentrated on the bottom scattering

part, although some of the methods and results are applicable to volume scattering in the water column as well.

1.1 Motivation

Ocean bottom scattering is a process of considerable importance in the operation of underwater acoustic systems. In some cases, bottom scattering is a major source of interfering reverberation that restricts sonar performance; in other cases, it provides an effective means of remotely measuring the physical properties of the ocean bottom. For basic understanding of the creation and distribution of the bottom scatterers, please see Kennett[2].

A great deal of research has been concentrated on water/bottom rough interface scattering. A number of bottom roughness models have been developed over the years to estimate the magnitude of either backscatter or forwardscatter from the seabed boundary, as a function of incident/scattering angles, frequency, bottom type and roughness[3,4,5,6,7,8]. All these models are developed by modifying rough ocean surface scattering theories which impose a pressure-release boundary condition. Their success is limited because the scatterers beneath the water/bottom interface are ignored. Especially when the bottom is smooth, the roughness models fail to predict the correct scattering strength and frequency dependence[9,10,13].

It is generally accepted that volume scattering caused by the inhomogeneities beneath the water/bottom interface cannot be neglected[11,12,9,13]. In some cases, when the interface is smooth, volume inhomogeneities are the dominant contributor to scattering [8,9,13]. A number of researchers have developed volume scattering theories for the bottom. Stockhausen[14] developed a scattering model for a bottom consisting of a uniform set of spherical particles, in which the scatterers are

not correlated. Ivakin and Lysanov [10] and Ivakin[15] employed Chernov's[16] work on wave propagation in inhomogeneous media to develop bottom scattering models. They do not include the lateral wave contributions. Hines[9,13] followed a similar approach but included lateral wave contributions. He compared his model with his own laboratory measurements and with other available data. Both Ivakin/Lysanov's model and Hines' model considered the scatterers in the bottom as correlated random quantities, and this approach appears to be appropriate after comparing it with high-frequency experimental data.

Efforts have also been made to incorporate roughness and volume inhomogeneities into a single model. Ivakin and Lysanov[17] include refraction at a randomly rough interface in their sediment scattering model. Refraction by large-scale roughness is considered, but diffraction by the smaller scales is neglected. Jackson *et al.*[12] developed a composite roughness model for high-frequency backscattering, where the volume scattering is converted into equivalent surface scattering under the assumption that high absorption rates prevent acoustic energy from penetrating deep into the bottom.

However, problems in bottom scattering still exist. First, none of the existing volume scattering theories considers the coherent sound energy loss due to scattering while propagating in the random medium, and only absorption of sound due to heat conversion is included. When the acoustic frequency is so high that the heat absorption is much greater than the scattering loss, these theories work well. For low frequencies, however, ignoring volume scattering loss is not justified. This effect is yet to be addressed in the literature.

Secondly, when taking bottom inhomogeneities as a random process, the understanding of the auto-correlation function of this process is essential for modeling this process. The existing theories concentrate only on finding the acoustic scattering strength, without going further to examine the spatial correlation of the

scattered acoustic field. The acoustic scattering strength (standard deviation of the randomly scattered field) does not give a complete characterization of the statistical properties of the wave field. The statistical properties of the fluctuations of the wave field can be characterized more completely by using a correlation function of the scattered field. However, the question of how to find and utilize the correlation of the scattered field in the bottom scattering process, which is of both theoretical and practical interest, has not yet received much attention.

Thirdly, it has been argued that when the water/bottom interface is not very rough, the volume scattering contribution to the total bottom scattering process will become important. However, there is no quantitative description of this effect. More precisely, given the random parameters of the volume inhomogeneity, what degree of interface roughness will result in an equivalent amount of scattering for a given frequency range?

Fourthly, bottom anisotropy (i.e., the bottom random parameters have different values if measured along different directions) is yet to be investigated. When the bottom random processes is not isotropic, what impact it will have upon the scattered field?

Finally, all existing volume scattering models use a far-field assumption, and the scattering cross section or the scattering coefficient is used to characterize the scatterers. However, for low-frequency scattering in a layered random medium, both near- and far-field solutions are necessary, and the classical definition of scattering cross section is no longer appropriate.

So far, almost all bottom scattering experiments are conducted by using a single source and a single receiver. A typical example can be found in Merklinger's paper[11]. In his experiment, the source and the receiver are placed along a vertical line and are arranged as close together as possible to ensure monostatic backscat-

tering geometry. By assuming the only scatterers are along the water/bottom interface, and that these scatterers are homogeneously distributed, he finds the insonified area, an annulus controlled by the source duration and the sound speed in the water, and calculates the backscattering strength as a function of incident angle. He noticed that there are some features in the data which cannot be explained by interface roughness, and he speculates that these features are caused by sub-bottom inhomogeneities. However, single-source-single-receiver experiments of this type cannot distinguish interface scattering from sub-bottom volume scattering.

Because of the fast development of technology, it is now feasible to use acoustic arrays to measure bottom scattering. Frisk[18] proposes to use vertical arrays to measure low-frequency bottom scattering. Motivated by Frisk's proposal, this thesis intends to address the aforementioned problems. An integro-differential equation method will be used to formulate the problem. The major contributions of this thesis are:

1 The coherent energy loss due to scattering is estimated. As a result, the scattering theory developed in this thesis improves upon the Born approximation.

2 For the first time in bottom scattering problems, spatial correlation of the scattered field is studied in detail for two fluid half-spaces with the lower half-space being random. This extends our understanding of the bottom scattering process and a technique to invert random parameters in the bottom is proposed.

3 Scattering from a rough interface on top of a layer of volume inhomogeneity is studied, and a comparison between rough interface scattering and scattering due to volume inhomogeneities is made. We handled the interface scattering part by using the boundary perturbation theory[19] and assumed the roughness and the

volume inhomogeneity are uncorrelated. The result of this analysis suggests the possibility of distinguishing the two scattering mechanisms experimentally.

4 The methods used in this thesis allow the inclusion of anisotropy of the scatterers, and so the anisotropic influences on scattering are also discussed at length.

5 The Scattering Correlation Coefficient is introduced, which clarifies the ambiguities of using the concept of scattering cross section in bottom scattering problems. A formulation is found based on the Scattering Correlation Coefficient to calculate the scattering field due to a point source. It will help us understand conceptually the physical process of volume scattering in complicated media, and it can be used as the starting point to solve the near-field problem.

1.2 Review of Relevant Literature

The purpose of this section is not to provide an exhaustive review of all the existing literature on bottom scattering. Since this research involves several different areas, it is intended only to discuss the references which are directly relevant to each area.

1.2.1 On wave propagation in a random medium

There are three excellent books, one by Chernov[16], one by Tatarskii[20], and the third by Ishimaru[22], which contain systematic treatments of the theory of wave propagation in a medium with random inhomogeneities. They include the study of wave propagation using the ray approximation; the diffraction theory of wave propagation and related approximation methods; the application of quantum

field theory; the influences of fluctuations in the incident wave on the diffraction image formed by a focusing system; and some experimental data analyses. Many basic concepts in propagation and scattering in a random medium are clearly described. Since the authors treat the problem of wave propagation as a general physical phenomenon, the books cover almost all branches of wave motion. However, the problem of wave propagation in a random medium with discontinuous interfaces is not included since this is still an on going research subject.

Also, there is a review paper by Barabanenkov *et al.* [40] on the "status of the theory of propagation of waves in a randomly inhomogeneous medium", where the authors restrict their review to volume scattering in media without discontinuous interfaces. The method of small perturbations, and scattering by large-scale inhomogeneities are discussed in detail. There is also a very insightful introduction to the theory of multiple scattering. Literature cited ranges from scattering in radio physics, optics, acoustics to scattering in plasma physics and other branches of physics.

Flatté[23,24] and his colleagues have performed extensive studies on acoustic waves propagating in a temporally and spatially varying ocean, with emphasis on the effect of internal waves.

1.2.2 On volume scattering

The Born approximation is the most widely used method in underwater acoustics in solving weak volume scattering problems. The original form of the Born approximation[64] is for those scattering problems that the medium is homogeneous except for the scatterers. Later the Born approximation is extended to cover the case that the background medium is stratified[10]. We will call it the Extended Born approximation in this thesis. When the background medium is stratified, both the background wave and the scattered wave become more complicated because of

multi-path effect.

Ivakin and Lysanov[10,25,15] followed Chernov's theory[16], assuming that the random scattering is caused by "sharply anisotropic random inhomogeneities (fluctuations of the refractive index): large-scale in the horizontal plane and small-scale in depth". They used the Extended Born approximation and the far-field assumption (steepest-descent method) to obtain a backscattering formula. The authors explained the distinctive features observed in the frequency and angular dependence of the backscattering coefficient at small grazing angles. Although the water/bottom interface discontinuity is accounted for by using the Extended Born approximation, the authors ignored the interface wave contribution in their calculations.

Hines' Ph.D. thesis[9] in 1988 is a systematic study of high-frequency acoustic wave backscattering from volume inhomogeneities. It contains an extensive literature survey on wave scattering both from rough interfaces and from volume inhomogeneities. Hines' theory also followed Chernov's approach [16], and the Extended Born approximation and the far-field approximation is used to calculate volume backscattering. His assumption of bottom randomness is that both the sound speed and the density fluctuate, and the two are perfectly correlated through medium porosity. The correlation function he used is exponential. One step further than Ivakin and Lysanov, Hines also included the interface wave contribution. The results are compared to his own high frequency laboratory measurements as well as published experimental data conducted by other researchers.

1.2.3 On the integro-differential equation method

This method is the so-called "bi-local" approximation to the Dyson equation for calculating the coherent part of the acoustic field. (For reference see Tatarskii, Bourret and Keller [20,26,27]). This approach broadens the domain of validity of

the single-scattering (Born) approximation to a considerable extent. Most of the research is for the case of an unbounded random medium. When a random medium is confined to a finite region, it is a much more difficult mathematical problem. Rosenbaum[28] studied the interface effects and concluded that the introduction of interfaces will change the solution of the integro-differential equation. For a one-dimensional random medium, the interface perturbs the coherent wave motion to a significant extent over a large distance from it; for the three dimensional model which Rosenbaum used, the interface effects are confined to a well-defined "transition" layer of the order of a wavelength. However he only considered the case of normal incidence. Kupiec *et al.*[29] studied the reflection for a special medium where the average refractive index in the random portion is equal to the refractive index in the homogeneous region.

Kurtepov[30] demonstrated one of the very few applications of the integro-differential equation method in underwater acoustics. He studied the influence of internal waves on shallow water propagation. Assuming that both boundaries of the shallow water waveguide are impenetrable, he obtained the attenuation coefficients for each propagating normal mode.

1.2.4 On the rough interface model

Due to the volume of work done on this subject, it is virtually impossible to outline all related papers. A good review paper by Fortuin[31] summarizes pressure-release rough surface scattering theories up to 1969. When the roughness height is relatively small, compared with the acoustic wavelength, perturbation methods are widely used. Kuperman[6] employed the perturbation method developed by Bass[32] for the rough sea surface, and obtained a set of boundary conditions to calculate the reflection and transmission at a two-fluid rough interface. Later Kuperman and Schmidt[7] extended the model to handle elastic wave scattering

in a horizontally stratified ocean. Theories on large amplitude roughness will not be cited here since this thesis studies only the case where the interface is relatively smooth. Recently, there are researchers who model the rough ocean bottom as fractals [33,34,35,36,37]. One major advantage of this approach is that if the rough boundary is indeed fractal, the self-similar property of the fractal will enable us to just measure the statistics of the roughness at one scale and predict the statistics of the roughness on all other scales. In this thesis, Bass and Fuks'[19] single scattering model will be used as the means to compare the relative scattering strengths of volume and rough interface scatterings.

1.2.5 On spatial coherence of scattered field

In underwater acoustics, there has been of little study on the spatial coherence of the bottom scattered field. However, research on spatial coherence of rough surface scattered fields exists. Notably, Clay and Medwin [42,43] in 1970 studied the dependence of the spatial and temporal correlation of forward-scattered sound on the rough surface statistics. They used the Kirchhoff approximation to formulate the problem, and related the spatial and temporal correlations of the acoustical field to the statical description of the rough surface. In a laboratory experiment, a wind-driven sea surface was simulated, and the spatial and temporal correlation of the acoustic field was measured and compared with their theory.

Kinney and Clay[44] studied spatial coherence by using the facet-ensemble method in 1984. They compared the experimental result by Medwin and Clay[43] with Eckart theory and the facet-ensemble method, and found good agreement between the experiment data and the theory. In another paper[45], the same authors studied if the spatial wavenumber power spectrum of a rough surface is sufficient to predict the amplitude and spatial coherence of acoustic energy scattered from that surface, and the conclusion was negative.

1.3 Outline of the Content of Each Chapter

Chapter 2 defines the volume scattering scenario. Assuming the scattering is caused by the random variation of sound speed in a layer beneath the water/bottom interface, the wave equation is split into two coupled equations, governing the coherent component and the random component of the total field. The relationship between these two components is discussed.

Chapter 3 is devoted to solving for the coherent wave field. An incident plane wave is assumed, and the coherent reflection coefficient between two fluid half-spaces is obtained for all incident angles and different frequencies. Different background parameters will be used in the calculation, and the results are compared to the reflection coefficients when no volume inhomogeneities are present, but heat absorption is included.

Chapter 4 calculates the randomly scattered field, and studies the spatial correlations (vertical and horizontal) of this field. It is found that the spatial correlation of the scattered field depends strongly on the correlation length of the bottom random sound speed variation; as a result, by sweeping frequencies, the bottom correlation length can be determined experimentally. The results are compared with that of the Extended Born approximation, and some conclusions are made as to the applicability of the Extended Born approximation. Finally, the influence of bottom anisotropy is examined. If the bottom correlation function has a longer correlation length in one direction and a shorter one in the orthogonal direction, it is found that the longer and the shorter correlation length of the bottom correlation function are both sensitive to the acoustic frequency and the orientation the the receiving arrays.

Chapter 5 compares the differences between scattering from volume inhomogeneities and scattering from small interface roughness. We consider for various

parameters, which of the two mechanisms will be dominant. When either is dominant, the spatial correlation of the combined scattered field is investigated, and the possibility of using it to distinguish the two mechanisms is discussed.

In Chapter 6, the classical definition of scattering cross section of ocean bottom scattering is questioned. A new set of parameters, the "Scattering Correlation Coefficients", is defined which does not have the ambiguities associated with the conventional notion of scattering cross section. The mathematical formulation for point source scattering is given in detail. The significance of the formulation and the difficulties in solving this problem are examined.

Chapter 7 concludes the thesis and addresses future research works related to this thesis. What are the necessary geological parameters to be used as inputs in the theory developed in the thesis are discussed in detail.

Chapter 2

FORMULATION

2.1 The Integro-differential Equation

In the thesis, we are interested in acoustical wave scattering by an inhomogeneous ocean bottom. The medium under study is schematically shown in Fig.2.1.

The upper half-space, $z > 0$, is composed of homogeneous water having constant density ρ_1 and constant sound speed c_1. The lower half-space, $z < 0$, is a homogeneous fluid ocean bottom having constant density ρ_2 and constant sound speed c_2, except for the layer between $z = 0$ and $z = -h$, where the medium has the same constant density ρ_2 as the rest of the bottom, but the sound speed is composed of a constant c_2 and superimposed with a random component δc, where δc is a function of position (x, y, z):

$$c_{layer} = c_2 + \delta c(x, y, z). \tag{2.1}$$

We also assume $\langle \delta c(x, y, z) \rangle = 0$, and so $\langle c_{layer} \rangle = c_2$, where the brackets $\langle \cdots \rangle$ indicate the ensemble average. The thickness of the random layer is a free parameter, which can be chosen as large as infinity. The coherent reflection and random

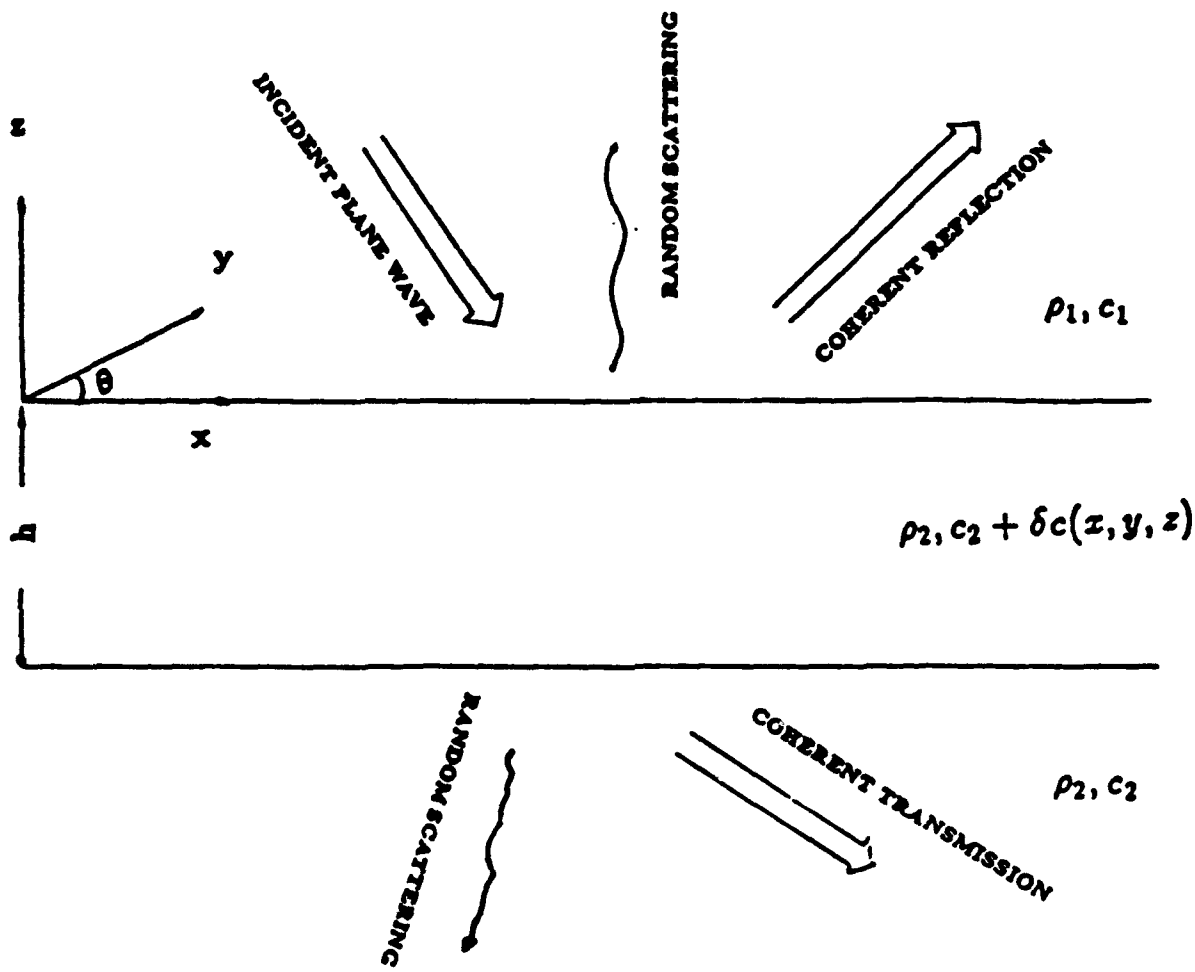
z
y
θ
x
INCIDENT PLANE WAVE
RANDOM SCATTERING
COHERENT REFLECTION
ρ_1, c_1
h
$\rho_2, c_2 + \delta c(x, y, z)$
RANDOM SCATTERING
COHERENT TRANSMISSION
ρ_2, c_2

scattering from this random layer is the primary concern in this thesis.

The validity of the theory that will be developed is not restricted to the layered fluid media as shown in Fig.2.1. The bottom can be any fluid, fluid-elastic, or elastic layered media, and the random layer is not necessarily immediately beneath the water; there can be other homogeneous layers beneath the water and above the random layer. Further, more than one random layer is allowed. For a more complete model, attenuation of both compressional waves and shear waves should be included. The attenuation can be incorporated into the present theory without difficulty. Another important issue is to model the background sound speed profile in the random layer with a gradient, which is closer to a real sediment sound speed profile[63]. This profile will allow the incident wave to refract back into the water column, hence causing additional scattering.

However, in this thesis we will restrict the study to the case shown in Fig.2.1, emphasizing the basic physics of scattering from a simple random layer. This will allow us to closely observe the consequences of the random layer on the behavior of the acoustic wave scattering.

Generally, the density of the random layer should be treated as a random parameter as well. We must therefore know the correlation between the random sound speed and the random density. However, there is little experimental data available to extract such a relationship. We will only study the scattering by sound speed fluctuations in this thesis. The effects of density fluctuations can be incorporated into the present theory when the sound speed-density correlation is known.

This theory will be suitable for studying scattering by a sedimented bottom,

where the interface roughness does not necessarily dominate the scattering process, so volume scattering can be important; also the inhomogeneities can be treated as small perturbations since the scatterers are due to inhomogeneous sedimentation, where the sound speed variation is not very large. Scattering by rocky bottoms and bottoms with ocean ridges should be treated differently.

For the remainder of this thesis, we shall use the following subscript notations. We use 1, 2, and 3 to respectively designate: the water ($z > 0$), the random layer ($0 > z > -h$), and the homogeneous half-space beneath the random layer ($z < -h$). With suppressed time dependence $e^{-i\omega t}$, the pressure wave equation for the homogeneous water medium is:

$$\nabla^2 P_1 + k_1^2 P_1 = 0. \qquad (z > 0) \tag{2.2}$$

Likewise, the pressure wave equation for the homogeneous bottom medium ($z < -h$) is:

$$\nabla^2 P_3 + k_2^2 P_3 = 0, \qquad (z < -h) \tag{2.3}$$

where $k_1 = \omega/c_1$ is the wavenumber in the water, and $k_2 = \omega/c_2$ is the wavenumber in the homogeneous bottom. We note that the average wavenumber in the random layer equals the wavenumber of the homogeneous bottom. The pressure wave equation in the random layer is:

$$\nabla^2 P_2 + (\frac{\omega}{c_2 + \delta c})^2 P_2 = 0. \quad (0 > z > -h) \tag{2.4}$$

We assume the random part of the sound speed is small, $\delta c/c_2 \ll 1$, the wavenumber in the random layer will take on the form:

$$\frac{\omega}{c_2 + \delta c} \approx \frac{\omega}{c_2}(1 - \frac{\delta c}{c_2}). \tag{2.5}$$

Hence

$$(\frac{\omega}{c_2 + \delta c})^2 \approx \frac{\omega^2}{c_2^2}(1 - \frac{2\delta c}{c_2}) = k_2^2[1 + \epsilon(x, y, z)], \tag{2.6}$$

where $\epsilon(x,y,z) = -2\delta c/c_2$.

Therefore, Eq.(2.4) becomes:

$$\nabla^2 P_2 + k_2^2[1+\epsilon(x,y,z)]P_2 = 0. \quad (0 > z > -h) \tag{2.7}$$

Since there is no general solution to the above Helmholtz equation with statistically random coefficient ϵ, we decompose P_i into a coherent part $\langle P_i \rangle$ and a scattered part p_i^s throughout the media:

$$P_i = \langle P_i \rangle + p_i^s. \quad (i = 1,2,3) \tag{2.8}$$

The wave equations governing $\langle P_1 \rangle$, p_1^s, $\langle P_3 \rangle$, and p_3^s are the same homogeneous Helmholtz equations as Eqs.(2.2) and(2.3), whereas the wave equation for the random layer, Eq.(2.7), becomes a pair of coupled differential equations governing the coherent part $\langle P_2 \rangle$ and the scattered part p_2^s respectively:

$$\nabla^2 \langle P_2 \rangle + k_2^2 \langle P_2 \rangle = -k_2^2 \langle \epsilon p_2^s \rangle, \tag{2.9}$$

$$\nabla^2 p_2^s + k_2^2 p_2^s = -\epsilon k_2^2 \langle P_2 \rangle + k_2^2[\langle \epsilon p_2^s \rangle - \epsilon p_2^s]. \tag{2.10}$$

These are inhomogeneous Helmholtz equations with unknown source terms to the right of the equalities. Notice that the term in square brackets of Eq.(2.10) is of second-order smallness. By eliminating that term (called bi-local approximation[20]), we see that the coherent field determines the source strength of the scattered field in Eq.(2.10); in turn, the scattered field determines the source strength of the coherent field in Eq.(2.9). Applying Green's Theorem to Eq.(2.10), we have[20]

$$p_2^s(\vec{R}) = \frac{k_2^2}{4\pi} \int\int_{v'} \int \epsilon(\vec{R}') \langle P_2(\vec{R}') \rangle G(\vec{R}\,|\vec{R}') dv', \tag{2.11}$$

where v' is the random region, and $\vec{R}$ and $\vec{R}'$ indicate source position (x',y',z') and receiver position (x,y,z), respectively. G is the Green's function which will be given in detail later. Substituting Eq.(2.11) into Eq.(2.9), we find that the

coherent part of the pressure field in the random layer fulfills the following integro-differential equation:

$$\nabla^2\langle P_2(\vec{R})\rangle + k_2^2\langle P_2(\vec{R})\rangle = - \left(k_2^4/4\pi\right)\int\int_{v'}\int \langle\epsilon(\vec{R})\epsilon(\vec{R}')\rangle\langle P_2(\vec{R}')\rangle G(\vec{R}\,|\vec{R}')dv'. \qquad (2.12)$$

The above equation, along with the coherent fields in media 1 and 3 and appropriate boundary conditions, determines the coherent field in the random layer. After finding $\langle P_2\rangle$, we will be able to use Eq.(2.11) to calculate the scattered field. Notice that in Eq.(2.11), if we substitute P_2^0, the pressure field in the absence of ϵ, instead of using $\langle P_2\rangle$, then it becomes the Extended Born approximation[9].

Eq.(2.12) has been studied for cases without velocity discontinuities by a number of authors for various kinds of isotropic correlation functions[20,28,29]. In the present problem, there is a sound speed discontinuity at the water/bottom interface. The presence of this discontinuity will result in a more complicated Green's Function compared with that when the discontinuity is absent. The way the interface problem is handled will be given in Chapter 3. In the rest of this chapter, we will introduce the Green's Function G and the correlation function $\langle\epsilon(\vec{R})\epsilon(\vec{R}')\rangle$.

2.2 The Green's Function

Since we have chosen that $\langle c_{layer}\rangle = c_2$, the background sound speed is just two homogeneous half-spaces. The Green's Function for two half-spaces with source located in the lower half-space satisfies:

$$(\nabla^2 + k_1^2)G_1(\vec{R}\mid\vec{R}') = 0, \qquad z > 0 \qquad (2.13)$$

$$(\nabla^2 + k_2^2)G_2(\vec{R}\mid\vec{R}') = -4\pi\delta(\vec{R}-\vec{R}'), \qquad z < 0 \qquad (2.14)$$

and the boundary conditions at $z = 0$ are:

$$G_1(x, y, 0 \mid x', y', z') = G_2(x, y, 0 \mid x', y', z'), \tag{2.15}$$

$$\frac{1}{\rho_1}\frac{\partial}{\partial z}G_1(x, y, 0 \mid x', y', z') = \frac{1}{\rho_2}\frac{\partial}{\partial z}G_2(x, y, 0 \mid x', y', z'). \tag{2.16}$$

The Green's function for the lower half-space can be expressed in the following integral form[54]:

$$G_2(\vec{R} \mid \vec{R}') = \int_{-\infty}^{\infty}\int (\frac{-1}{2\pi i \xi_2}) \left[e^{i\xi_2|z-z'|} + v_{21}e^{i\xi_2|z'|-i\xi_2 z}\right] e^{i\vec{\kappa}\cdot\vec{l}}d^2\vec{\kappa}, \tag{2.17}$$

where v_{21} is the plane wave reflection coefficient with the plane wave incident from below the water/bottom interface:

$$v_{21} = \frac{\rho_1\xi_2 - \rho_2\xi_1}{\rho_1\xi_2 + \rho_2\xi_1}, \tag{2.18}$$

and ξ_1 and ξ_2 are the vertical wave numbers in the upper and lower half-spaces respectively:

$$\xi_1 = \sqrt{k_1^2 - \kappa^2}, \tag{2.19}$$

$$\xi_2 = \sqrt{k_2^2 - \kappa^2}, \tag{2.20}$$

and $\vec{l}$ is the vector connecting the horizontal coordinates of the source and the observation points:

$$\vec{l} = \vec{r} - \vec{r'} = (x - x')\vec{i} + (y - y')\vec{j}. \tag{2.21}$$

Notice that the Green's function for a medium without any discontinuity would be the same as Eq.(2.17) except that $v_{21} = 0$. The inclusion of v_{21} in the Green's function makes the solution of the coherent field much more difficult to find than in the case when $v_{21} = 0$.

2.3 The Correlation Function

We assume that the correlation function of the quantity $\epsilon(\vec{R})$ has the following stationary and anisotropic form, which is horizontally and vertically decoupled[10,50]:

$$\langle \epsilon(\vec{R})\epsilon(\vec{R}') \rangle = 4\langle \frac{\delta c(\vec{R})}{c_2} \frac{\delta c(\vec{R}')}{c_2} \rangle = 4\sigma^2 N(\vec{l}) M(|z-z'|), \tag{2.22}$$

where $\vec{R}$ and $\vec{R}'$ indicate the positions (x,y,z) and (x',y',z'), the horizontal vector $\vec{l} = (x-x')\vec{i} + (y-y')\vec{j}$, and σ^2 is the standard deviation of the random quantity $\delta c/c_2$. Further, we assume that

$$\int_{-\infty}^{\infty} M(|z-z'|)dz' = z_0, \tag{2.23}$$

where z_0 is a measure of the vertical correlation length, which is assumed much smaller than the horizontal correlation length l_0 given below. This assumption is based on the fact that in the sediment, the medium is much better correlated horizontally than vertically. Finally, we choose the correlation function, $N(\vec{l})$, and its associated spectrum, $S(\vec{\kappa})$, to have one of the following forms:

$$\begin{aligned} N(\vec{l}) &= exp[-(|\vec{l}|/l_0)], && \textit{(isotropic exponential)} \\ S(\vec{\kappa}) &= \frac{2\pi l_0^2}{[1+(\kappa l_0)^2]^{3/2}}; \end{aligned} \tag{2.24}$$

$$\begin{aligned} N(\vec{l}) &= exp[-\frac{|l_x|}{l_{x0}} - \frac{|l_y|}{l_{y0}}], && \textit{(anisotropic exponential)} \\ S(\vec{\kappa}) &= \frac{4l_{x0}l_{y0}}{(1+(\kappa_x l_{x0})^2)(1+(\kappa_y l_{y0})^2)}; \end{aligned} \tag{2.25}$$

$$\begin{aligned} N(\vec{l}) &= exp[-(l_x/l_{x0})^2 - (l_y/l_{y0})^2], && \textit{(anisotropic Gaussian)} \\ S(\vec{\kappa}) &= \pi l_{x0}l_{y0} exp[-\frac{1}{4}(\kappa_x^2 l_{x0}^2 + \kappa_y^2 l_{y0}^2)]. \end{aligned} \tag{2.26}$$

Where $N(\vec{l})$ and $S(\vec{\kappa})$ are related as Fourier transforms:

$$S(\vec{\kappa}) = \int\int N(\vec{l}) e^{i\vec{l}\cdot\vec{\kappa}} d^2\vec{l}. \tag{2.27}$$

For the isotropic exponential case, l_0 is the correlation length; whereas for the anisotropic exponential case, l_{x0} and l_{y0} are correlation lengths along x and y directions. Even when $l_{x0} = l_{y0}$, it will not degenerate to the isotropic case, since there are discontinuities across the l_x and l_y axes. The discontinuity problem can be corrected by introducing a second length scale[10], however this will not be discussed here. As for the Gaussian case, l_{x0} and l_{y0} are the same as in the anisotropic exponential case. However when $l_{x0} = l_{y0}$, it does degenerate to the isotropic case. Since anisotropic correlations are incorporated in the formulation, we can study the anisotropic effects on the scattered field, which will be covered in Chapter 4.

We notice that since there is little experimental data to support any particular type of correlation functions, the ones we choose are based on mathematical simplicity. The correlation length in all three types of correlation functions we choose is described by parameters l_0, or $\sqrt{l_{x0}^2 + l_{y0}^2}$. Whether the modeling is enough for real ocean bottoms has to be determined by geological measurements. However, the formulation developed in this thesis is flexible in terms of fitting other types of correlation functions as long as they are given in the form of two dimensional spectrums.

Now we have completed the formulation of the problem. In Chapter 3, we will solve the problem of coherent reflection when a plane wave is incident onto the random bottom, and in Chapter 4 , we will concentrate on the scattered field. Note that we ignored the second order term in Eq.(2.10), assuming it is much smaller than the first order term. This assumes that multiple scattering is not important. However, when the sound speed variation in the random layer is so large that multiple scattering cannot be ignored, the present approximation will fail.

Chapter 3

COHERENT REFLECTION

In Chapter 2, we decomposed the total acoustic wave field into two parts: the coherent field $\langle P \rangle$ and the randomly scattered field p^s. In this chapter, we will use the formulation developed in the previous chapter to study the coherent part of the total field $\langle P \rangle$ when a plane wave in an oblique angle impinges from the water to the bottom. In the absence of the random layer, the reflection problem of plane waves from the interface of two homogeneous half-spaces is well known. As introduced in Chapter 2, we have a random layer in the bottom in which sound speed has a random component (see Fig.2.1). Since we have assumed that the sound speed fluctuations in the random layer are small compared with the background bottom sound speed, we would expect that there is a small loss in the coherent component of the sound field.

Assume that a plane wave with horizontal wave vector $\vec{\kappa_0}$ is incident upon the bottom. Since the coherent pressure field in the water obeys the Helmholtz equation, it has to take on the following form:

$$\langle P_1 \rangle = e^{i\vec{\kappa_0}\cdot\vec{r}} \left(e^{-i\sqrt{k_1^2-\kappa_0^2}z} + \langle V \rangle e^{i\sqrt{k_1^2-\kappa_{r0}^2}z} \right); \tag{3.1}$$

likewise, the coherent wave in the homogeneous bottom (medium 3) will have the following form:

$$\langle P_3 \rangle = \langle T \rangle e^{i\vec{\kappa_0}\cdot\vec{r}} e^{-i\sqrt{k_3^2-\kappa_0^2}z}, \tag{3.2}$$

where $\langle V \rangle$ and $\langle T \rangle$ are the coherent reflection and coherent transmission coefficients, respectively. They are constants to be determined.

Next we will find the solution of $\langle P_2 \rangle$ in the random layer and then use the boundary conditions at $z = 0$ and $z = -h$ to obtain the coherent reflection coefficient $\langle V \rangle$.

Inserting the correlation function, Eq.(2.22), into Eq.(2.12), the integro-differential equation becomes:

$$\nabla^2\langle P_2(\vec{R})\rangle + k_2^2\langle P_2(\vec{R})\rangle = -\frac{k_2^4\sigma^2}{\pi}\int\int_{v'}\int N(\vec{l})M(|z-z'|)\langle P_2(\vec{R}')\rangle G_2(\vec{R}\,|\vec{R}')dv'. \tag{3.3}$$

Since the incident wave is in the $\vec{\kappa_0}$ direction, and the randomness is assumed stationary, the horizontal wave vector $\vec{\kappa_0}$ in the coherent wave remains constant throughout the medium. Letting

$$\langle P_2(\vec{R})\rangle = P(z)e^{i\vec{\kappa_0}\cdot\vec{r}}, \tag{3.4}$$

we obtain from Eq.(3.3):

$$\left[\frac{d^2}{dz^2} + k_2^2 - \kappa_0^2\right] P(z)e^{i\vec{\kappa_0}\cdot\vec{r}} = -\frac{k_2^4\sigma^2}{\pi}\int\int_{v'}\int N(\vec{l})M(|z-z'|)P(z')e^{i\vec{\kappa_0}\cdot\vec{r}'}G_2(\vec{R}\,|\vec{R}')dx'dy'dz'. \tag{3.5}$$

To solve for $P(z)$, we consider the case $z_0 \ll \lambda$, i.e. the acoustic wavelength is much larger than the vertical correlation length, where λ is the acoustic wavelength.

Therefore, we can write the vertical correlation as a delta function, $M(|z-z'|) = z_0\delta(z-z')$, where z_0 is a measure of the vertical correlation length. By doing so, the integration over z' is eliminated. The assumption that the random sound speed is vertically uncorrelated is supported by sediment core data[50]. Switching the integration variables from (x', y') to $\vec{l} = \vec{r} - \vec{r}'$, the above equation can be simplified to:

$$\left[\frac{d^2}{dz^2} + k_2^2 - \kappa_0^2\right] P(z) = -\frac{k_2^4\sigma^2 z_0}{\pi} P(z) \int\int N(\vec{l}) e^{-i\vec{\kappa_0}\cdot\vec{l}} G_2(\vec{l}, z, z')|_{z=z'} d^2\vec{l}. \tag{3.6}$$

Substituting the expression for G_2 in Eq.(2.17) into Eq.(3.6) with $z' = z$, and rearranging the terms, we have:

$$\left[\frac{d^2}{dz^2} + \eta^2\right] P(z) = -f(z)P(z) \tag{3.7}$$

where η^2 and $f(z)$ are defined as follows:

$$\eta^2 = k_2^2(1 - \frac{\kappa_0^2}{k_2^2} + c(\kappa_0)), \tag{3.8}$$

$$f(z) = \frac{k_2^4\sigma^2 z_0}{2\pi^2} \int\int S(\vec{\kappa} - \vec{\kappa_0})(\frac{i}{\xi_2}) v_{21} e^{-i2\xi_2 z} d^2\vec{\kappa}. \tag{3.9}$$

Here $c(\vec{\kappa_0})$ is a constant given by

$$c(\vec{\kappa_0}) = \frac{k_2^2\sigma^2 z_0}{2\pi^2} \int\int S(\vec{\kappa} - \vec{\kappa_0})(\frac{i}{\xi_2}) d^2\vec{\kappa}, \tag{3.10}$$

and $S(\vec{\kappa} - \vec{\kappa_0})$ is the shifted two-dimensional spectrum of $N(\vec{l})$:

$$S(\vec{\kappa} - \vec{\kappa_0}) = \int\int N(\vec{l}) e^{i(\vec{\kappa}-\vec{\kappa_0})\cdot\vec{l}} d^2\vec{l}. \tag{3.11}$$

Note that if there is no interface discontinuity at $z = 0$, v_{21} in Eq.(3.9) will vanish, likewise $f(z)$ also vanishes. Eq.(3.7) then becomes:

$$\left[\frac{d^2}{dz^2} + \eta^2\right] P(z) = 0. \tag{3.12}$$

This is a homogeneous Helmholtz equation with complex wavenumber η. Therefore, in the absence of the interface discontinuity, the solutions in the random layer are still plane waves, but with complex wavenumbers; stated in another way, the solutions are inhomogeneous plane waves. Explained physically, the random layer subtracts energy from the coherent propagation. This case has been studied by several authors mentioned in Chapter 1.

By including the water/bottom interface discontinuity, we have an extra term, $f(z)$, in Eq.(3.7). Now plane waves are no longer solutions to Eq.(3.7) since Eq.(3.7) is no longer a Helmholtz equation with constant wavenumbers. However, observing that $f(z)$ is always much smaller than η^2, since v_{21} is a quantity whose magnitude is equal or smaller than one, we solve Eq.(3.7) by iteration. The zeroth order solution is

$$P_0(z) = Ae^{-i\eta z} + Be^{i\eta z}, \tag{3.13}$$

and the first order solution is

$$\begin{aligned} P(z) &= Ae^{-i\eta z} + Be^{i\eta z} - \frac{1}{2i\eta}\int_{-h}^{0} f(z')P_0(z')e^{i\eta|z-z'|}dz' \\ &= Ae^{-i\eta z} + Be^{i\eta z} - \frac{1}{2i\eta}\int_{-h}^{z} f(z')(Ae^{-i\eta z'} + Be^{i\eta z'})e^{i\eta(z-z')}dz' \\ &\quad -\frac{1}{2i\eta}\int_{-z}^{0} f(z')(Ae^{-i\eta z'} + Be^{i\eta z'})e^{-i\eta(z-z')}dz', \end{aligned} \tag{3.14}$$

where A and B are unknown constants. The integration over depth z' will be carried out numerically.

Then the approximate solution of the coherent pressure field in the random layer is:

$$\langle P_2(\vec{R})\rangle = P(z)e^{i\vec{\kappa}_0\cdot\vec{r}}. \tag{3.15}$$

Now we have solutions for the coherent fields in media 1, 2 and 3, i.e., Eqs.(3.1), (3.2) and (3.15), with four unknown constants $\langle V\rangle$, $\langle T\rangle$, A and B. By requiring the continuity of the mean pressure and mean vertical particle velocity along the interfaces $z = 0$ and $z = -h$,

$$\langle P_1(\vec{r},0)\rangle = \langle P_2(\vec{r},0)\rangle, \tag{3.16}$$

$$\frac{1}{\rho_1}\frac{\partial}{\partial z}\langle P_1(\vec{r},0)\rangle = \frac{1}{\rho_2}\frac{\partial}{\partial z}\langle P_2(\vec{r},0)\rangle, \tag{3.17}$$

$$\langle P_2(\vec{r},-h)\rangle = \langle P_3(\vec{r},-h)\rangle, \tag{3.18}$$

$$\frac{\partial}{\partial z}\langle P_1(\vec{r},-h)\rangle = \frac{\partial}{\partial z}\langle P_2(\vec{r},-h)\rangle, \tag{3.19}$$

we obtain the coherent reflection coefficient $\langle V\rangle$:

$$\langle V\rangle = \frac{(v_{01} + v_{12} + v_b v_{01} v_{23} e^{2i\eta h} + t_{12} v_{23} e^{2i\eta h})}{(1 + v_{01}v_{12} + v_b v_{23} e^{2i\eta h} + t_{12} v_{01} v_{23} e^{2i\eta h})}. \tag{3.20}$$

In the above expression, there are several quantities that will be defined. Most of them involve the quantities η or σ due to the small fluctuations of sound speed in the layer. They are:

$$v_{01} = \frac{\rho_2\sqrt{k_1^2 - \kappa_0^2} - \rho_1\sqrt{k_2^2 - \kappa_0^2}}{\rho_2\sqrt{k_1^2 - \kappa_0^2} + \rho_1\sqrt{k_2^2 - \kappa_0^2}}, \tag{3.21}$$

$$v_{12} = \frac{\sqrt{k_2^2 - \kappa_0^2}\beta - \eta\xi}{\sqrt{k_2^2 + \kappa_0^2}\beta + \eta\xi}, \tag{3.22}$$

$$v_b = \frac{(\sqrt{k_2^2 - \kappa_0^2} - \eta)\alpha}{\sqrt{k_2^2 + \kappa_0^2}\beta + \eta\xi}, \tag{3.23}$$

$$v_{23} = -\frac{(\sqrt{k_2^2 - \kappa_0^2} - \eta)\alpha}{\sqrt{k_2^2 + \kappa_0^2}\gamma + \eta\phi}, \tag{3.24}$$

$$t_{12} = \frac{(\sqrt{k_2^2 - \kappa_0^2} + \eta)\alpha}{\sqrt{k_2^2 + \kappa_0^2\beta + \eta\xi}}. \tag{3.25}$$

The quantities $\alpha, \beta, \gamma, \xi$ and ϕ are:

$$\alpha = 1 - \frac{1}{2i\eta}\int_{-h}^{0} f(z')dz', \tag{3.26}$$

$$\beta = 1 - \frac{1}{2i\eta}\int_{-h}^{0} f(z')e^{-2i\eta z'}dz', \tag{3.27}$$

$$\gamma = 1 - \frac{1}{2i\eta}e^{2i\eta h}\int_{-h}^{0} f(z')e^{2i\eta h}dz', \tag{3.28}$$

$$\xi = 1 + \frac{1}{2i\eta}\int_{-h}^{0} f(z')e^{-2i\eta z'}dz', \tag{3.29}$$

$$\phi = 1 + \frac{1}{2i\eta}e^{2i\eta h}\int_{-h}^{0} f(z')e^{2i\eta h}dz'. \tag{3.30}$$

Recall that the quantity $f(z)$ is given by Eq.(3.9).

By inspection, we observe that when σ approaches zero, $c(\vec{\kappa_0})$ and $f(z)$ also approach zero, $\eta = \sqrt{k_2^2 - \kappa_0^2}$, $\alpha, \beta, \gamma, \xi$ and ϕ all become unity, $\langle P_2(\vec{R})\rangle$ degenerates to the conventional transmitted wave, and $\langle V\rangle$ is merely the conventional plane-wave reflection coefficient for two half-spaces.

The coherent reflection coefficient, $\langle V\rangle$, in Eq.(3.20) is obtained by using Eqs.(3.21) through (3.30) and Eq.(3.9) through numerical integrations. The modulus and phase of $\langle V\rangle$ versus incident angle θ_0 for different values of the statistical parameters, including the case of non-random reflection for comparison, are shown in Figs.3.1-3.6. Among them, Figs.3.1-3.4 are for the case of a "fast" bottom, i.e. $c_2 > c_1$, and Figs.3.5-3.6 are for the case of a "slow" bottom, $c_2 < c_1$. Figs.3.1 and 3.2 are the magnitude and phase of the coherent reflection coefficient for three different frequencies, 200 Hz, 300 Hz and 400 Hz. The top line is the reflection

coefficient with no randomness. The results show an increased energy loss with increasing frequency. Figs.3.3 and 3.4 show the magnitude and phase of the coherent reflection coefficient for the same set of acoustic background parameters with fixed frequency, but changing randomness size, respectively, $\sigma = 0, \sigma = 0.05$ and $\sigma = 0.10$. Here we see the energy loss increases with increasing σ. Compared with the case of reflection from a fast homogeneous half-space, the major effect due to the randomness is the disappearance of a sharp critical angle. We also notice that the phase change is not significant. Figs.3.5 and 3.6 are the magnitude and phase of $\langle V \rangle$ versus different frequencies for a slow bottom. In this case, total reflection does not occur. The change in magnitude is not as significant as for fast bottoms. However, the phase change is relatively large.

The behavior of $\langle V \rangle$ is similar to the reflection coefficient for a homogeneous absorbing bottom[56]. However, the mechanism of energy loss is different[58].

After finding $\langle V \rangle$, the other unknowns, A, B, and $\langle T \rangle$, can be found through Eqs.(3.16) to (3.19) to be:

$$A = \frac{1}{2\eta\rho_1}[\rho_2\sqrt{k_1^2 - \kappa_0^2} + \rho_1\eta + \langle V \rangle(\eta\rho_1 - \rho_2\sqrt{k_1^2 - \kappa_0^2})]; \tag{3.31}$$

$$B = \frac{1}{\alpha}[1 - \beta A + \langle V \rangle] \tag{3.32}$$

$$\langle T \rangle = exp[-i\sqrt{k_2^2 - \kappa_0^2}h][\alpha A exp(i\eta h) + \gamma B exp(-i\eta h)]. \tag{3.33}$$

Notice that when σ approaches zero, $\langle T \rangle$ degenerates to the conventional transmission coefficient. These results will be used in Chapter 4 to calculate the scattered field.

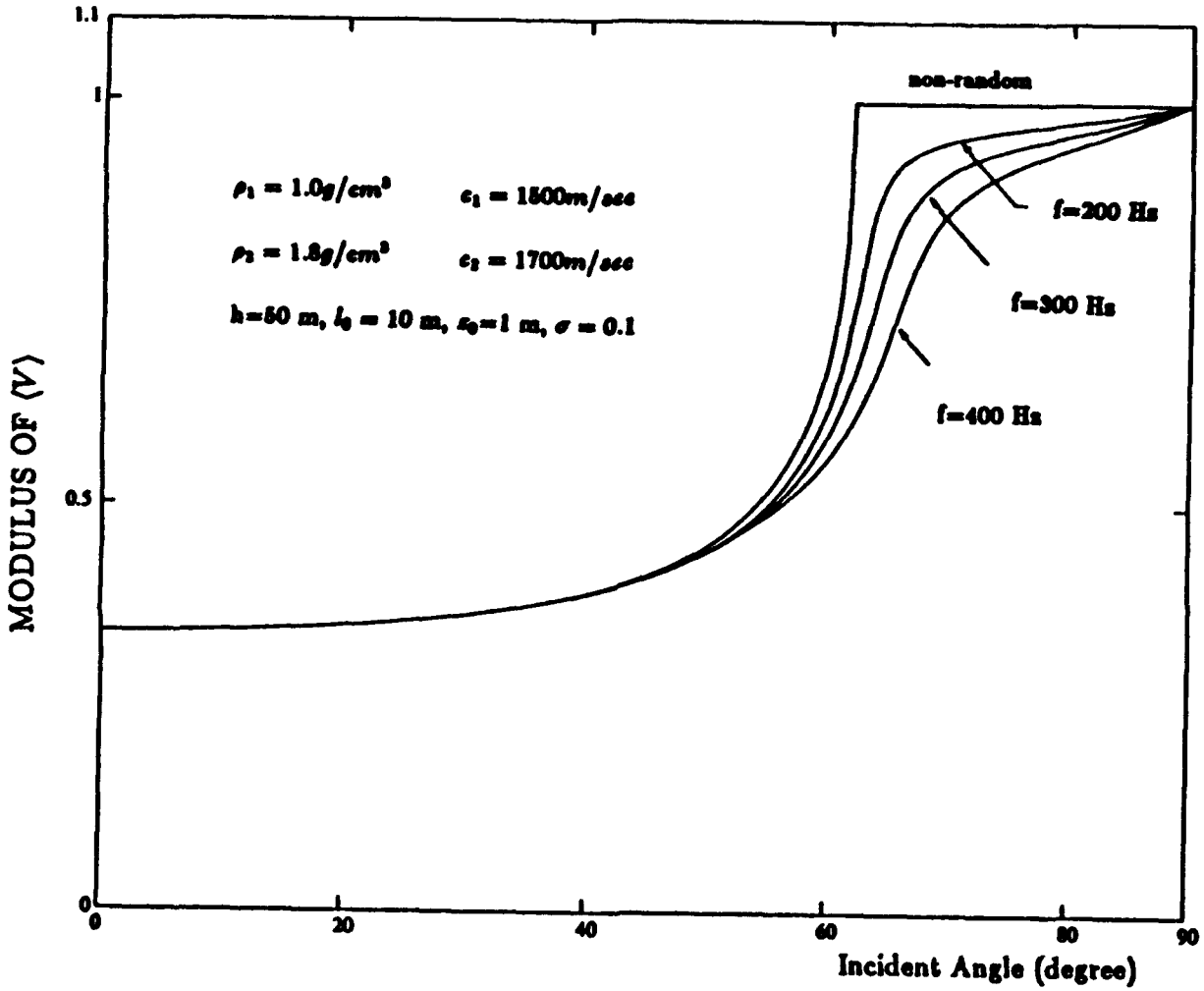

Figure 3.1: Magnitude of reflection coefficient for different frequencies (fast bottom)

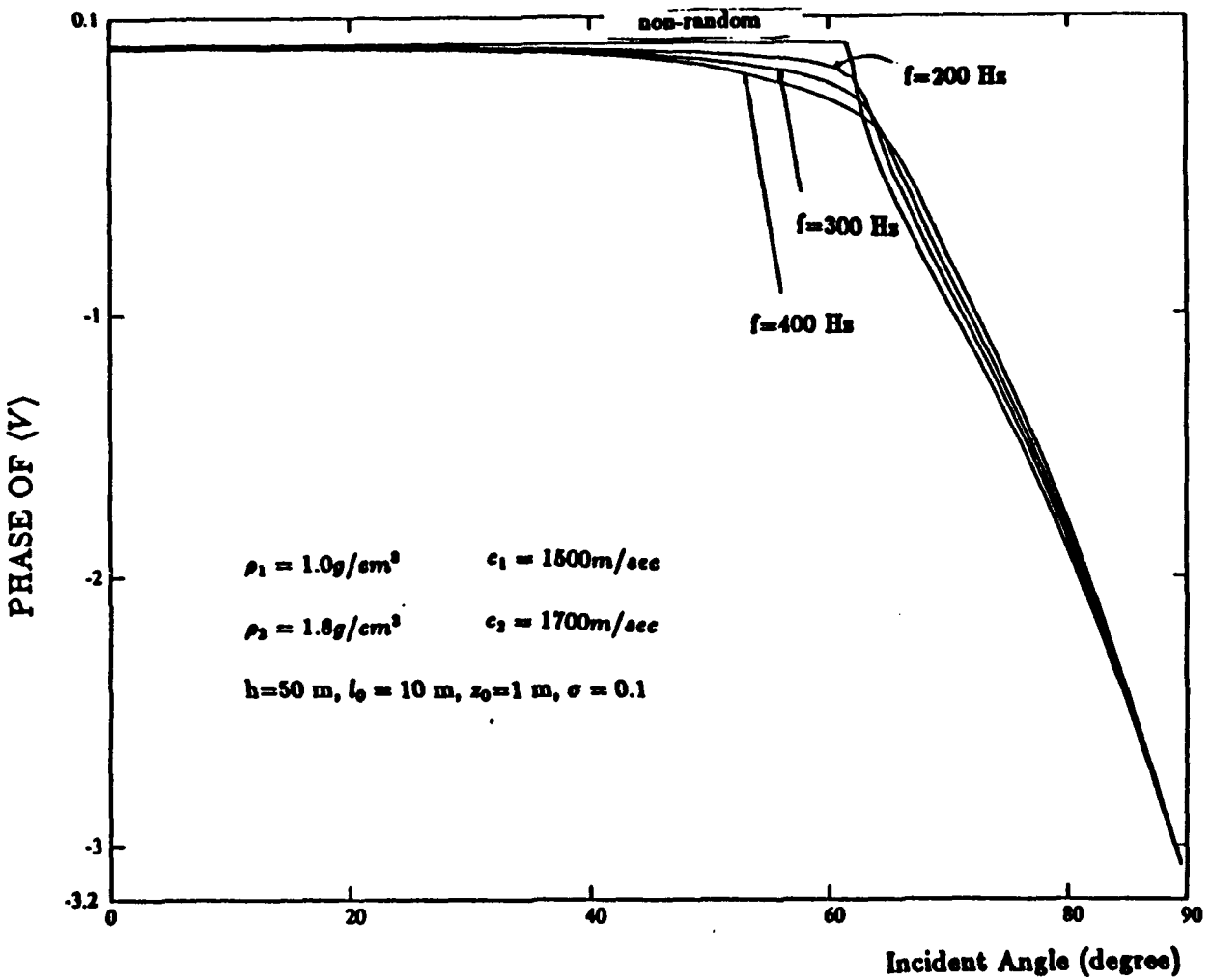

Figure 3.2: Phase of reflection coefficient for different frequencies (fast bottom)

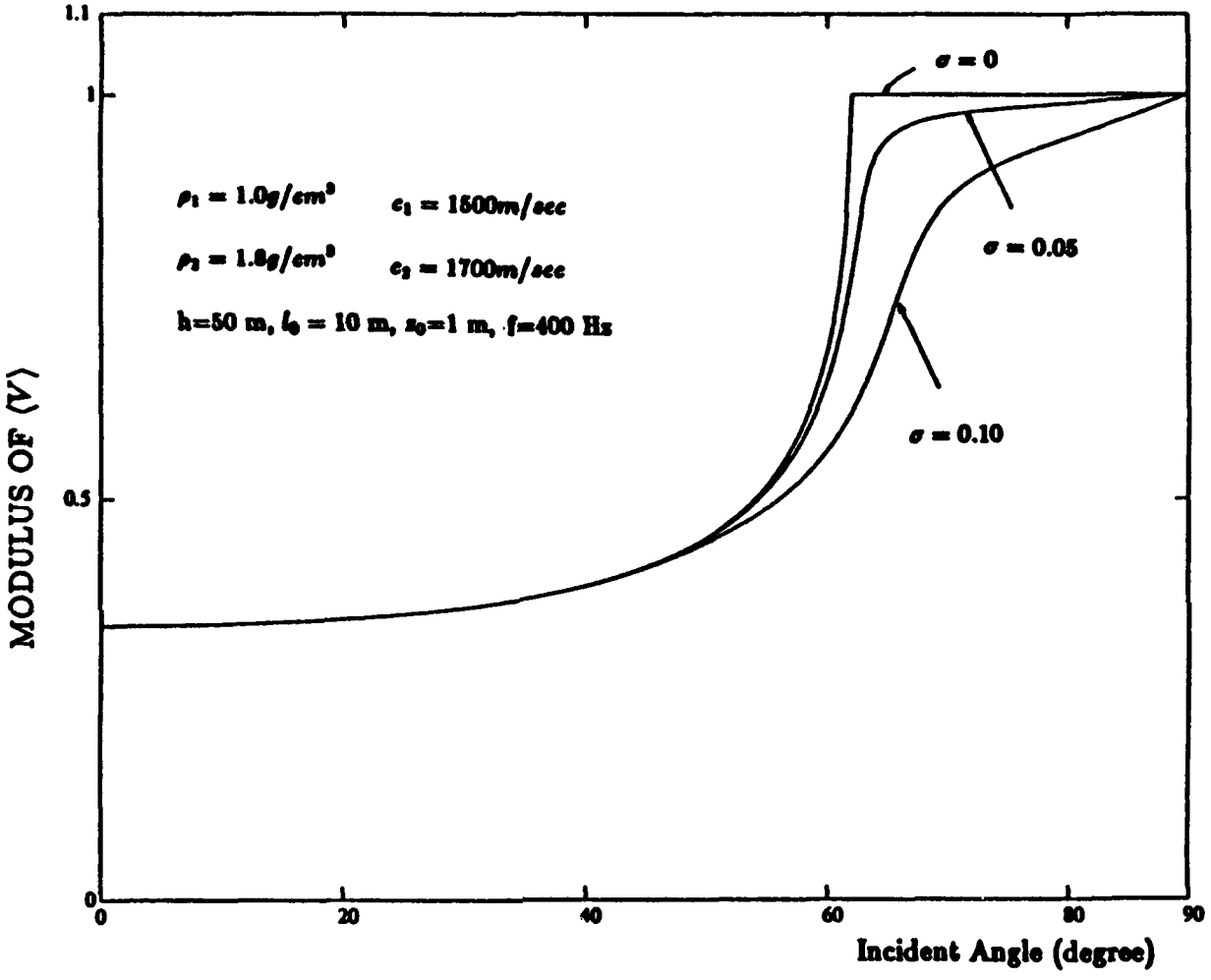

Figure 3.3: Magnitude of reflection coefficient for different σ's (fast bottom)

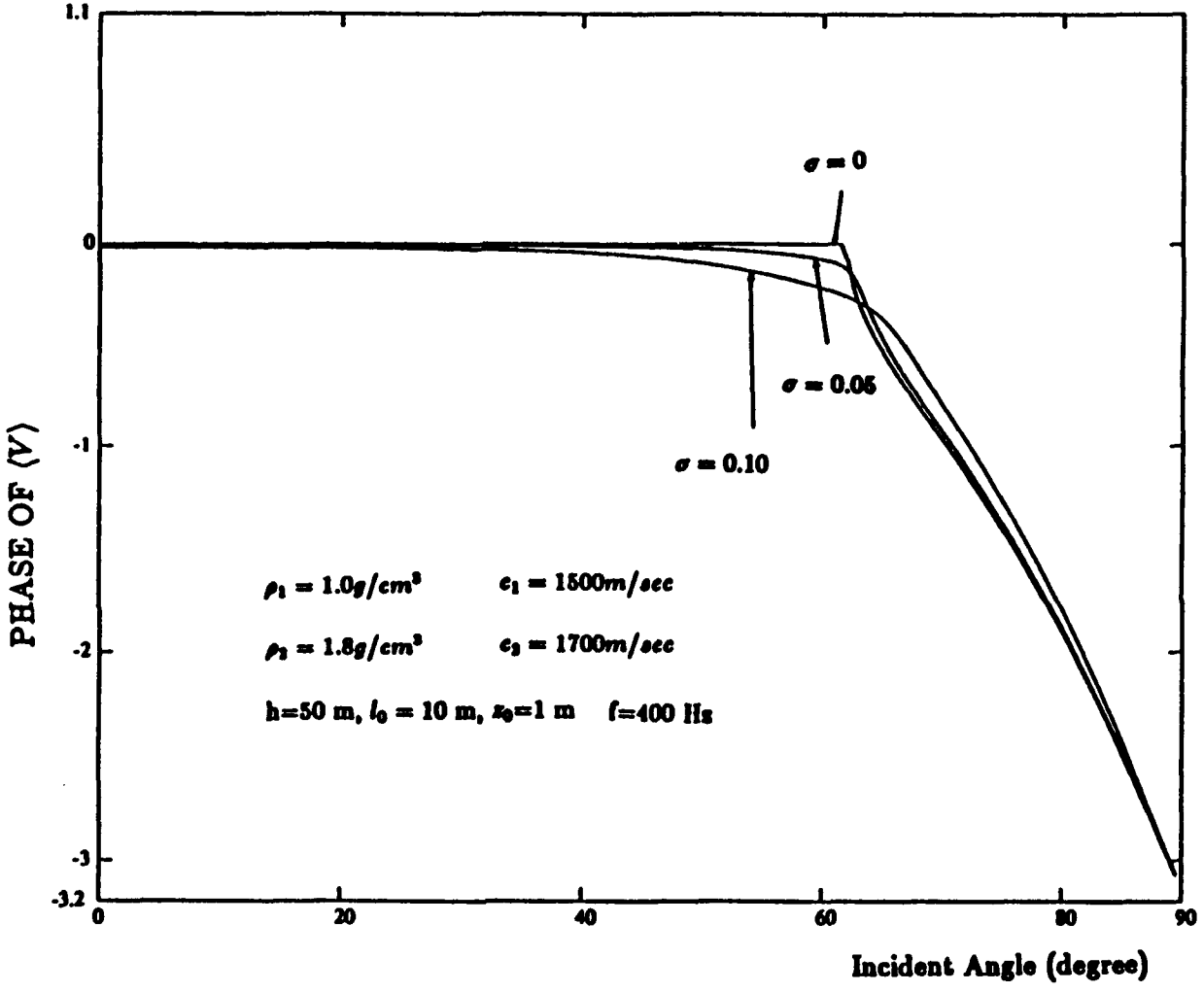

Figure 3.4: Phase of reflection coefficient for different σ's (fast bottom)

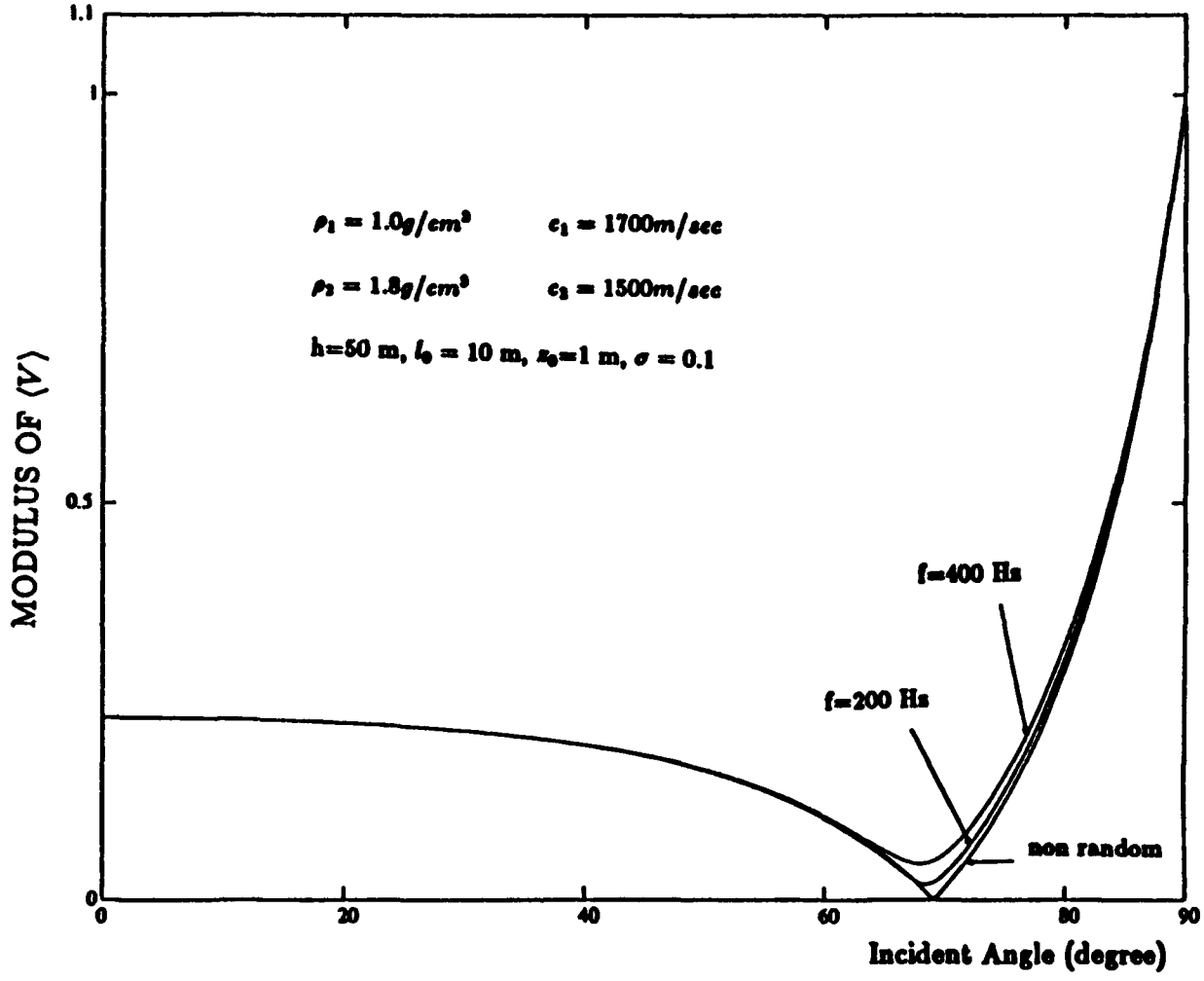

Figure 3.5: Magnitude of reflection coefficient for different frequencies (slow bottom)

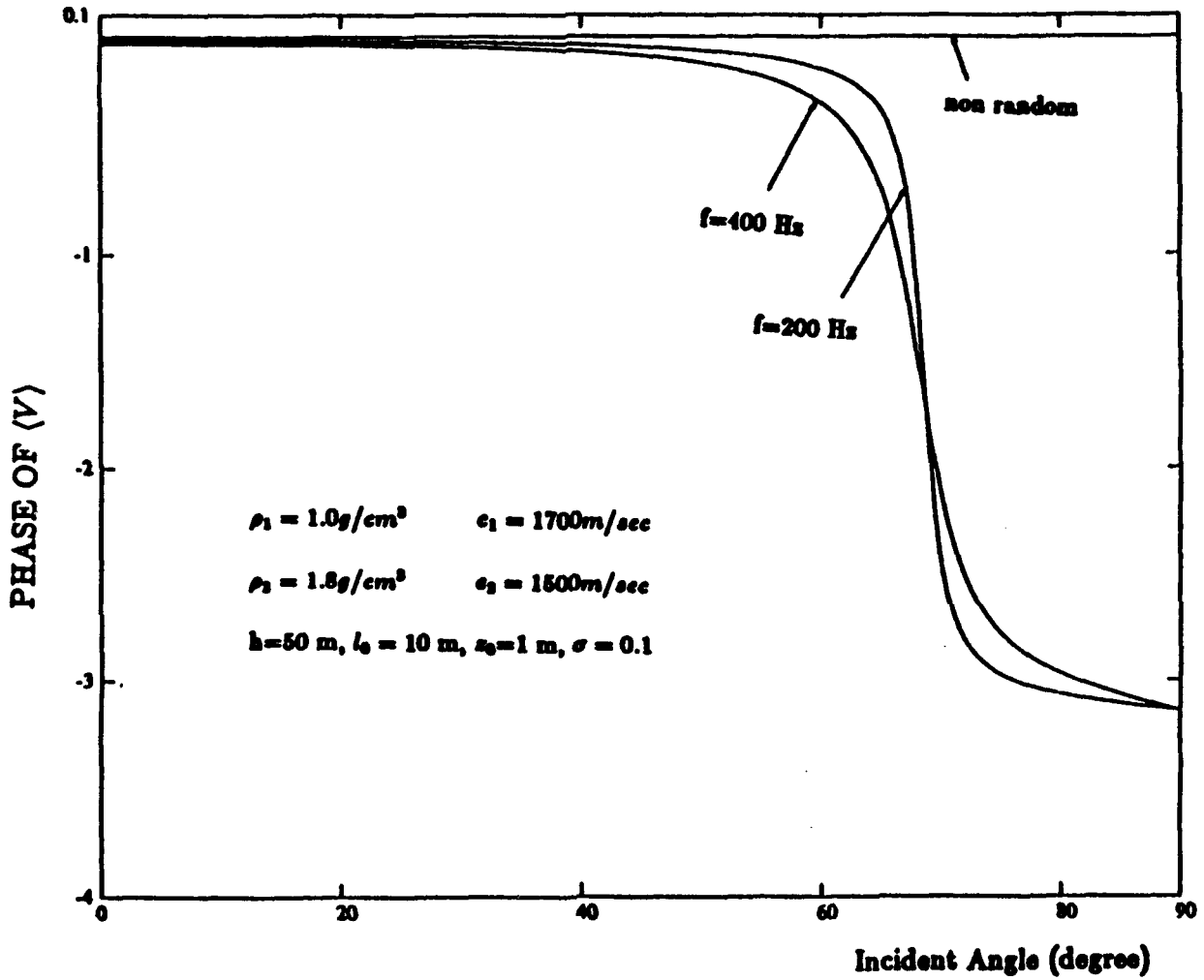

Figure 3.6: Phase of reflection coefficient for different frequencies (slow bottom)

Chapter 4

SPATIAL CORRELATION OF THE SCATTERED FIELD

In Chapters 2 and 3, we have found the solutions of the coherent reflection and transmission coefficients $\langle V \rangle$ and $\langle T \rangle$, and the constants A and B, hence the coherent field $\langle P_2(\vec{R}') \rangle$ is known. We can put the coherent field into Eq.(2.11) in Chapter 2 to find the randomly scattered field:

$$p_1^s(\vec{R}) = \frac{k_2^2}{4\pi} \int \int_{v'} \int \epsilon(\vec{R}') \langle P_2(\vec{R}') \rangle G(\vec{R} \,|\vec{R}') dv'. \tag{4.1}$$

We are interested in the scattered acoustic field in the water, as measured at the observation point $\vec{R}$ which is in the water column where $z > 0$. The only difference between Eq.(2.11) and Eq.(4.1) is that the observation point in Eq.(2.11) is in the random layer where $z < 0$. Therefore, the Green's function that will be used here is one with the source in the random layer ($z < 0$) and the observation point in the water ($z>0$).

Since the statistical average, i.e. the first moment, of the random quantity ϵ is zero, $\langle \epsilon \rangle = 0$, $\langle p^s \rangle = 0$ because p^s is proportional to ϵ. Hence we shall study the

spatial correlation function, i.e. the second moment of p^s, which is defined as:

$$C_v(\vec{R}_1, \vec{R}_2) = \langle p_1^s(\vec{R}_1) p_1^{s*}(\vec{R}_2) \rangle, \tag{4.2}$$

where R_1 and R_2 are two spatial positions where the receivers are located. Therefore, $C_v(\vec{R}_1, \vec{R}_2)$ is a measure of how well the scattered fields at different locations are correlated. Notice that the the spatial correlation of the scattered field, $C_v(\vec{R}_1, \vec{R}_2)$, defined above is not normalized; when $\vec{R}_1 = \vec{R}_2$, C_v is the scattering intensity.

Conventionally, only $C_v(\vec{R}_1, \vec{R}_1) = \langle |p^s(\vec{R}_1)|^2 \rangle$, the intensity of the scattered field, is studied. However, the intensity contains just a small portion of the information carried in the second moment of the scattered field. No effort has yet been made to study the spatial correlation of the quantity p^s in bottom acoustics. Results of this kind exist in electromagnetic wave and atmospheric acoustic wave studies[16], where the media are assumed infinite, and no medium discontinuities are present. The formulation given in Chapter 2 allows us to calculate the spatial correlation of the scattered field, not only the intensity. Recent technological developments in underwater acoustic experiments make it possible to investigate the spatial correlation of the scattered field. Some considerations on experiments of this kind will be given in Chapter 7.

Substituting Eq.(4.1) into Eq.(4.2), we have

$$\begin{aligned} C_v(\vec{R}_1, \vec{R}_2) \;=\; & \left(\frac{k_2^2}{4\pi}\right)^2 \int\int_{v'} \int dv' \int\int_{v''} \int dv'' \langle \epsilon(\vec{R}') \epsilon(\vec{R}'') \rangle \cdot \\ & \langle P_2(\vec{R}') \rangle \langle P_2^*(\vec{R}'') \rangle G(\vec{R}_1 | \vec{R}') G^*(\vec{R}_2 | \vec{R}''). \end{aligned} \tag{4.3}$$

The correlation function of ϵ is given in Eq.(2.22) of Chapter 2. If the acoustic wavelength is much larger than the vertical correlation length of ϵ, $\lambda >> z_0$, we can approximate the correlation function as follows:

$$\langle \epsilon(\vec{R})\epsilon(\vec{R}') \rangle = 4\langle \frac{\delta c(\vec{R})}{c_2} \frac{\delta c(\vec{R}')}{c_2} \rangle \approx 4 z_0 \sigma^2 N(\vec{l}) \delta(z - z'), \tag{4.4}$$

where $N(\vec{l})$ and its spectrum are assumed to have one of the forms given in Eqs.(2.24) to (2.26). The Green's function in which the source is located in the random layer and the observation point is located in the water has this form:

$$G(\vec{R}_1|\vec{R}') = \frac{1}{2\pi} \int\int g(\vec{\kappa}, z_1, z') e^{i\vec{\kappa}\cdot(\vec{r}-\vec{r}')} d^2\vec{\kappa}, \tag{4.5}$$

where $g(\vec{\kappa}, z_1, z')$ is the two dimensional Fourier transform of the Green's Function, $G(\vec{R}_1|\vec{R}')$, and is sometimes called the depth-dependent Green's function[54]. For the present case, it is:

$$g(\vec{\kappa}, z_1, z') = T_{21} \left(\frac{i}{\xi_2} \right) e^{i\xi_1 z - i\xi_2 z'}, \tag{4.6}$$

where ξ_1 and ξ_2 are vertical wavenumbers in the water and in the bottom, respectively corresponding to $\vec{\kappa}$:

$$\begin{aligned} \xi_1 &= \sqrt{k_1^2 - \kappa^2}, \\ \xi_2 &= \sqrt{k_2^2 - \kappa^2}, \end{aligned} \tag{4.7}$$

and T_{21} is the transmission coefficient from medium 2 to medium 1 in the absence of the the random quantity ϵ:

$$T_{21} = \frac{2\rho_1 \xi_2}{\rho_1 \xi_2 + \rho_2 \xi_1}. \tag{4.8}$$

Substituting the above expressions into Eq.(4.3), we have

$$\begin{aligned} C_v(\vec{R}_1, \vec{R}_2) &= z_0 \left(\frac{\sigma k_2^2}{4\pi} \right)^2 \left(\frac{1}{2\pi} \right)^2 \int\int d^2\vec{r}' \int\int d^2\vec{r}'' \int dz' \int\int d^2\vec{\kappa} \int\int d^2\vec{\kappa}' \cdot \\ &\quad |P(z')|^2 N(\vec{l}) g(\kappa, z_1, z') g^*(\kappa', z_2, z') e^{i\vec{\kappa}_0\cdot\vec{l}} e^{i\vec{\kappa}\cdot(\vec{r}'-\vec{r}_1)} e^{i\vec{\kappa}'\cdot(\vec{r}_2-\vec{r}'')} \\ &= z_0 \left(\frac{\sigma k_2^2}{2\pi} \right)^2 \int dz' \int\int d^2\vec{\kappa} |P(z')|^2 S(\vec{\kappa} - \vec{\kappa}_0) \cdot \\ &\quad g(\kappa, z_1, z') g^*(\kappa, z_2, z') e^{i\vec{\kappa}\cdot(\vec{r}_1-\vec{r}_2)}. \end{aligned} \tag{4.9}$$

The above formula is the basis for the calculation of the spatial correlation of the scattered field. It consists of two wavenumber integrals and one depth integral over the random layer. $|P(z')|$ is the z-dependent part of the coherent field in the random layer; it can be calculated through Eqs.(3.14), (3.31), (3.32), and (3.33) in Chapter 3. As a comparison, we can also use the Extended Born approximation in Eq.(4.9). To do so, instead of using the coherent solution, we use the background field, i.e. the field in the absence of the randomness:

$$P(z) = T_{12} e^{-i\sqrt{k_2^2 - \kappa^2} z}, \tag{4.10}$$

where T_{12} is the transmission coefficient from medium 1 to 2:

$$T_{12} = \frac{2\rho_2 \xi_1}{\rho_1 \xi_2 + \rho_2 \xi_1}. \tag{4.11}$$

Later in this chapter, a comparison between using the coherent field and using the Extended Born approximation will be made.

In order to integrate Eq.(4.9) numerically, we change the wavenumber integrals into polar coordinates. Letting the polar coordinates for the quantities $\vec{\kappa}$, $\vec{\kappa_0}$ and $\vec{r} - \vec{r_0}$ respectively be:

$$\begin{aligned} \vec{\kappa} &= (\kappa, \phi), \\ \vec{\kappa_0} &= (\kappa_0, \phi_0), \\ \vec{r} - \vec{r_0} &= (R, \theta), \end{aligned} \tag{4.12}$$

Eq.(4.9) becomes:

$$\begin{aligned} C_v(R,\theta) \;=\; & z_0 \left(\frac{\sigma k_2^2}{2\pi}\right)^2 \int dz' |P(z')|^2 \int d\kappa \kappa g(\kappa, z_1, z') g^*(\kappa, z_2, z') \\ & \int d\phi S(\kappa cos\phi - \kappa_0 cos\phi_0, \kappa sin\phi - \kappa_0 sin\phi_0) e^{i\kappa R cos(\phi - \theta)}, \end{aligned} \tag{4.13}$$

where R is the horizontal separation distance of the two receivers, and θ is the horizontal angle between the line linking the two receivers and the x-axis. The following

results for the spatial correlation of the scattered field are obtained from Eq.(4.13).

Fig.4.1 shows the receiver geometry. Since the two receiver points in Eq.(4.9) are completely arbitrary, we will choose them to be either in a vertical line parallel to the z-axis, or a horizontal line, perpendicular to the z-axis. The orientation of the horizontal receivers is indicated by the azimuthal angle θ. The incident wave direction is determined by the incident angle θ_0 and the azimuthal angle ϕ_0. Although the anisotropy of the bottom correlation function is assumed to be aligned in the xy-plane (see Eqs.(2.24) to (2.26)), neither the incident wave nor the horizontal receivers have to be so aligned; therefore this configuration is arbitrary in terms of the incident wave direction and receiver orientation.

For clarity, Fig.4.2 specifies the environmental parameters upon which all the following results are calculated except for those separately indicated. Since there is little experimental data available, especially those concerning the random distribution of sound speed in the layer, the parameters are chosen to meet the theoretical requirements and to be in the reasonable range of reality. How to experimentally measure these parameters will be discussed in Chapter 7.

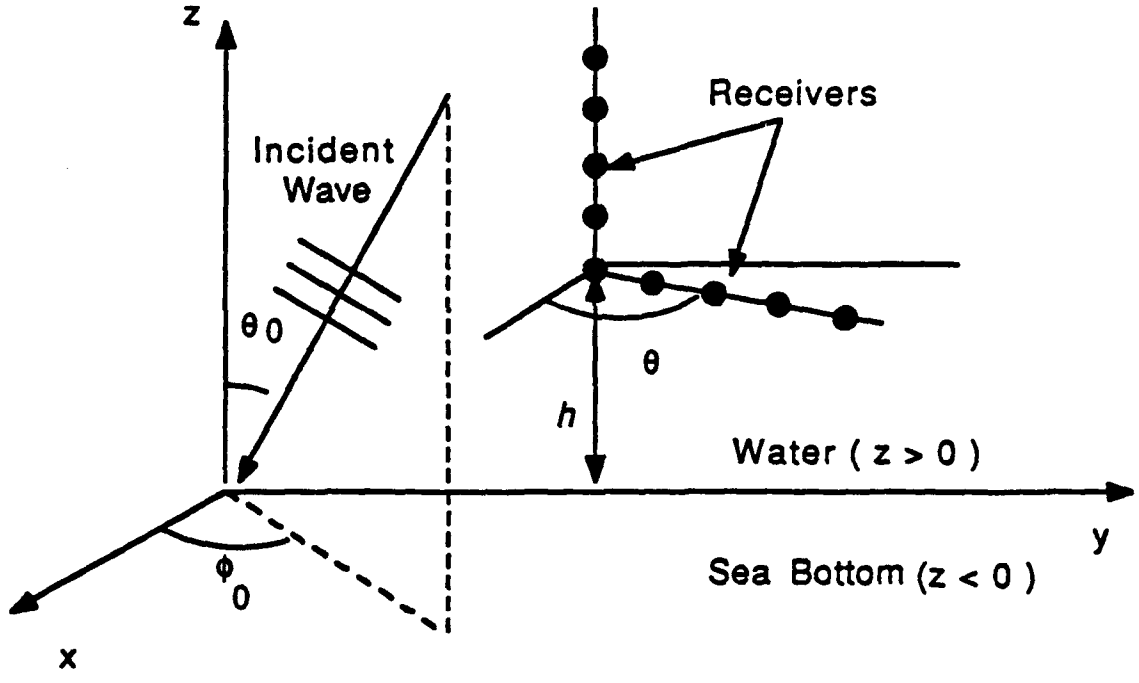

Fig. 4.1 Incident wave and receiver arrangement

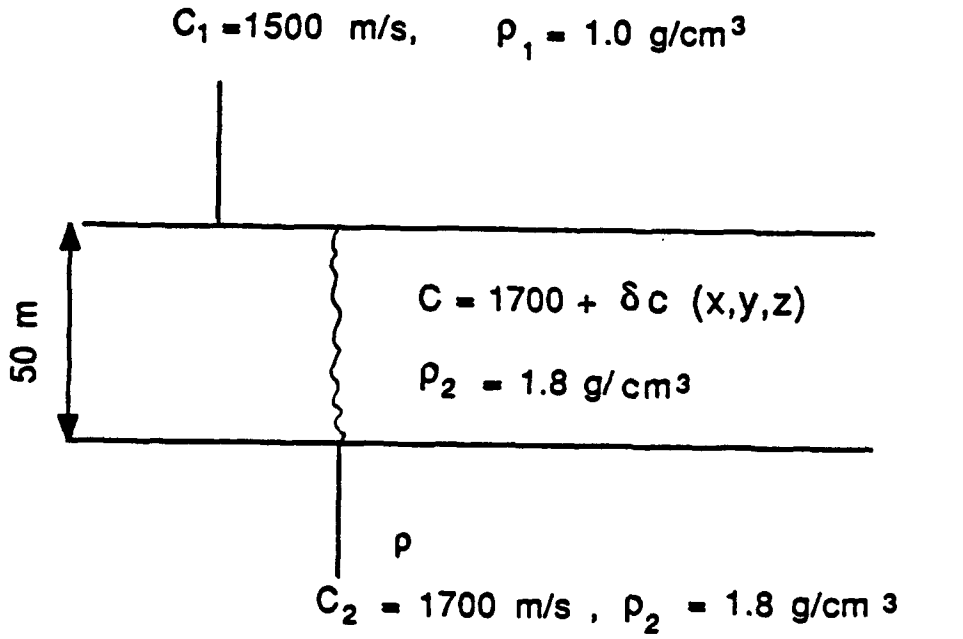

$$\frac{\langle \delta^2 c \rangle}{c_2^2} = \sigma^2 = (\ 0.05.\ )^2, \quad l_0 = 5.0\ \text{m};\ z_0 = 0.5\ \text{m}$$

Fig. 4.2 Environment parameters

4.1 Angular Dependence

First, we examine the angular dependence of the horizontal correlation. In the present case, we choose the incident angle θ_0 to be either 30° or 60°, and $\phi_0 = 0$, so the incident wave is in the x direction. The bottom correlation function is isotropic Gaussian (see Eq.(2.26)). In calculating the horizontal correlation of the scattered field, $C_v(R, \theta)$, we keep one receiver at a fixed point, and the second receiver takes sequential measurements away from the first receiver in the horizontal plane. The distance between the two receivers is R. The second receiver may also move in different directions, which correspond to different orientation angles. Since the incident direction is fixed in the x-direction, we are going to examine the differences in horizontal correlations among different receiver orientations. Throughout Fig.4.3 to Fig.4.8, the acoustic frequency is 100 Hz. The x-direction is referred to as along-propagation direction, and the y-direction is referred to as the cross-propagation direction. Fig.4.3 shows the comparison between the horizontal correlation in the along-propagation direction ($\theta = 0°$) and the horizontal correlation in the cross-propagation direction ($\theta = 90°$) while the incident angle $\theta_0 = 30°$. The horizontal axis is expressed in the non-dimensional unit R/λ. Notice that while the cross-propagation correlation ($\theta = 90°$) has a clear null near 0.6 wavelengths, the along-propagation correlation ($\theta = 0°$) does not. In other words, the correlation along the propagation direction is greater than the correlation across the propagation direction. For better views, Figs.4.4 and 4.5 show two side views of the gradual change of $|C_v(R, \theta)|$ against different θ's ranging from 0° to 90°. One of the two axes is still R/λ, the other one is θ.

Figs.4.6, 4.7 and 4.8 are the same as Figs.4.3, 4.4 and 4.5 except that the incident angle is increased to 60°.

Chernov[16] mentioned a similar angular dependence for the case of scattering in infinite media. Physically, since the incident wave is a plane wave, receivers across the propagation direction will have the same phase, whereas along other directions the phase differs, and the difference reaches maximum when the receivers are aligned along the propagation direction. Later it will be shown that the null in the correlation can be used to estimate the bottom correlation length by an inverse procedure. Therefore in an experiment, the receivers should be deployed across the incident wave propagation direction to identify the null.

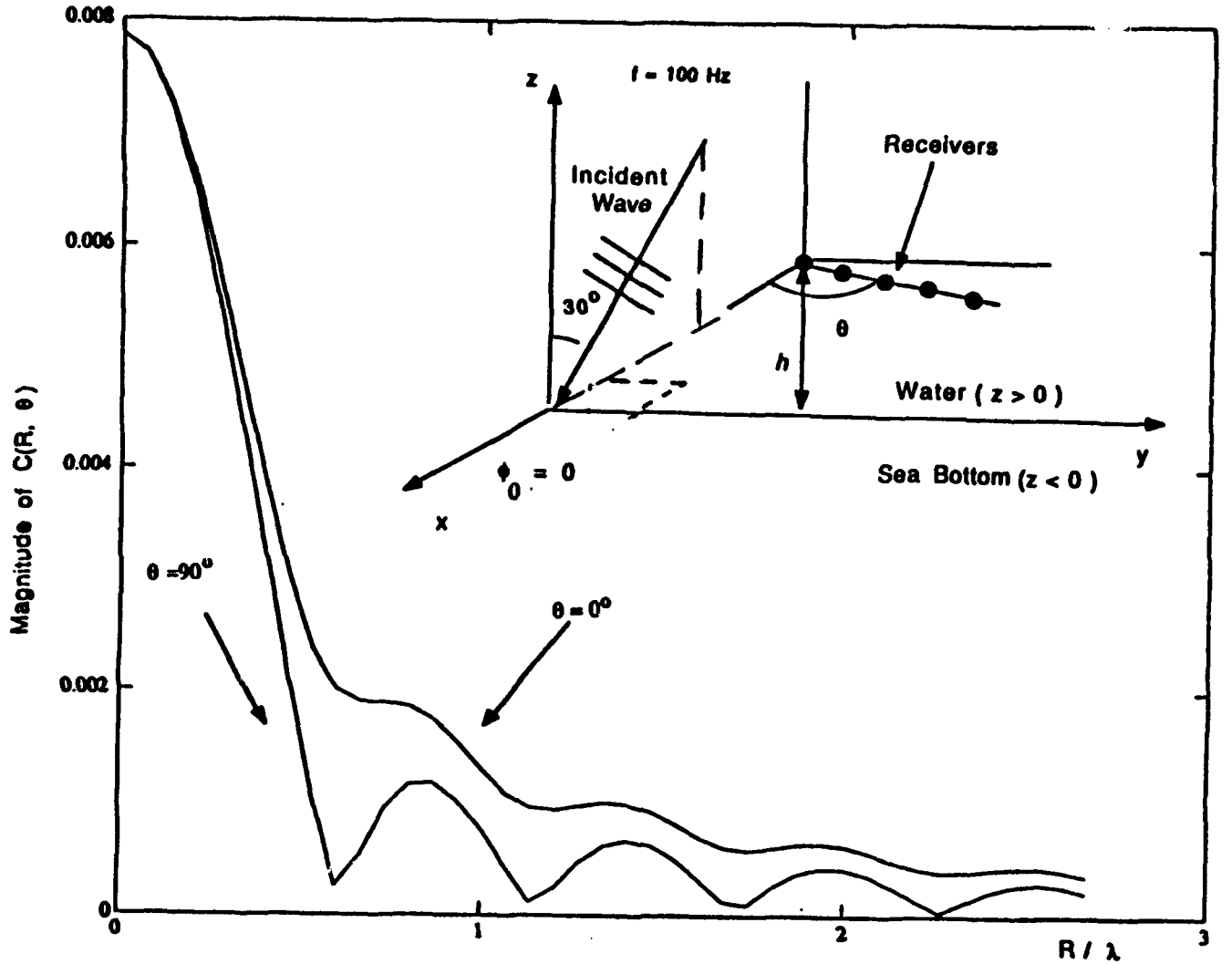

Figure 4.3: Comparison on receiver orientation, $\theta_0 = 30°$

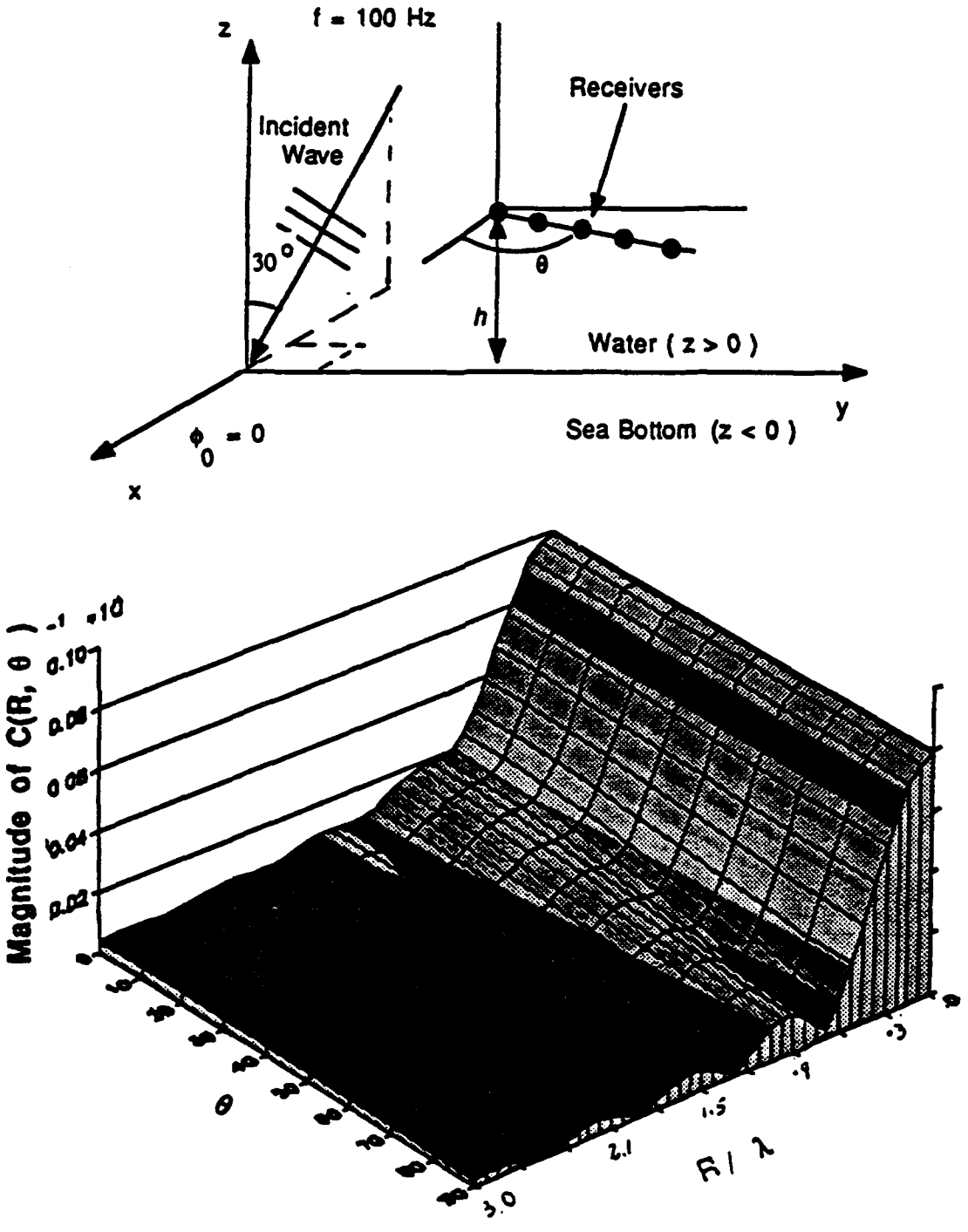

Figure 4.4: Comparison on receiver orientation, $\theta_0 = 30°$

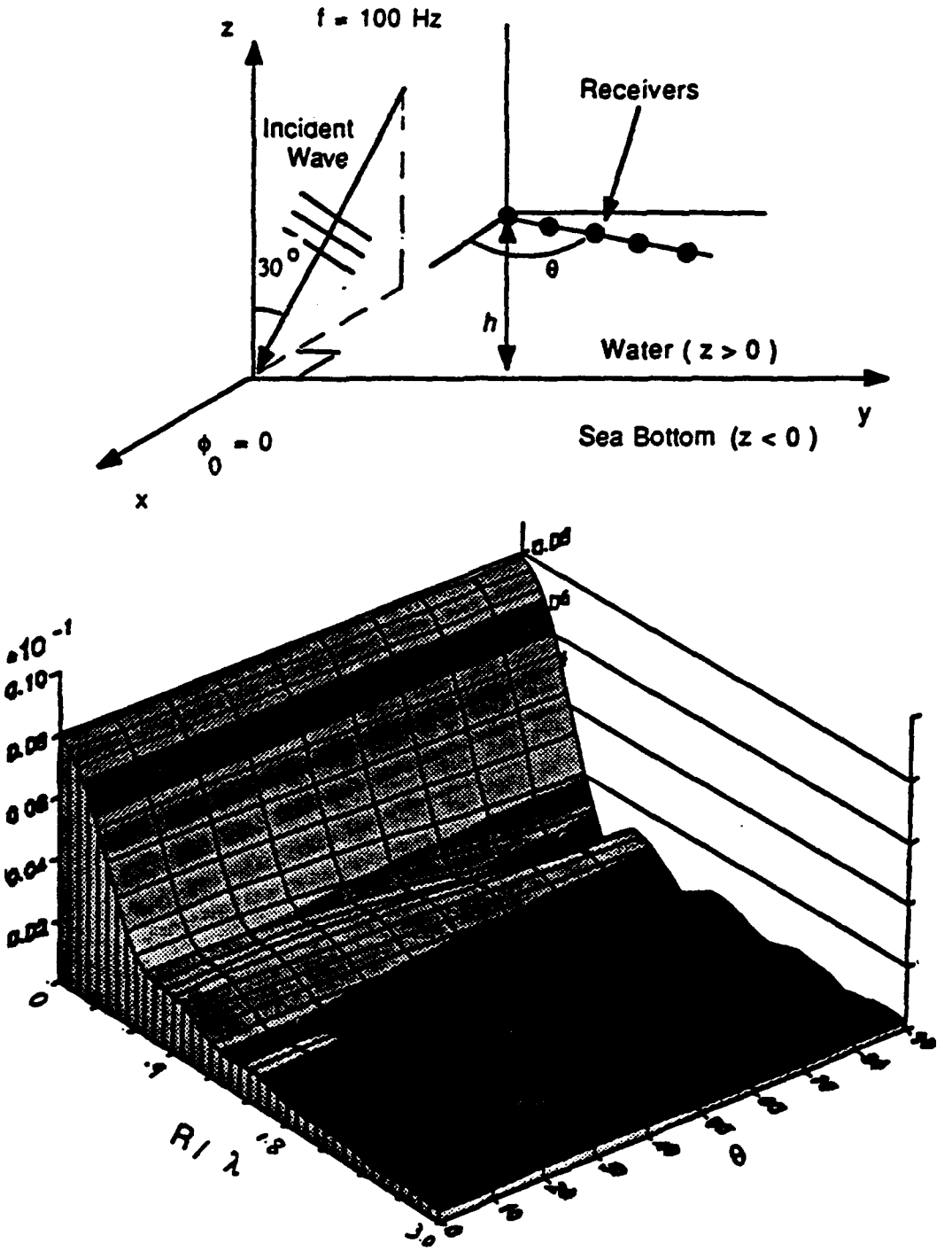

Figure 4.5: Comparison on receiver orientation, $\theta_0 = 30°$

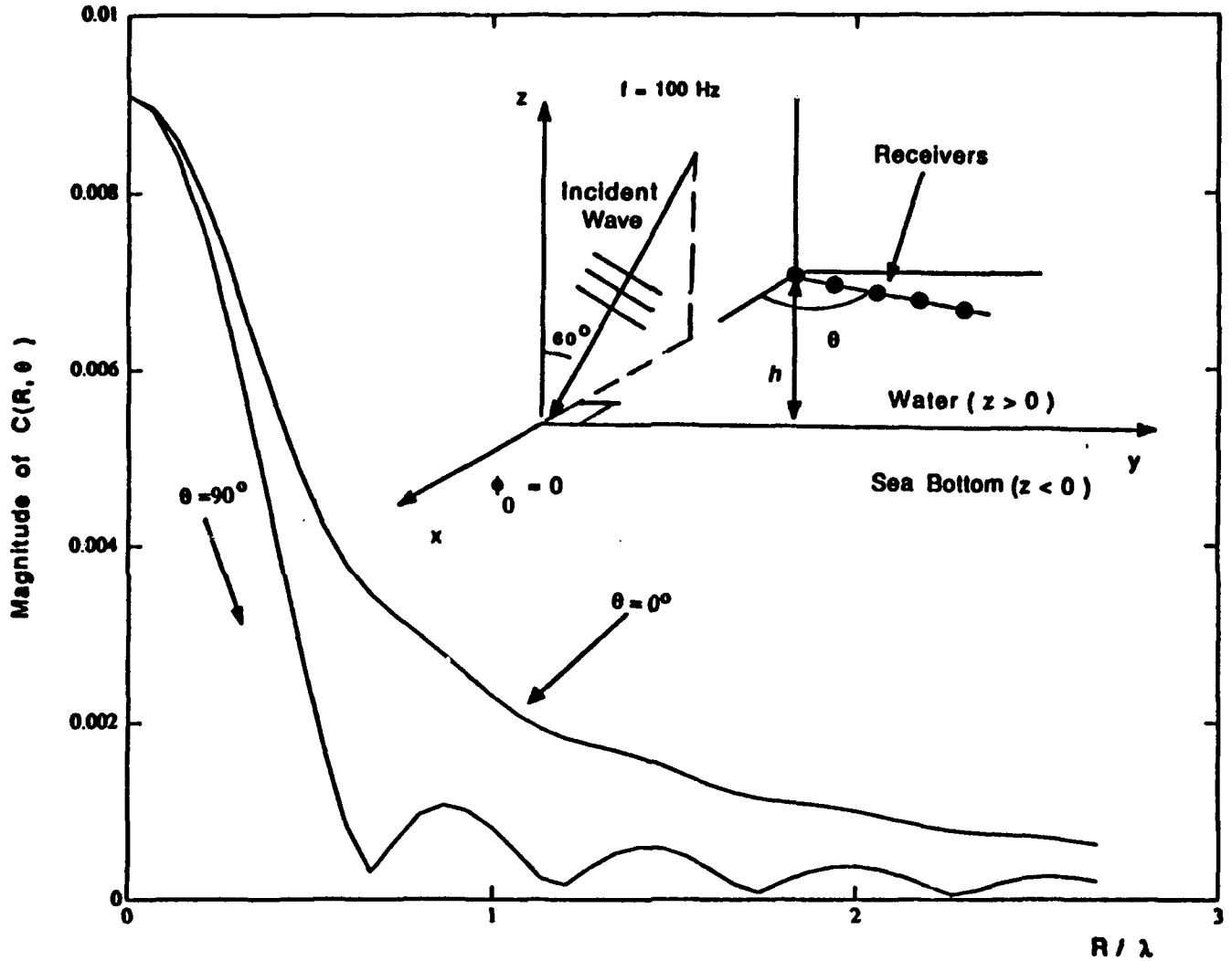

Figure 4.6: Comparison on receiver orientation, $\theta_0 = 60°$

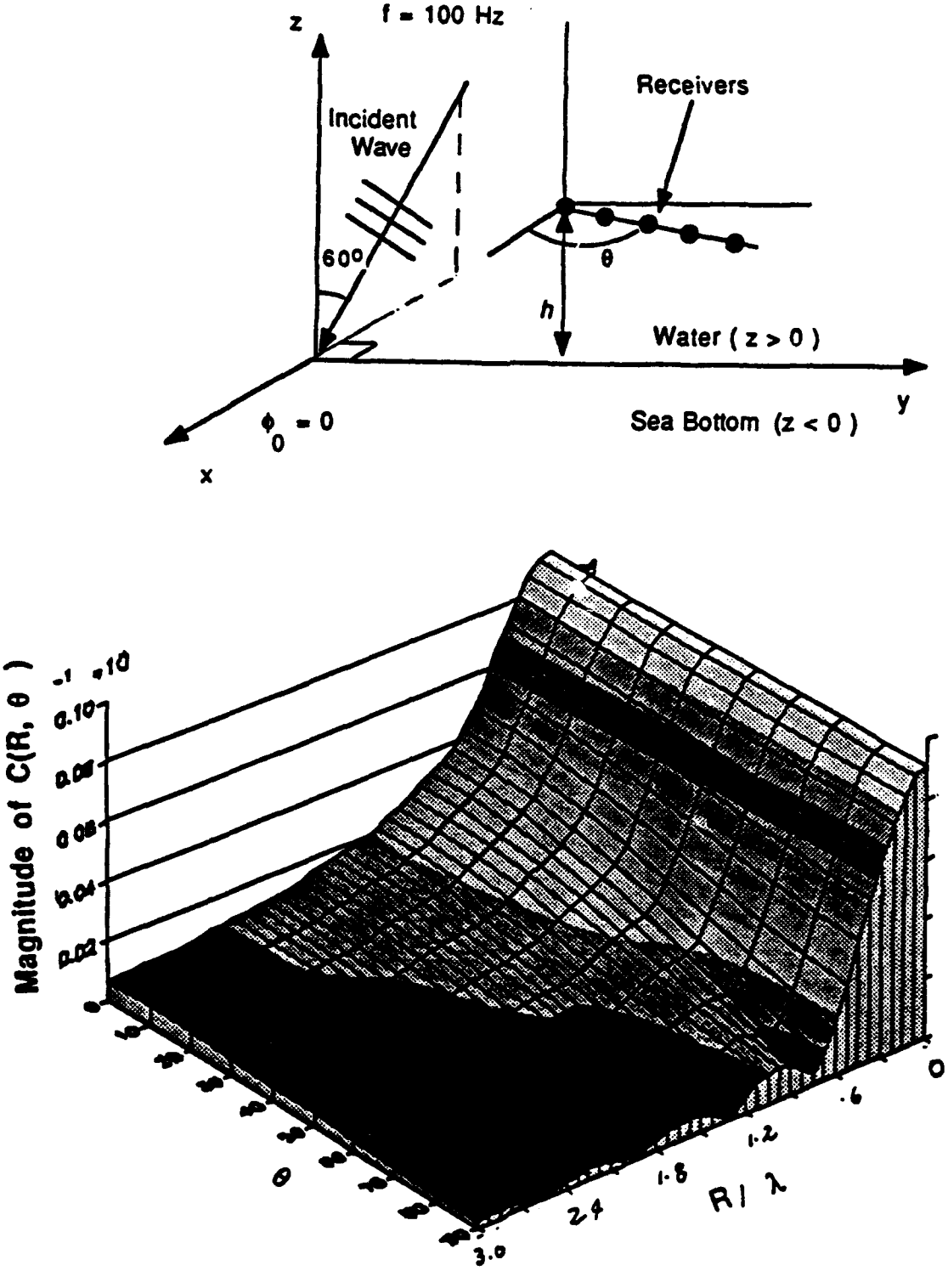

Figure 4.7: Comparison on receiver orientation, $\theta_0 = 60°$

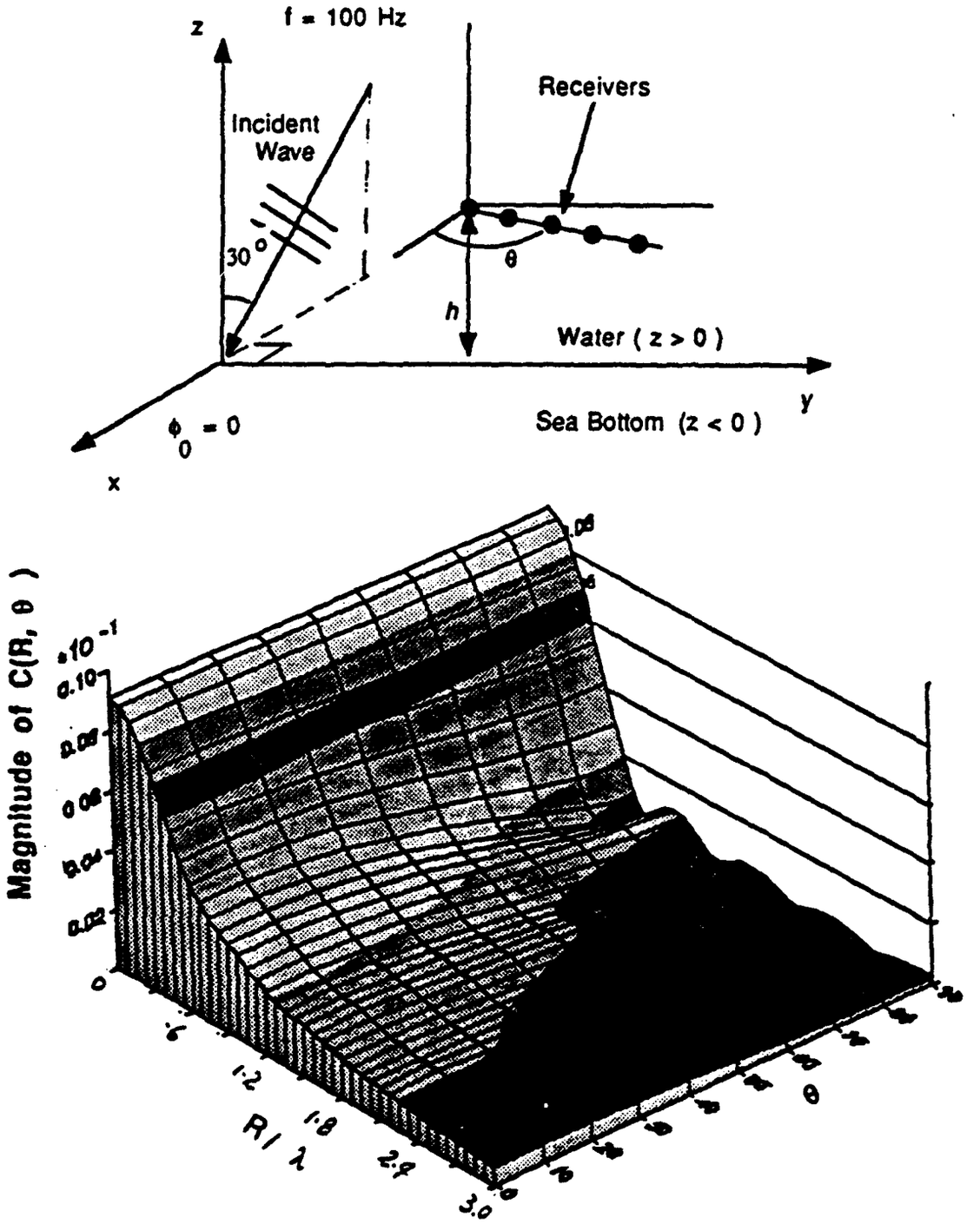

Figure 4.8: Comparison on receiver orientation, $\theta_0 = 60°$

4.2 Frequency Dependence

Next we investigate the frequency dependence of the spatial correlation function $C_v(R, \theta)$. We will emphasize the relationship between the physical size of the scatterer expressed by twice the horizontal correlation length, i.e. $2l_0$, and the acoustic wavelength used. Again we choose the correlation function to be Gaussian in this section. Since we have assumed that $l_0 = 5$ meters throughout this section, the physical size of the volume scatterer has a diameter of roughly 10 meters. For comparison, we vary the acoustic frequencies. Because the acoustic wavelength λ is a function of frequency, it is not convenient to use the unit R/λ for the horizontal axis as we did in the last section; therefore, the horizontal axes of the Figures in this section are all expressed in terms of R in the units of meters.

Fig.4.9 shows the horizontal correlations when the incident angle θ_0 is 30° for three different frequencies, 40 Hz, 60 Hz and 80Hz, respectively. The corresponding acoustic wavelengths are 37.5m, 25m and 18.75m respectively and they are all larger than the volume scatterer size of 10 meters. We find that the first null of the correlation changes accordingly when the acoustic frequency increases. It changes in such a fashion that the null position on the R/λ axis will be fixed. In Fig.4.10, the acoustic frequencies are 160 Hz, 180 Hz and 200 Hz, and the corresponding wavelengths are 9.38m, 8.33m and 7.5m respectively. They are all smaller than the scatterer size of 10 meters. This time the null positions are independent of frequency; more importantly, the half-value point on the correlation curve roughly equals to 5 meters, which is the correlation length l_0 of the random sound speed.

These results show that when the acoustic wavelength is comparable or smaller than the size of the scatterer, the position of the first null is independent of fre-

quency, and the half-value point equals the correlation length of that of ϵ. However, when the acoustic wavelength is larger than the size of the scatterer, the first null changes with frequency.

In order to see this more clearly, we show in Fig.4.11 a three dimensional plot of the correlation $C_v(R,\theta)$. The two horizontal axes are correlation distance R in meters and frequency in Hz. Note the two regions where the first null locus has different behavior against frequency; it curves into smaller values for increasing frequency starting from the low frequency end; and as the frequency increases further when the acoustic wavelength is smaller than 10 meters, the null position stablizes at 10 meters.

Physically, when the acoustic wavelength is larger than the linear dimension of the scatterer, the wave cannot distinguish the scatterer size, and so what is reflected on the correlation of the scattered field of the random scatterers is the character equivalent to what of a white random process[65] would have. When the acoustic wavelength becomes smaller than the linear dimension of the volume scatterer, the spatial correlation of the scattered field will reflect the size of the volume scatter.

Figs.4.12, 4.13, and 4.14 are the same as Figs.4.9, 4.10, and 4.11 except that the incident angle is 60° rather than 30°. Figs.4.15, 4.16, and 4.17 are also the same as Figs.4.9, 4.10, and 4.11, but show the vertical correlation, rather than the horizontal correlation. The label Z in the figures is the vertical separation distance between the two receivers in meters. In all these figures, the characteristic frequency dependence of the correlation is the same. This is a very important result in terms of inverting the ocean bottom parameters. If we sweep the acoustic frequency in an experiment to measure the spatial correlation of the scattered field,

and form the correlations on either horizontal arrays or vertical arrays for different frequency bins, we should find a dividing point at which the first null will stop changing with increasing frequency. That point will indicate the correlation length of the bottom random sound speed distribution. In a real experiment, there will be ambient noise compounded into the scattering field and make the identification of the nulls difficult. However, we can always pick the half-value point on the correlation curve to estimate the size of the scatterers.

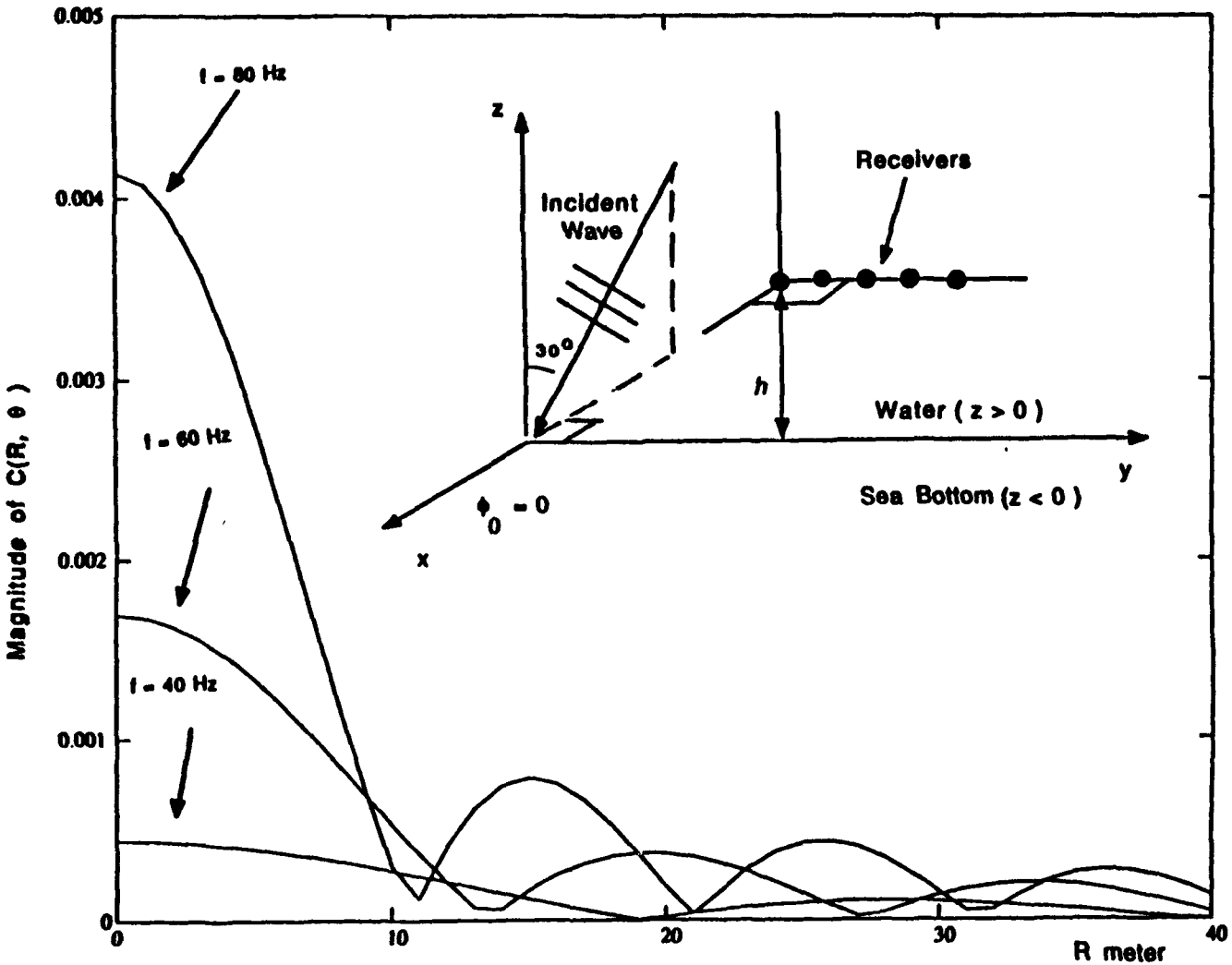

Figure 4.9: Frequency dependence, low frequency case, $\theta_0 = 30°$

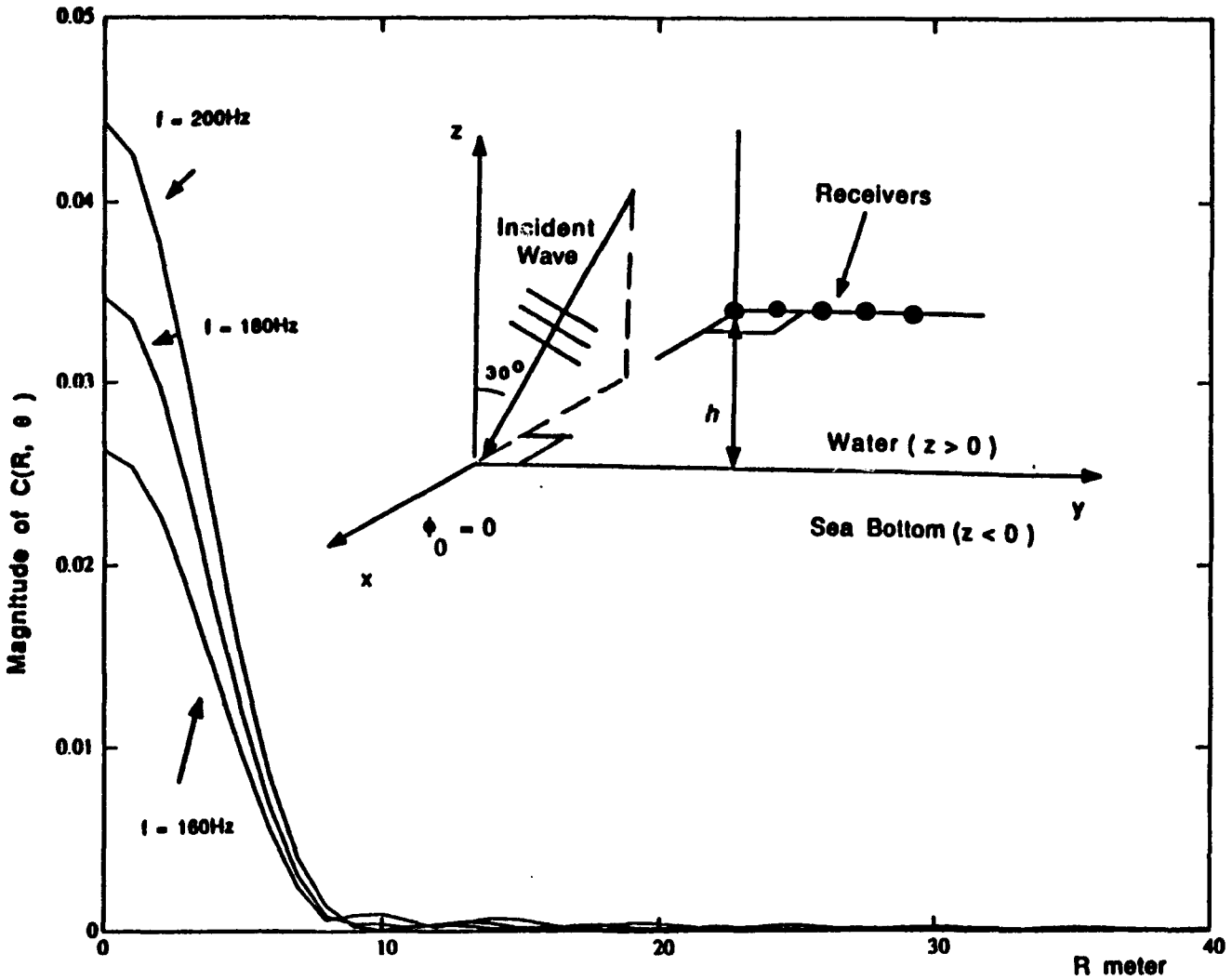

Figure 4.10: Frequency dependence, high frequency case, $\theta_0 = 30°$

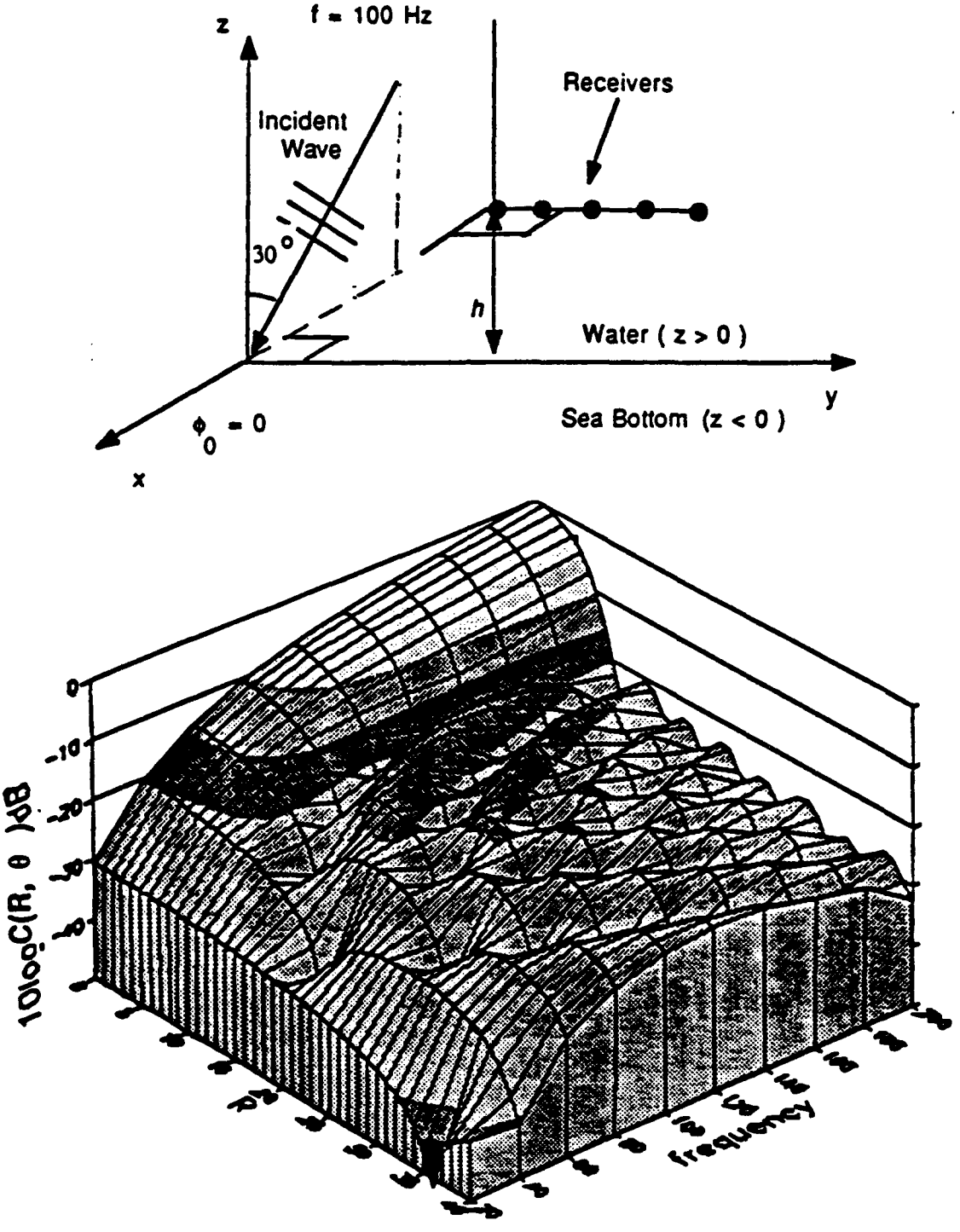

Figure 4.11: Frequency dependence, $\theta_0 = 30°$

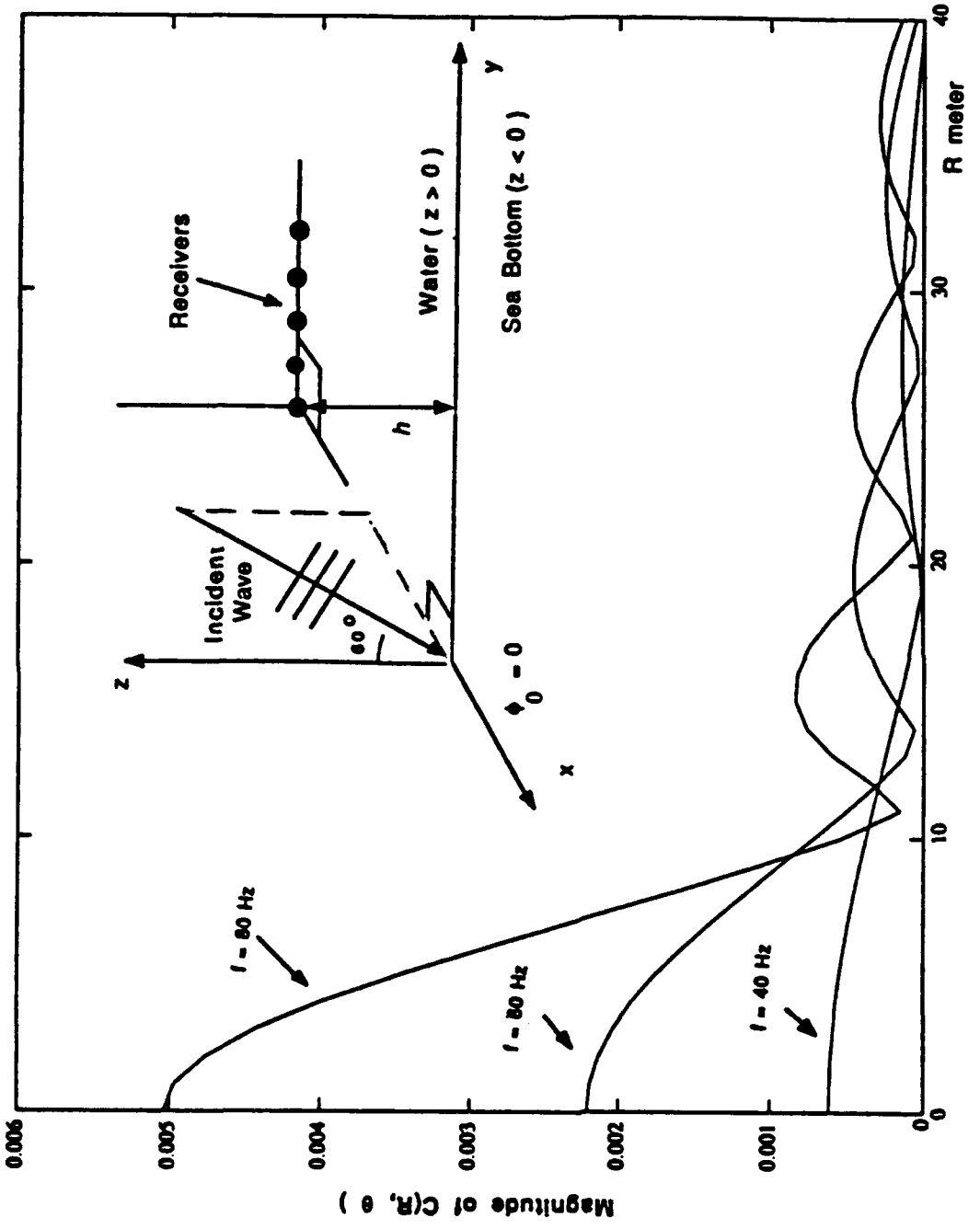

Figure 4.12: Frequency dependence, low frequency case, $\theta_0 = 60°$

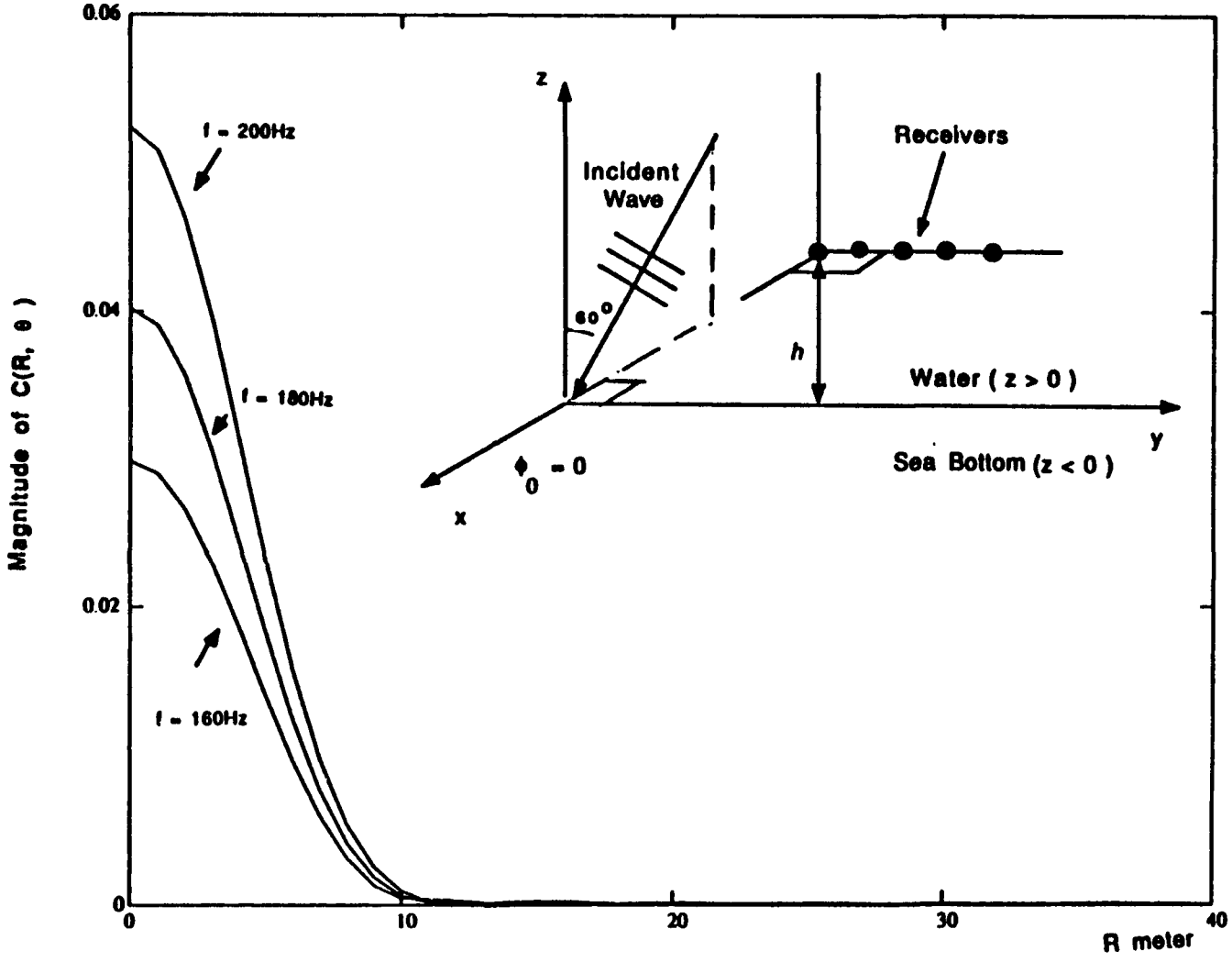

Figure 4.13: Frequency dependence, high frequency case, $\theta_0 = 60°$

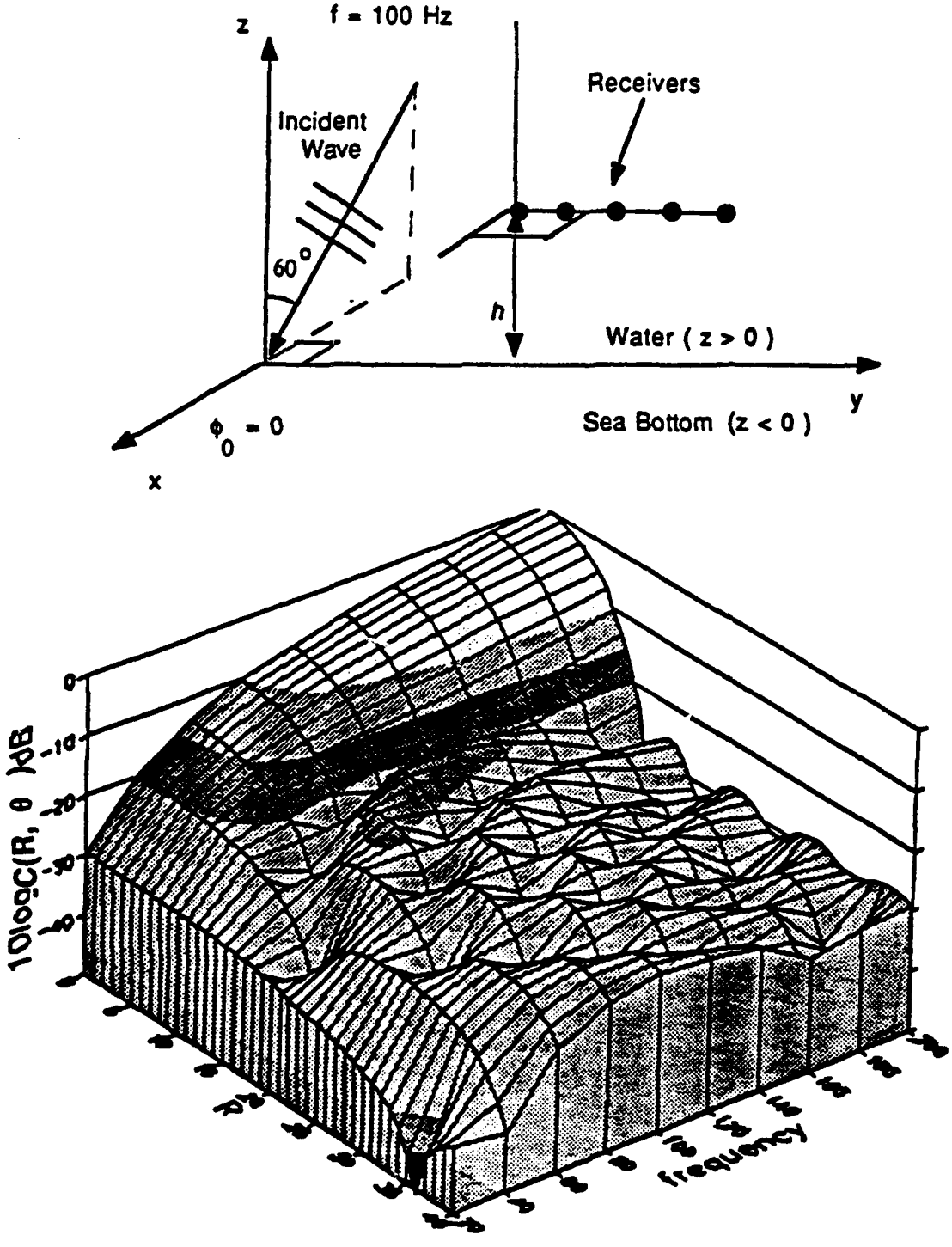

Figure 4.14: Frequency dependence, $\theta_0 = 60°$

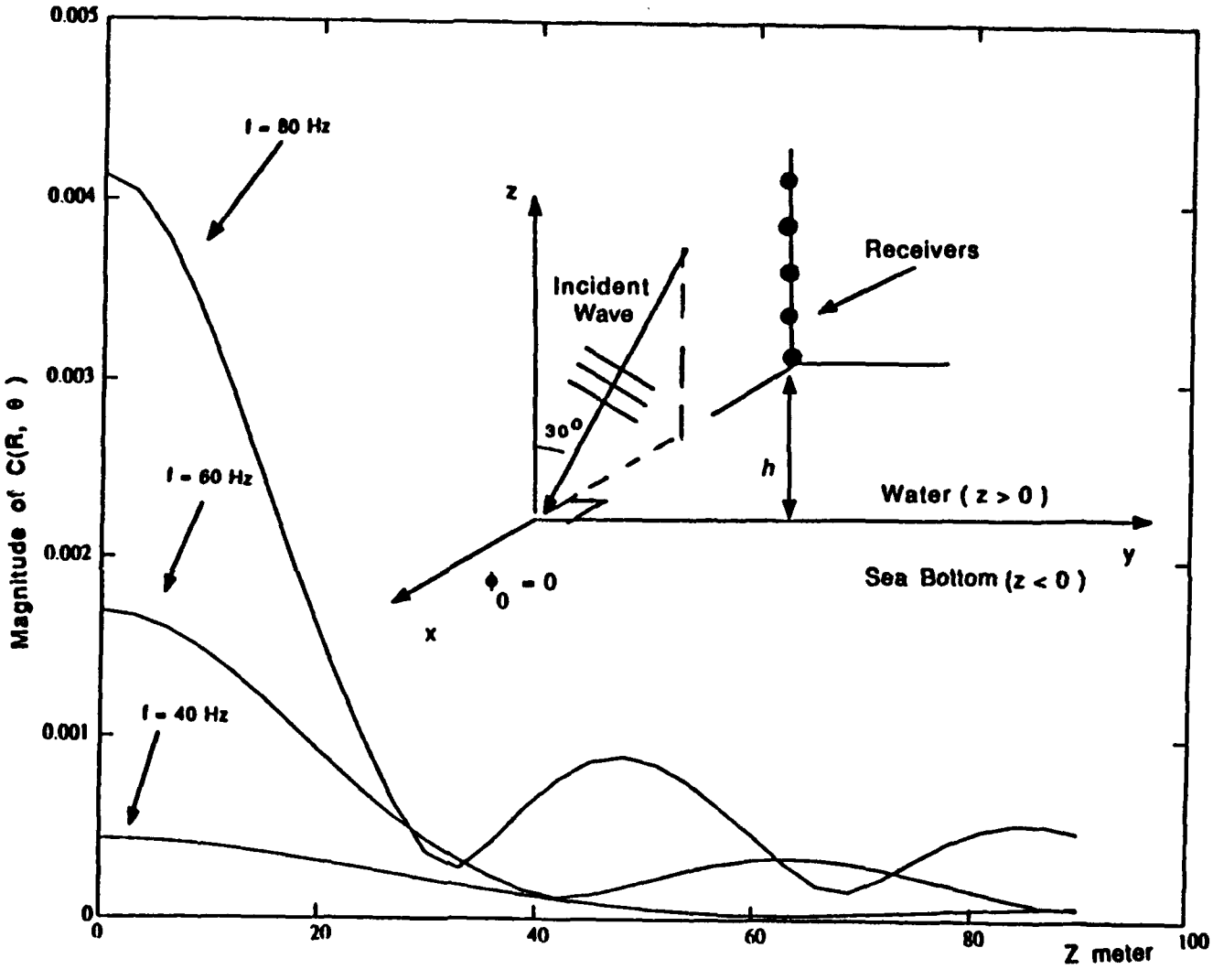

Figure 4.15: Frequency dependence, low frequency case, $\theta_0 = 30°$

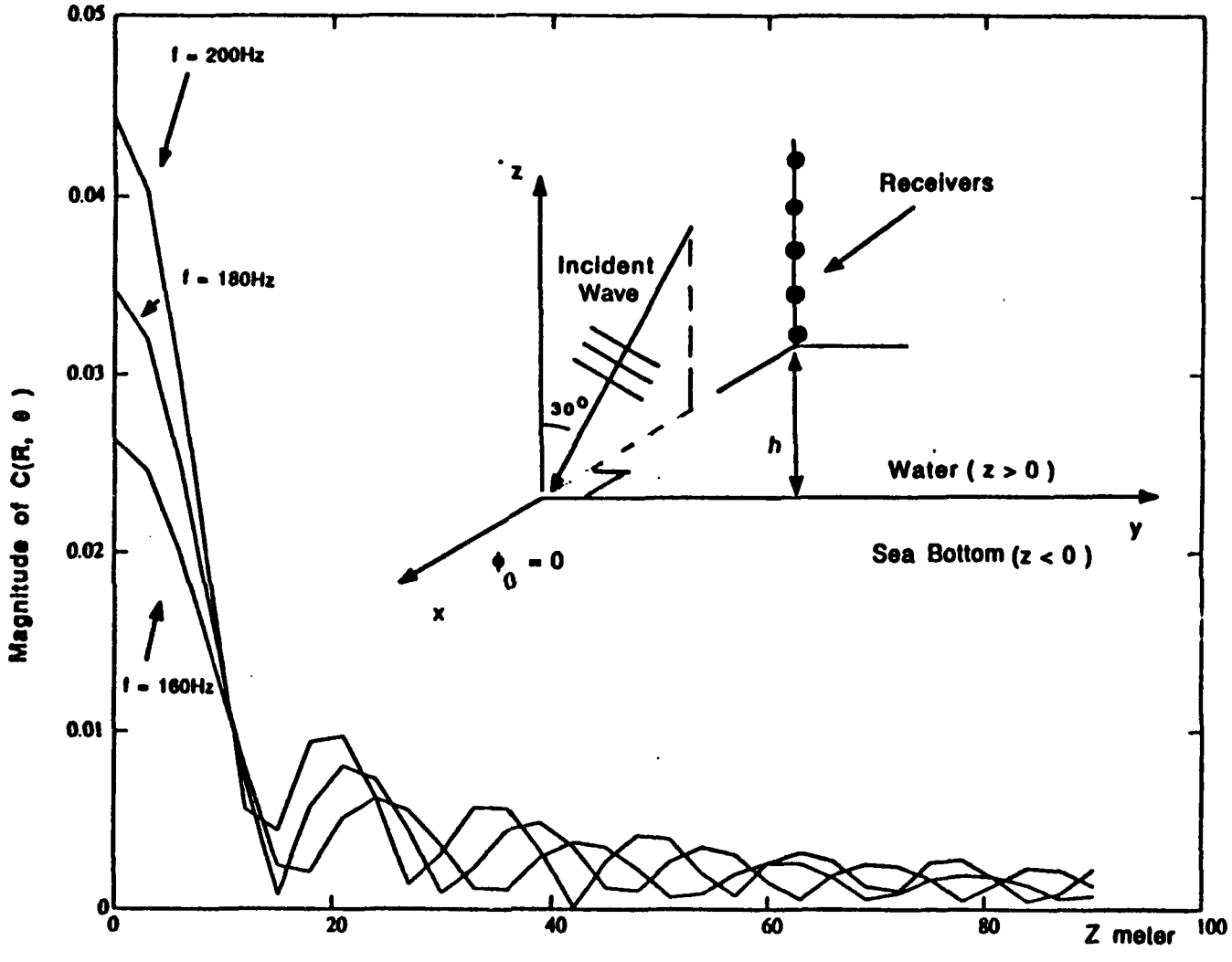

Figure 4.16: Frequency dependence, high frequency case, $\theta_0 = 30°$

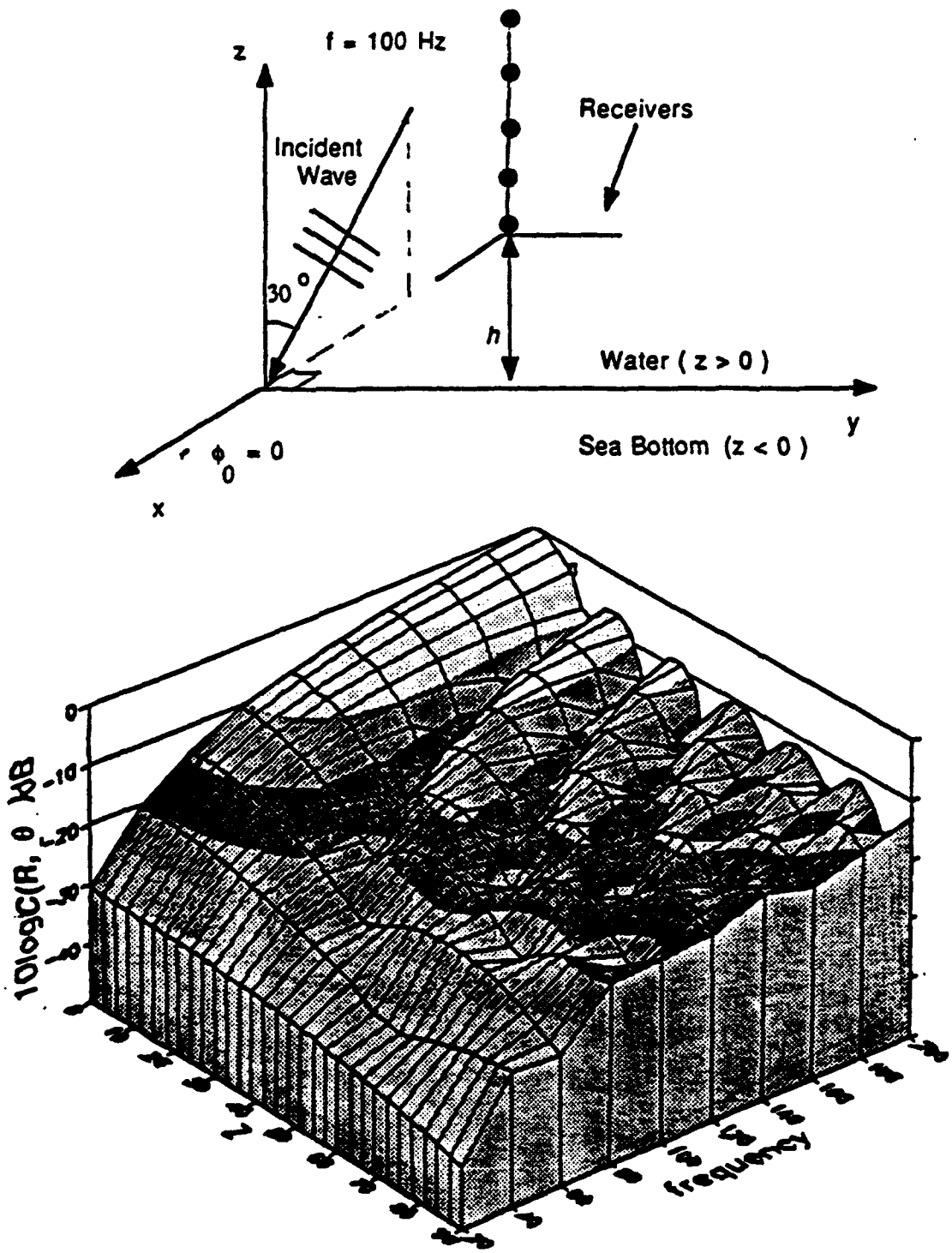

Figure 4.17: Frequency dependence, $\theta_0 = 30°$

4.3 Comparison with the Born approximation

The Born approximation has been used extensively in the calculation of weak scattering problems. However, when the size of the scatterer is large compared to the wavelength, the Born approximation fails since it does not include the energy loss in the incident wave due to scattering. The bi-local approximation used in this thesis takes into account the loss of energy in the coherent part of the field as discussed in Chapters 2 and 3. In this section we compare the two methods. In Eq.(4.13), if the bi-local approximation is used, the quantity $|P(z')|$ is given by Eq.(3.14) in Chapter 3; if the Extended Born approximation is used, $|P(z')|$ is given by Eq.(4.10) in this chapter. The difference between the two approximations is that the vertical wavenumber in the Born approximation is real, and therefore there is no energy loss while propagating deep into the random layer, whereas the vertical wavenumber is complex in the bi-local approximation, hence the wave is evanescent, and wave energy is taken away due to scattering while propagating deep into the random layer. Fig.4.18 shows the horizontal correlations of the scattered field when the thickness of the random layer equals six acoustic wavelengths. We see little difference between the two results. In Fig.4.19, all parameters are kept the same as in Fig.4.18 except that the layer thickness is sixty times the acoustic wavelength. There we find the horizontal correlation of the scattered field is apparently different. The Born approximation overestimates the scattering intensity (R=0). At the same time we notice that the correlation patterns obtained from the two methods are essentially the same. Figs.4.20 and 4.21 repeat the results in Figs.4.18 and 4.19, except they are vertical correlations, and likewise we find the results are similar. Therefore, we can conclude that the Born approximation can be used as a fast way to examine the correlation pattern, whereas when the scattering intensity is concerned, the Born approximation will result in more error. If the random layer

is a random half-space, the Born approximation will not converge, but the bi-local approximation will still be applicable.

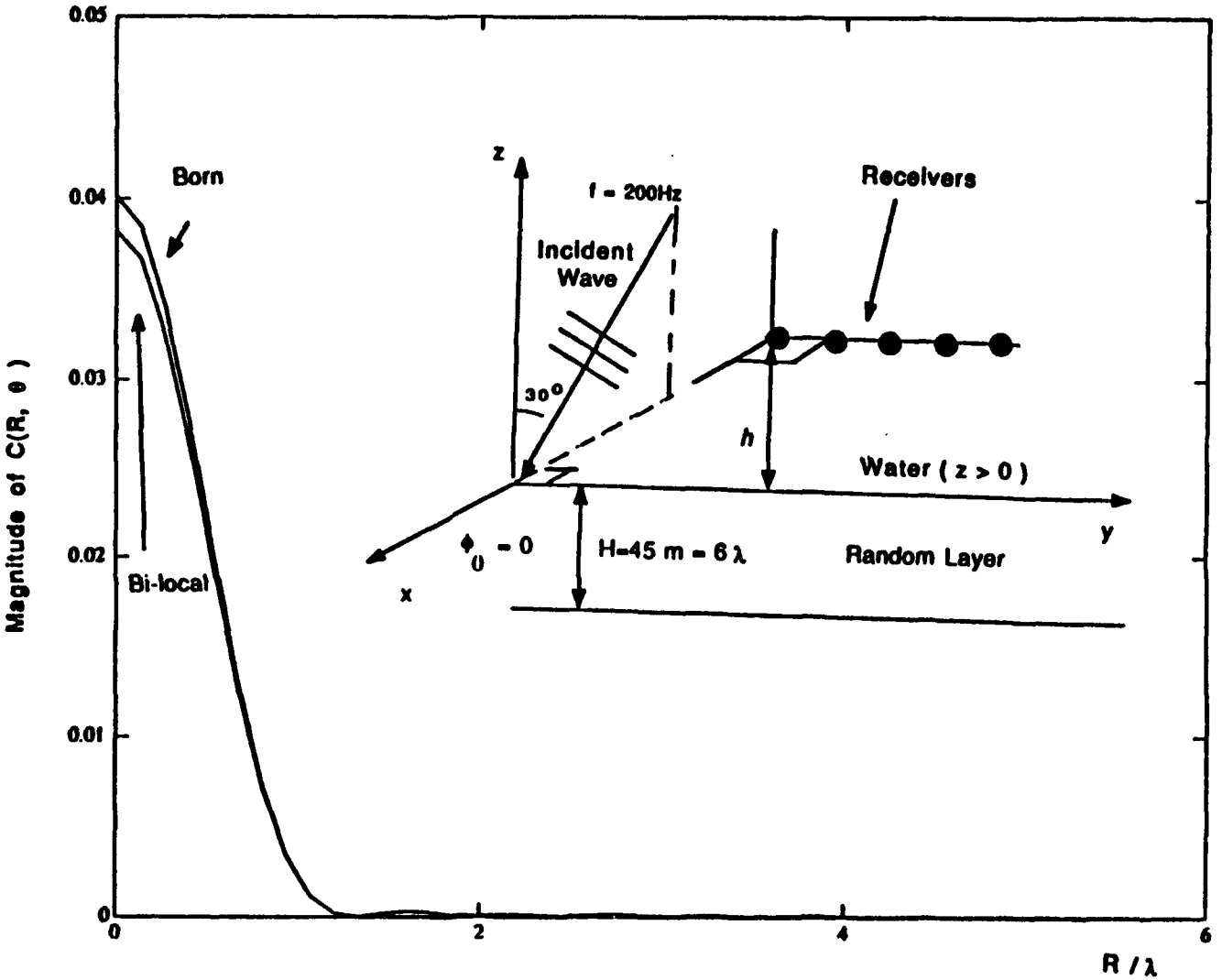

Figure 4.18: Comparison with the Born approximation, thin layer, horizontal correlation

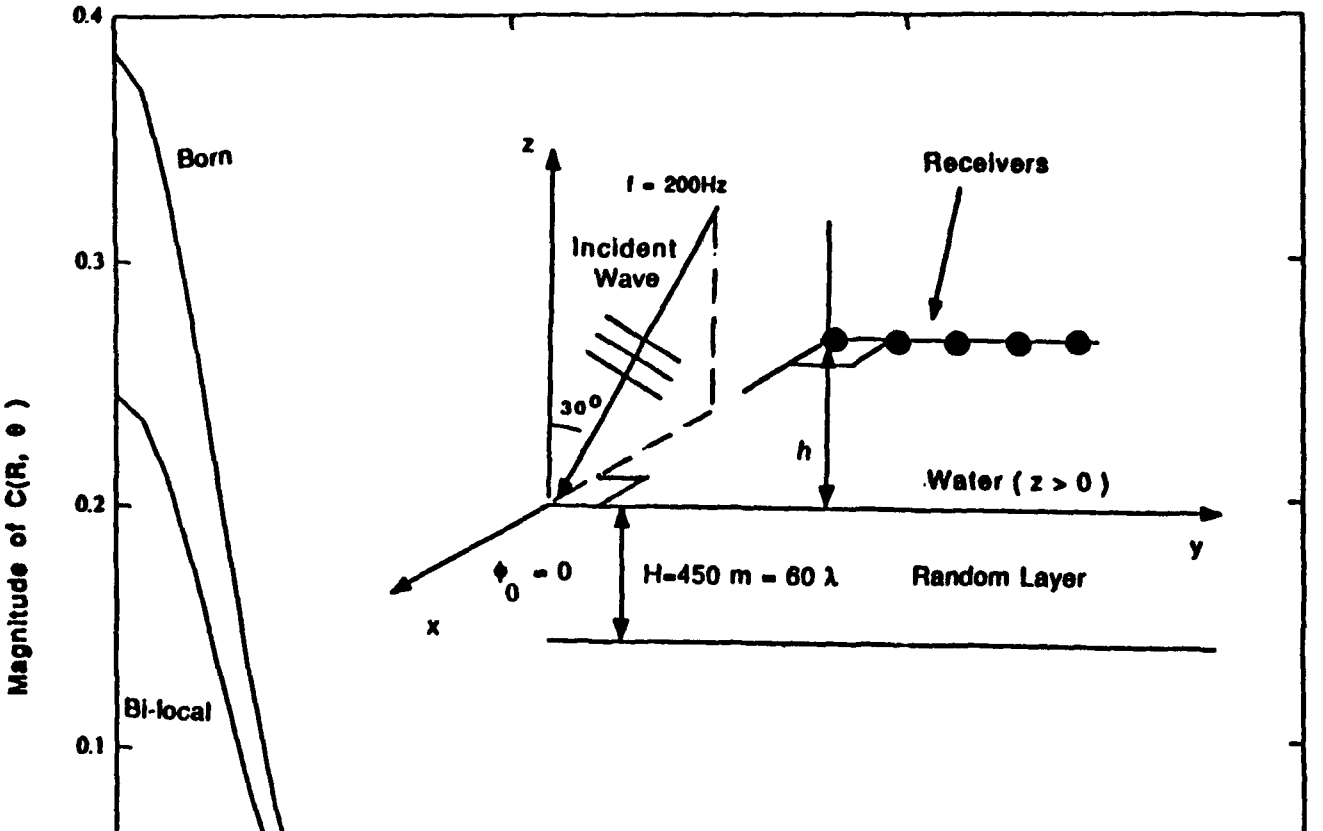

Figure 4.19: Comparison with the Born approximation, thick layer, horizontal correlation

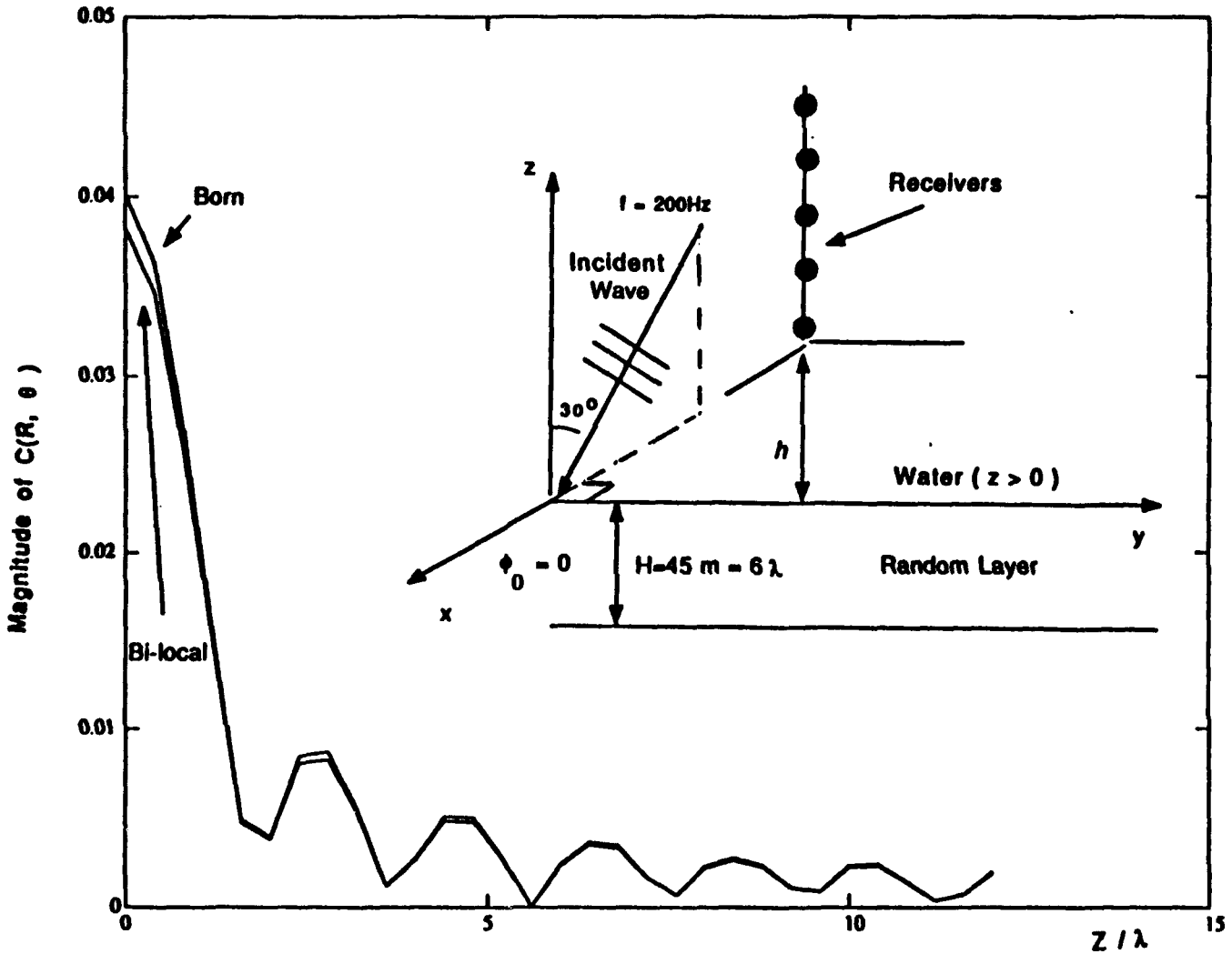

Figure 4.20: Comparison with the Born approximation, thin layer, vertical correlation

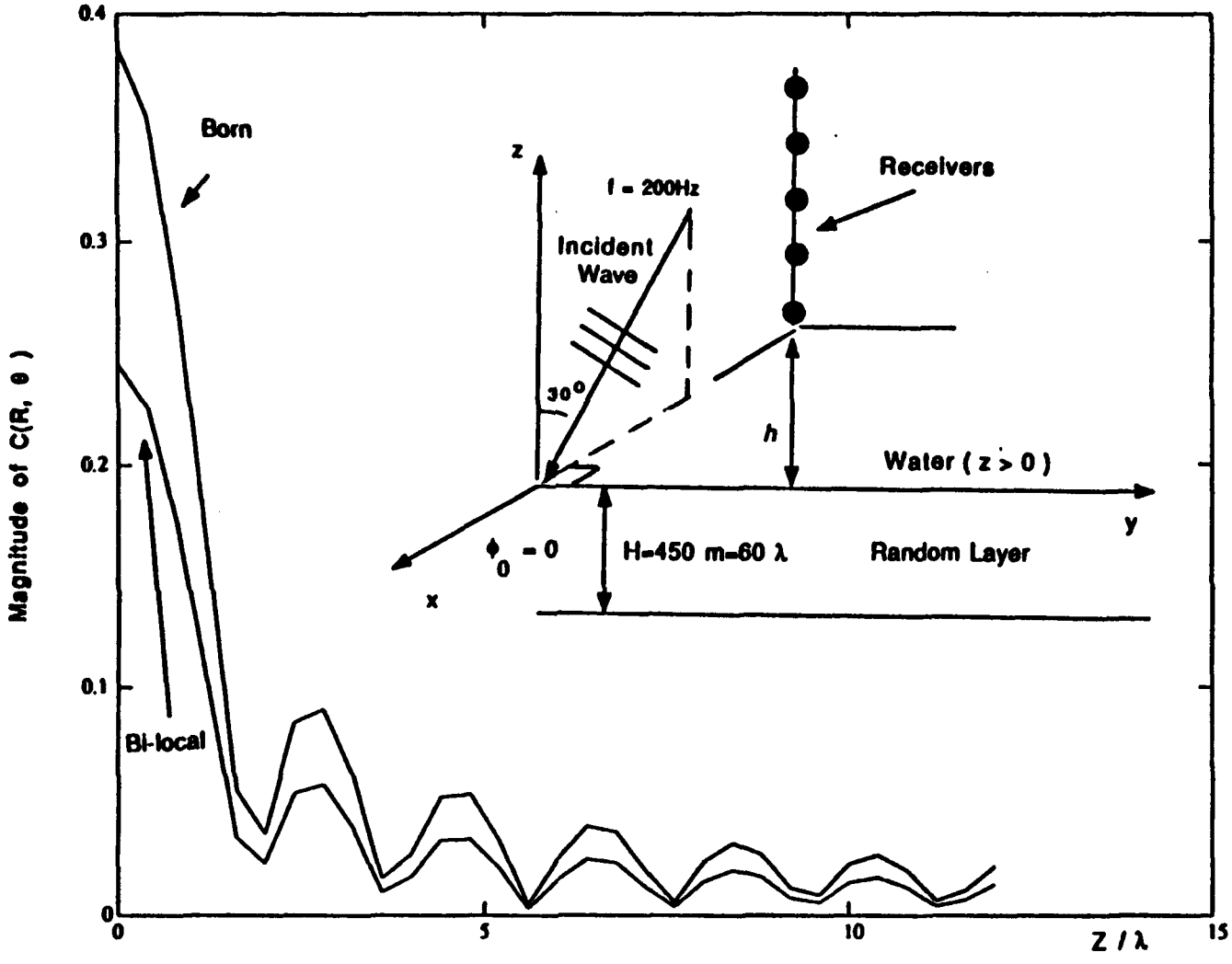

Figure 4.21: Comparison with the Born approximation, thick layer, vertical correlation

4.4 The Anisotropy

So far we have only studied the case where the bottom correlation functions is isotropic, i.e. $l_{x0} = l_{y0}$. It is also important to examine the influence of anisotropic correlation of ϵ on the spatial correlation of the scattered field. The formulation developed in this thesis allows such anisotropic correlations. In the following examples, the environmental parameters will be kept the same as in Fig.4.2 except:

1) $l_{x0} = 2.0m$, and $l_{y0} = 10.0m$, so the sound speed variation in the random layer is more correlated in the y-direction than in the x-direction.

2) In Figs.4.22-4.24, the correlation functions are still Gaussian, but in Figs.4.25-4.27, the correlation functions are 2-d exponential type.

All the examples are horizontal correlations of the scattered field measured across the propagation direction.

Figs.4.22, 4.23, and 4.24 show the examples for incident wave frequencies of 50, 100, and 200 Hz, respectively. The curves corresponding to $\phi_0 = 0$ are those when the incident wave is in the x-direction, therefore confronting the wide side of the volume scatterer; the other curves corresponding to $\phi_0 = 90^o$ are those when the incident wave is in the y-direction, confronting the narrow side of the volume scatterer. We see that the $\phi_0 = 0$ curves all indicate a 10 meter correlation length on their first nulls. It is clear that when the incident wave comes in the direction of the wide side of the scatterer, the longer correlation length will be reflected on $C_v(R, \theta)$. We notice that the nulls on the $\phi_0 = 90^o$ curves change with frequency. This is because when the incident wave is in the direction of the narrow side of the

scatterer, the null position will not stablize until the acoustic wavelength is shorter than the smaller correlation length, i.e. 2 meters in these examples. Figs.4.25, 4.26, and 4.27 are the same as Fig.4.22, 4.23, and 4.24, except that the Gaussian correlation function is changed to 2-d exponential correlation function. We find similar results in these examples.

We conclude that anisotropic correlation functions will influence the spatial correlation functions of the scattered field considerably. When the null position is used to invert for the correlation length, it is necessary to change the direction of the incident wave to see whether anisotropy exists.

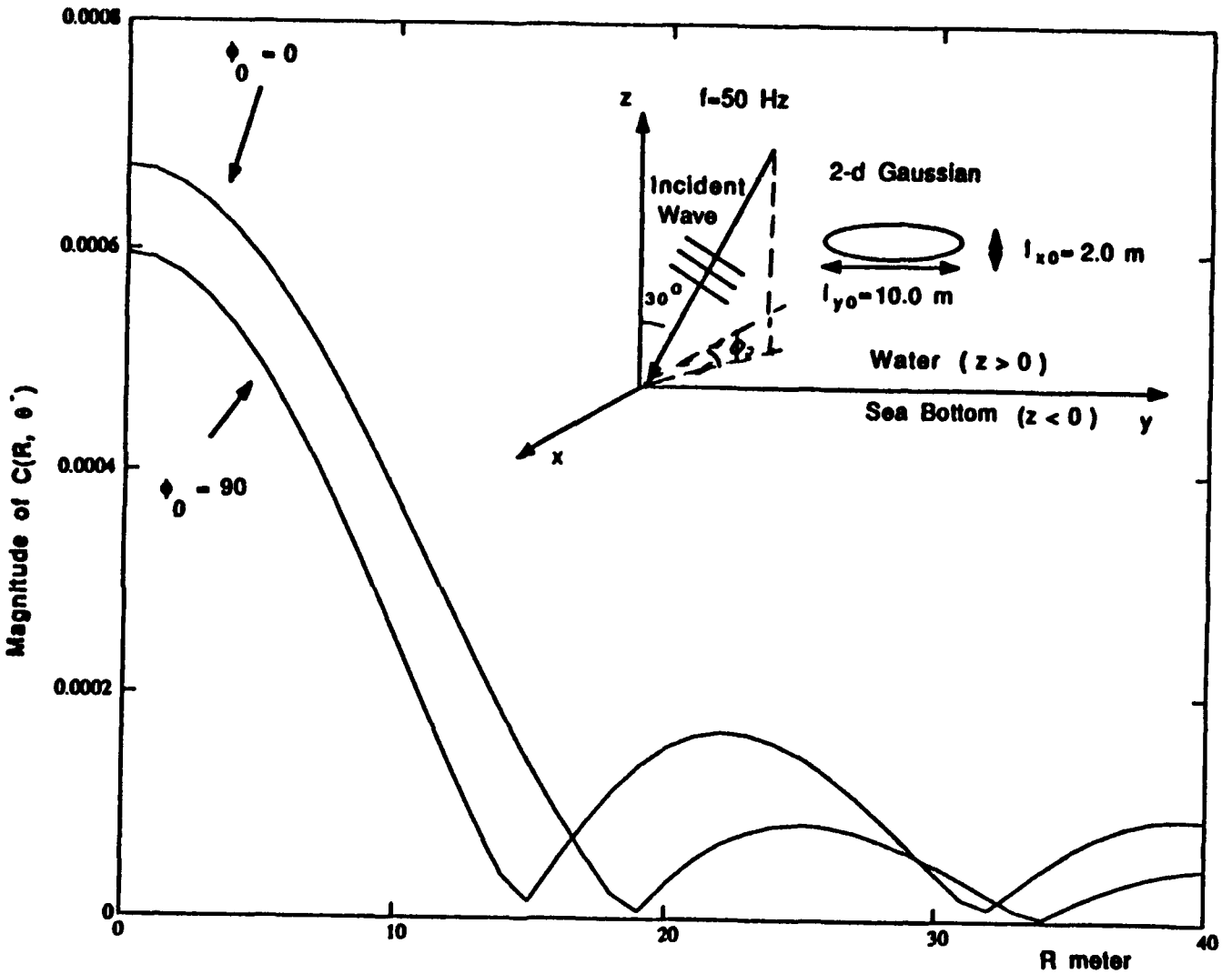

Figure 4.22: Anisotropy effect, f=50 Hz

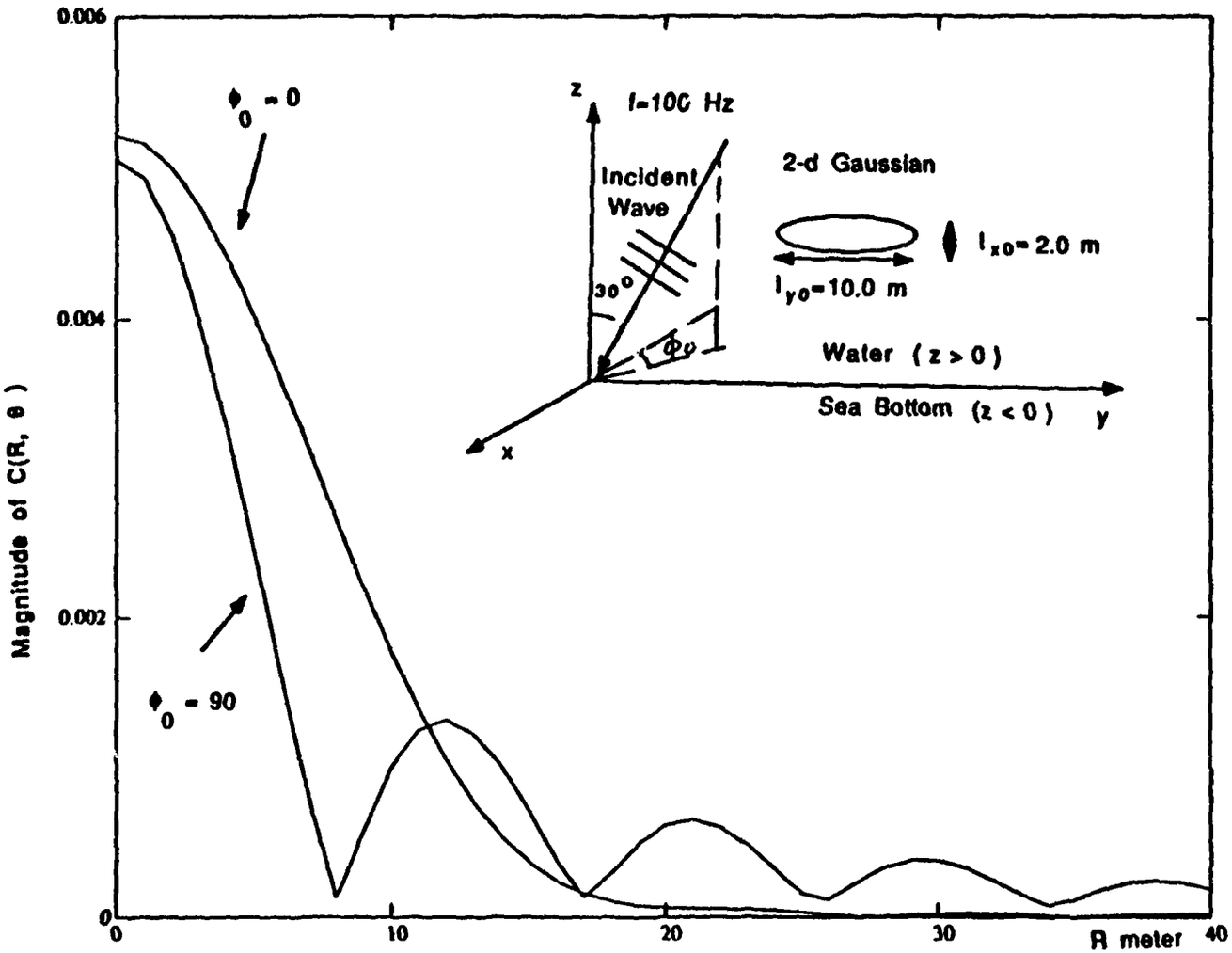

Figure 4.23: Anisotropy effect, f=100 Hz

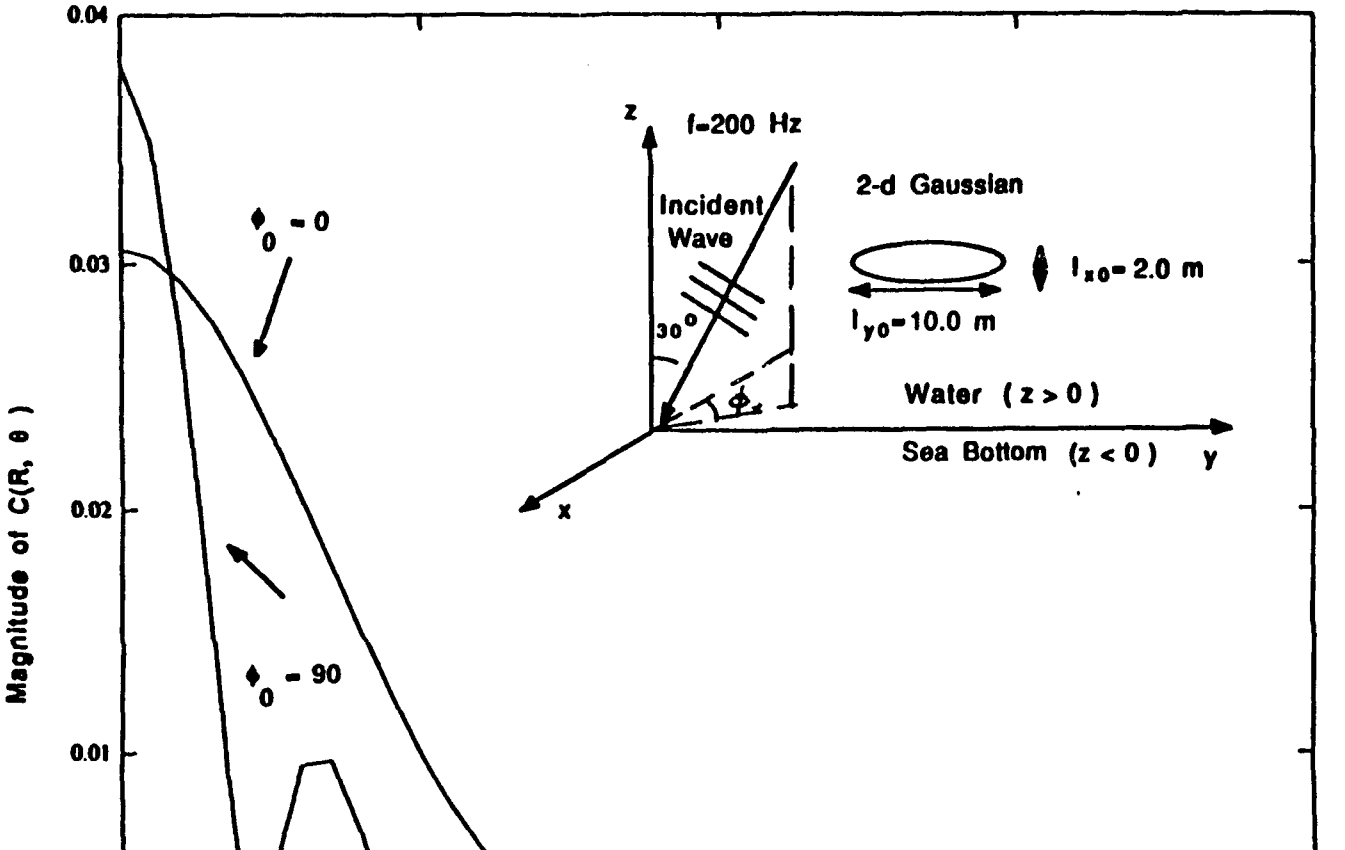

Figure 4.24: Anisotropy effect, f=200 Hz

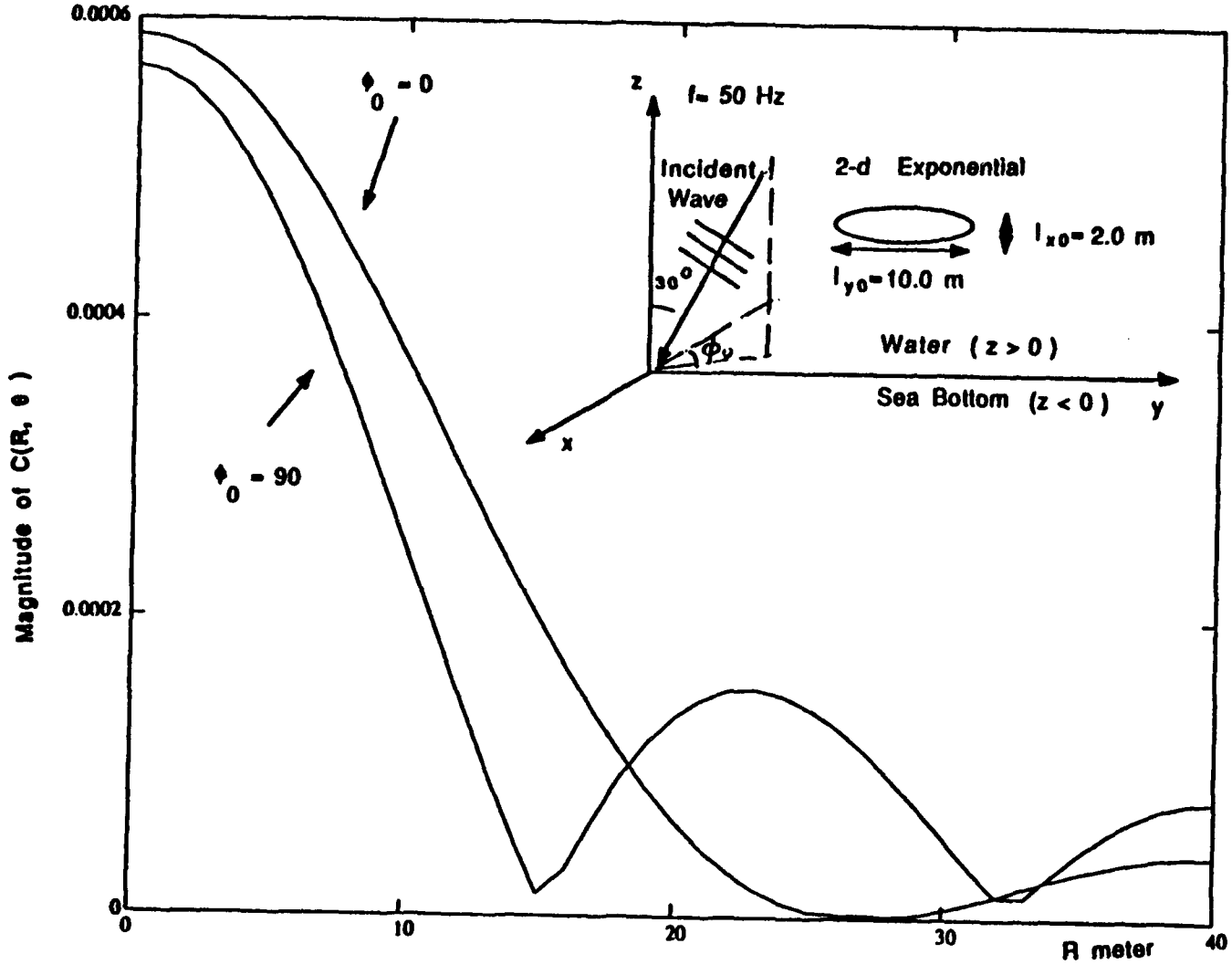

Figure 4.25: Anisotropy effect, f=50 Hz

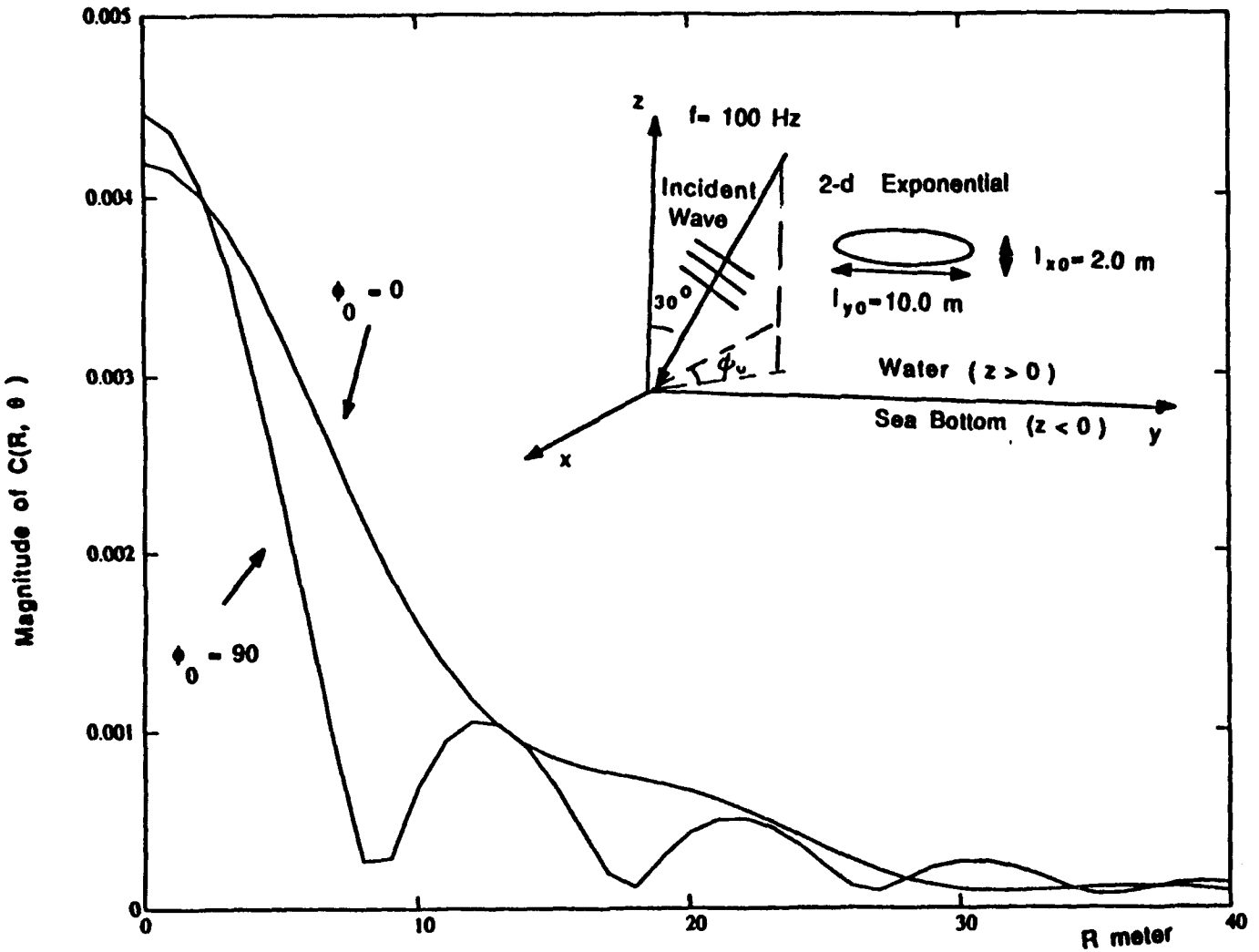

Figure 4.26: Anisotropy effect, f=100 Hz

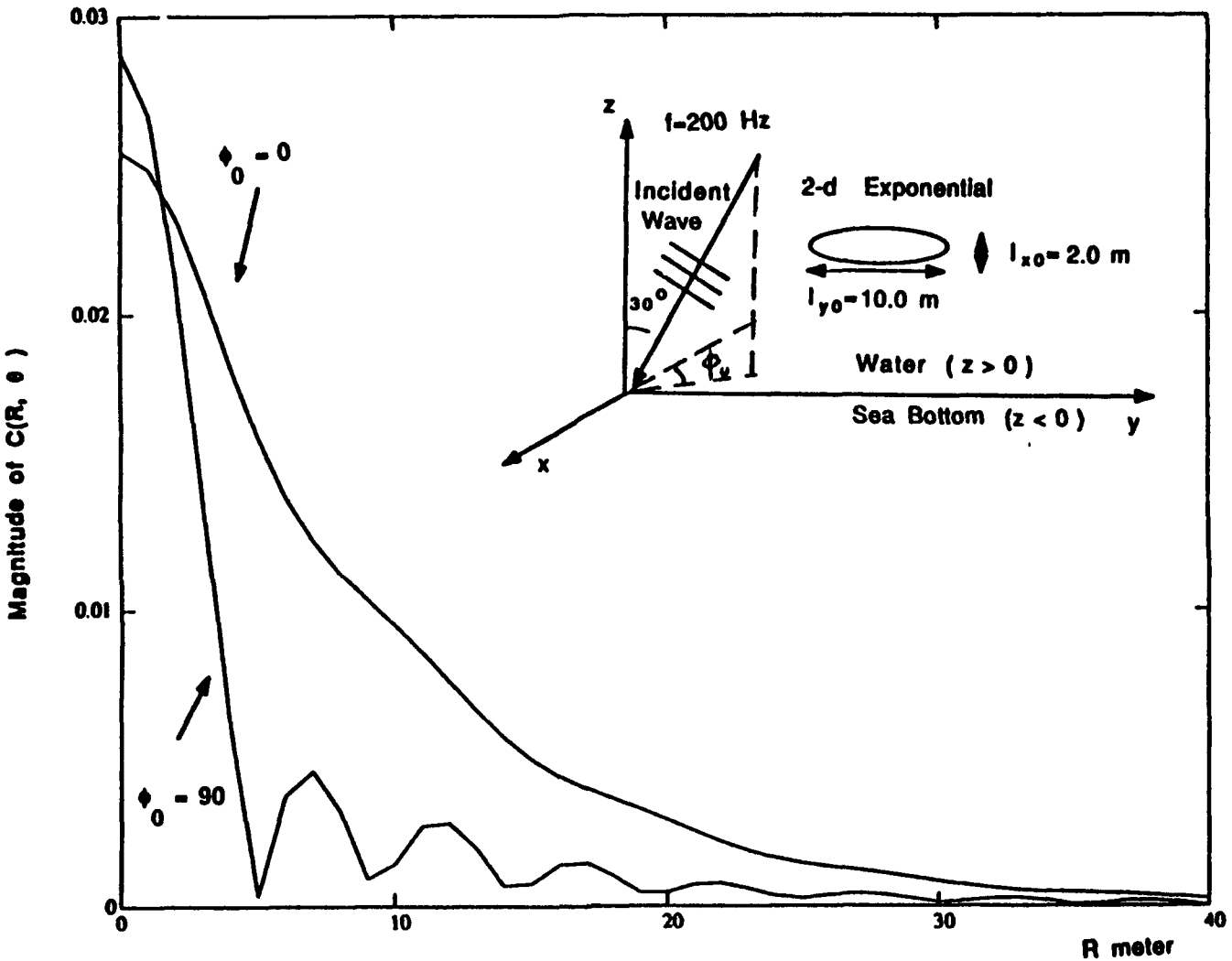

Figure 4.27: Anisotropy effect, f=200 Hz

In Chapters 2, 3, and 4, we studied the wave scattering from a random bottom. One major goal in this research is to invert for the bottom sound speed parameters. We concluded that the correlation length of the bottom random sound speed is related to the spatial correlation length of the scattered field. It is worthwhile to compare this research with work on scattering from a deterministic inhomogeneous ocean bottom. There is an enormous literature on inverse problems of this kind. Notably, Cohen and Bleinstein[59,60,61,62], along with other researchers, studied the velocity inversion problem when the velocity variation is non-random and small. They expressed the sound velocity variation through an integral equation related to received signal by using the Born approximation. The studies of random scattering problems can be linked to the studies of non-random scattering problems by introducing randomness to the formulated non-random problem and properly averaging the results to invert for the bottom parameters related to the non-random problem.

Chapter 5

VOLUME SCATTERING VS. ROUGH INTERFACE SCATTERING

As mentioned in the Introduction, both bottom inhomogeneities and interface roughness contribute to ocean bottom scattering. If the interface is very rough, and has length dimensions which are large relative to the acoustic wavelength, one can expect that rough interface scattering will dominate the scattered field; if the roughness is small relative to the acoustic wavelength and gentle in slope, the scattered field may be the combined result of volume and interface scattering mechanisms.

Since there is no existing theory that models both the roughness and the volume inhomogeneity in one unified approach, there is little quantitative understanding of the relative importance of the two scattering mechanisms. This chapter is intended to investigate the relative strengths of the scattered fields resulting from interface roughness and from volume inhomogeneities, and if both scattering mechanisms

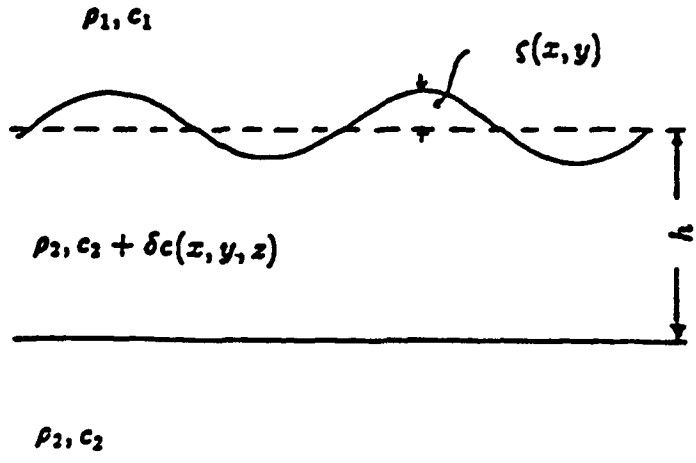

Figure 5.1: Geometry of roughness on top of volume inhomogeneity

are important in one location, whether it is possible to distinguish between the two scattering mechanisms.

The geometry is shown in Fig.5.1. We assume that the water/bottom interface roughness is random and small in amplitude and slope, and the bottom sound speed variation δc is random and small and superimposed upon a constant c_2 as in the previous chapters. Further we assume that there are no statistical correlations between the interface roughness and the volume inhomogeneities. The total randomly scattered field p^s_{total} can be written as the summation of the interface scattered field p^s_s and volume scattered field p^s_v:

$$p^s_{total} = p^s_s + p^s_v. \tag{5.1}$$

Therefore, the second moment of the total scattered field is:

$$\begin{aligned} \langle p^s_{total} p^{s*}_{total} \rangle &= \langle (p^s_s + p^s_v)(p^{s*}_s + p^{s*}_v) \rangle \\ &= \langle p^s_s p^{s*}_s + p^s_v p^{s*}_v + p^s_s p^{s*}_v + p^{s*}_s p^s_v \rangle \end{aligned}$$

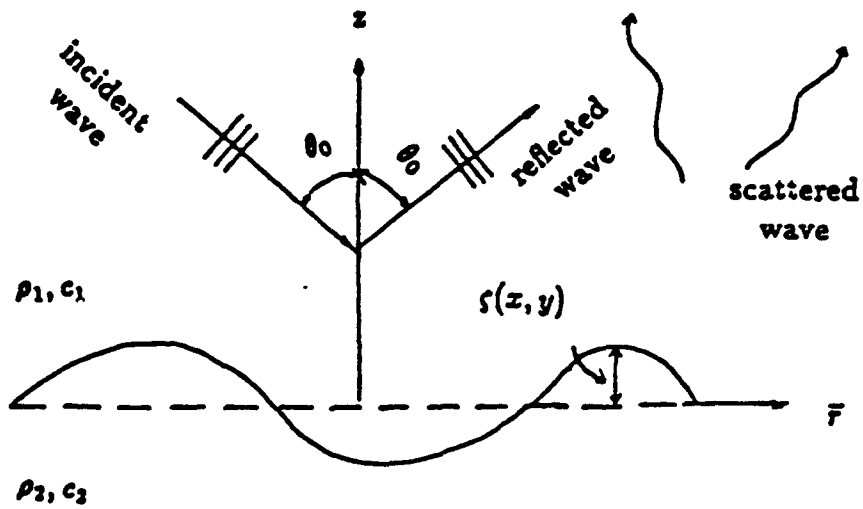

Figure 5.2: Schematic diagram of wave scattering from interface

$$= \langle p_s' p_s^{**} \rangle + \langle p_v' p_v^{**} \rangle, \tag{5.2}$$

where the cross correlation terms between the interface scattered field and the volume scattered field have been omitted because the two random processes are assumed statistically independent. So, the correlation of the total scattered field is simply the summation of the correlations of the interface scattered field and the volume scattered field. This means that the two scattering mechanisms can be examined separately under the above mentioned assumptions.

The Bass and Fuks'[19] perturbation theory will be used to find the scattered field correlation caused by the rough interface alone, and the spatial correlation of the volume scattered field obtained in the previous chapters will be combined, to investigate the combined effects.

According to Bass and Fuks[19], let two media be separated by the rough interface $z = \varsigma(x, y)$ and the sound speed and density in each medium are given in

Fig.5.2. If we designate P_s as the acoustic pressure, the vertical particle velocity and the pressure are continuous across the interface, *i.e.*

$$P_{s1} = P_{s2}; \quad \frac{1}{\rho_1}\frac{\partial P_{s1}}{\partial n} = \frac{1}{\rho_2}\frac{\partial P_{s2}}{\partial n}, \tag{5.3}$$

where n is the normal of the interface. We decompose P_{s1} and P_{s2} into the following forms:

$$P_{s1} = P_{s1}^0 + p_{s1}; \quad P_{s2} = P_{s2}^0 + p_{s2}, \tag{5.4}$$

where P_{s1}^0 and P_{s2}^0 are the pressure in the upper and lower media in the absence of the roughness, while p_{s1} and p_{s2} are the components related to the presence of small roughness.

Taking into account that

$$\frac{\partial}{\partial n} = (1+\gamma_x^2+\gamma_y^2)^{-1/2}\left(-\gamma_x\frac{\partial}{\partial x} - \gamma_y\frac{\partial}{\partial y} + \frac{\partial}{\partial z}\right), \quad \vec{\gamma} = \nabla\zeta, \tag{5.5}$$

and noticing that along $z = 0$,

$$P_{s1}^0 = P_{s2}^0, \quad \frac{1}{\rho_1}\frac{\partial P_{s1}^0}{\partial z} = \frac{1}{\rho_2}\frac{\partial P_{s2}^0}{\partial z}, \tag{5.6}$$

we expand the boundary conditions of Eq.(5.3) as a power series in ζ and γ, and retain the terms up to first order. Then the boundary conditions found for the scattered fields p_{s1} and p_{s2} at $z = 0$ are

$$\begin{aligned} &p_{s1} - p_{s2} = p(\vec{r}) \\ &\frac{1}{\rho_1}\frac{\partial p_{s1}}{\partial z} - \frac{1}{\rho_2}\frac{\partial p_{s2}}{\partial z} = v(\vec{r}), \end{aligned} \tag{5.7}$$

where $p(\vec{r})$ and $v(\vec{r})$, the pressure and vertical particle velocity discontinuities, respectively, along $z = 0$, are

$$\begin{aligned} p(\vec{r}) &= \frac{(\rho_2 - \rho_1)}{\rho_1}\frac{\partial P_{s1}^0}{\partial z}\zeta(\vec{r}) \\ v(\vec{r}) &= \frac{(\rho_2 - \rho_1)}{\rho_1\rho_2}\left[\nabla_\perp(\zeta\nabla_\perp P_{s1}^0) + \zeta\frac{k_1\rho_2^2 - k_2\rho_1^2}{\rho_2 - \rho_1}P_{s1}^0\right], \end{aligned} \tag{5.8}$$

and k_1 and k_2 are the wavenumbers in the upper and lower media, respectively, and $\nabla_\perp = (\frac{\partial}{\partial x}, \frac{\partial}{\partial y})$.

If the scattered field is written in the form of plane waves leaving the averaged interface, $z = 0$:

$$p_{s1}(\vec{R}) = \int_{-\infty}^{\infty} \tilde{p_{s1}}(\vec{\kappa}) e^{i(\vec{\kappa}\cdot\vec{r}+\kappa_{1z}z)} d^2\vec{\kappa}; \quad \kappa_{1z} = \sqrt{k_1^2 - \kappa^2}$$
$$p_{s2}(\vec{R}) = \int_{-\infty}^{\infty} \tilde{p_{s2}}(\vec{\kappa}) e^{i(\vec{\kappa}\cdot\vec{r}+\kappa_{2z}z)} d^2\vec{\kappa}; \quad \kappa_{2z} = \sqrt{k_2^2 - \kappa^2} \tag{5.9}$$

we then apply the Fourier transform to both sides of Eq.(5.7):

$$\tilde{p_{s1}}(\vec{\kappa}) - \tilde{p_{s2}}(\vec{\kappa}) = \tilde{p}(\vec{\kappa}),$$
$$\frac{i\kappa_{1z}}{\rho_1}\tilde{p_{s1}}(\vec{\kappa}) + \frac{i\kappa_{2z}}{\rho_2}\tilde{p_{s2}}(\vec{\kappa}) = \tilde{v}(\vec{\kappa}), \tag{5.10}$$

and note that $\tilde{p_{s1}}(\vec{\kappa})$ can be expressed as

$$\tilde{p_{s1}}(\vec{\kappa}) = \frac{\rho_1\kappa_{2z}\tilde{p}(\vec{\kappa}) - i\rho_1\rho_2\tilde{v}(\vec{\kappa})}{\rho_2\kappa_{1z} + \rho_1\kappa_{2z}}, \tag{5.11}$$

where $\tilde{p}$ and $\tilde{v}$ are Fourier transforms for $p(\vec{r})$ and $v(\vec{r})$, respectively.

Let a plane wave in the $(k_{x0}, k_{y0}, -k_{z0})$ direction be the incident wave, then

$$P_{s1}^0 = e^{i(k_{x0}x+k_{y0}y-k_{z0}z)} + V_0 e^{i(k_{x0}x+k_{y0}y+k_{z0}z)}, \tag{5.12}$$

and V_0 is the plane wave reflection coefficient:

$$V_0 = \frac{\rho_2 k_{z0} - \rho_1\sqrt{k_2^2 - k_1^2 + k_{z0}^2}}{\rho_2 k_{z0} + \rho_1\sqrt{k_2^2 - k_1^2 + k_{z0}^2}}. \tag{5.13}$$

Substituting Eq.(5.12) into Eq.(5.8), and applying the Fourier transform to both sides, we find that $\tilde{p}$ and $\tilde{v}$ take on the following forms:

$$\begin{aligned}
\tilde{p}(\vec{\kappa}) &= -ik_{z0}(1 - V_0)\frac{(\rho_2 - \rho_1)}{\rho_1}\tilde{\zeta}(\kappa_x - k_{x0}, \kappa_y - k_{y0}) \\
\tilde{v}(\vec{\kappa}) &= (1 + V_0)\frac{(\rho_2 - \rho_1)}{\rho_1\rho_2}\tilde{\zeta}(\kappa_x - k_{x0}, \kappa_y - k_{y0}) \\
&\quad \left[-k_{x0}\kappa_x - k_{y0}\kappa_y + \frac{k_1^2\rho_2 - k_2^2\rho_1}{\rho_2 - \rho_1}\right].
\end{aligned} \tag{5.14}$$

In these expressions, $\tilde{\zeta}$ is the Fourier transform of ζ:

$$\tilde{\zeta}(\kappa_x,\kappa_y)=\frac{1}{(2\pi)^2}\int\int\zeta(\vec{r})e^{-i(\kappa_x x+\kappa_y y)}dxdy. \tag{5.15}$$

Now, $\tilde{p_{s1}}$ in Eq.(5.11) can be solved by using Eq.(5.14)

$$\begin{aligned}\tilde{p_{s1}} &= -i\frac{\rho_2-\rho_1}{\rho_2\kappa_{1z}+\rho_1\kappa_{2z}}\tilde{\zeta}(\kappa_x-k_{x0},\kappa_y-k_{y0})\\ &\cdot\left[k_{x0}\kappa_{2z}(1-V_0)+(1+V_0)(-k_{x0}\kappa_x-k_{y0}\kappa_y+\frac{k_1^2\rho_2-k_2^2\rho_1}{\rho_2-\rho_1}\right].\end{aligned} \tag{5.16}$$

The scattered field in the upper medium is the inverse Fourier transform of $\tilde{p_{s1}}$:

$$p_{s1}(\vec{R})=\int_{-\infty}^{\infty}\int d^2\vec{\kappa}\tilde{p_{s1}}(\vec{\kappa})e^{i(\vec{\kappa}\cdot\vec{r}+\kappa_{1z}z)}. \tag{5.17}$$

Therefore, the spatial correlation of $p_{s1}(\vec{R})$, C_s, is

$$\begin{aligned}C_s(\vec{R_1},\vec{R_2}) &= \langle p_{s1}(\vec{R_1})p_{s1}^*(\vec{R_2})\rangle\\ &= \int\int d^2\vec{\kappa}\int\int d^2\vec{\kappa'}\langle\tilde{p_{s1}}(\vec{\kappa})\tilde{p_{s1}}^*(\vec{\kappa'})\rangle e^{i(\vec{\kappa}\cdot\vec{r_1}-\vec{\kappa'}\cdot\vec{r_2}+\kappa_{1z}z_1-\kappa'_{1z}z_2)};\end{aligned} \tag{5.18}$$

where

$$\langle\tilde{p_{s1}}(\vec{\kappa})\tilde{p_{s1}}^*(\vec{\kappa'})\rangle=f(\vec{\kappa})f^*(\vec{\kappa'})\langle\tilde{\zeta}(\kappa_x-k_{x0},\kappa_y-k_{y0})\tilde{\zeta}^*(\kappa'_x-k_{x0},\kappa'_y-k_{y0})\rangle, \tag{5.19}$$

and $f(\vec{\kappa})$ is defined:

$$\begin{aligned}f(\vec{\kappa}) &= \frac{(\rho_2-\rho_1)}{\rho_2\kappa_{1z}+\rho_1\kappa_{2z}}\\ &\left[k_{x0}\kappa_{2z}(1-V_0)+(1+V_0)(-k_{x0}\kappa_x-k_{y0}\kappa_y+\frac{k_1^2\rho_2-k_2^2\rho_1}{\rho_2-\rho_1})\right].\end{aligned} \tag{5.20}$$

Since $\tilde{\zeta}$ is the Fourier transform of ζ, therefore,

$$\begin{aligned}&\langle\tilde{\zeta}(\kappa_x-k_{x0},\kappa_y-k_{y0})\tilde{\zeta}^*(\kappa'_x-k_{x0},\kappa'_y-k_{y0})\rangle\\ &= \frac{1}{(2\pi)^4}\int\int dxdy\int\int dx'dy'\langle\zeta(\vec{r})\zeta(\vec{r'})\rangle\\ &\quad e^{-i[(\kappa_x-k_{x0})x-(\kappa'_x-k_{x0})x'+(\kappa_y-k_{y0})y-(\kappa'_y-k_{y0})y']}\\ &= \frac{\sigma_s^2}{(2\pi)^4}\int\int dl_x dl_y N_s(\vec{l})e^{-i[(\kappa_x-k_{x0})l_x+(\kappa_y-k_{y0})l_y]}\\ &\quad\int\int dx'dy'e^{-i[(\kappa_x-\kappa'_x)x'+(\kappa_y-\kappa'_y)y']}\\ &= \frac{\sigma_s^2}{(2\pi)^2}S_s(\kappa_x-k_{x0},\kappa_y-k_{y0})\delta(\vec{\kappa}-\vec{\kappa'}),\end{aligned} \tag{5.21}$$

where $N_s(\vec{l})$ is the auto-correlation function of ς, and σ_s^2 is the standard deviation of ς, and $S_s(\vec{\kappa})$ is the spectrum of $N_s(\vec{r})$. In the above derivation, variable $\vec{r}$ is replaced by $\vec{l} = \vec{r} - \vec{r'}$. Finally, substituting the above results into Eq.(5.18), we have

$$C_s(\vec{R}_1, \vec{R}_2) = \frac{\sigma_s^2}{(2\pi)^2} \int\int d^2\vec{\kappa} |f(\vec{\kappa})|^2 S_s(\kappa_x - k_{x0}, \kappa_y - k_{y0}) e^{i(\vec{\kappa}\cdot\vec{R} + \kappa_{1z}Z)}, \qquad (5.22)$$

where $\vec{R} = \vec{r_1} - \vec{r_2}$ is the horizontal distance between the two receivers; and $Z = z_1 - z_2$ is the vertical distance.

Assume $N_s(\vec{l})$ and its associated spectrum have one of the following forms:

$$\begin{aligned} N_s(\vec{l}) &= e^{-(l/l_0)}, \qquad (1-D \ \textit{exponential}) \\ S_s(\vec{\kappa}) &= \frac{2\pi l_0^2}{[1 + (\kappa l_0)^2]^{3/2}}; \end{aligned} \qquad (5.23)$$

$$\begin{aligned} N_s(\vec{l}) &= e^{-\frac{|l_x|}{l_{x0}} - \frac{|l_y|}{l_{y0}}}, \qquad (2-D \ \textit{exponential}) \\ S_s(\vec{\kappa}) &= \frac{4 l_{x0} l_{y0}}{(1 + (\kappa_x l_{x0})^2)(1 + (\kappa_y l_{y0})^2)}; \end{aligned} \qquad (5.24)$$

$$\begin{aligned} N_s(\vec{l}) &= e^{-(l_x/l_{x0})^2 - (l_y/l_{y0})^2}, \qquad (\textit{Gaussian}) \\ S_s(\vec{\kappa}) &= \pi l_{x0} l_{y0} e^{-\frac{1}{4}(\kappa_x^2 l_{x0}^2 + \kappa_y^2 l_{y0}^2)}, \end{aligned} \qquad (5.25)$$

we can evaluate Eq.(5.22)by numerical integration.

When the two receivers in Eq.(5.22) or in Eq.(4.9) of Chapter 4 are merged, $\vec{R}_1 = \vec{R}_2$, the result is the interface or volume scattering intensity, respectively. Using these two equations, we can examine the relative scattering intensities of interface scattering and volume scattering, given the same average background sound speed profiles. The average background profile for the following examples are two homogeneous half-spaces with sound speeds and densities given in Fig.5.3. Based on the background profile, we can perturb the interface to make it rough,

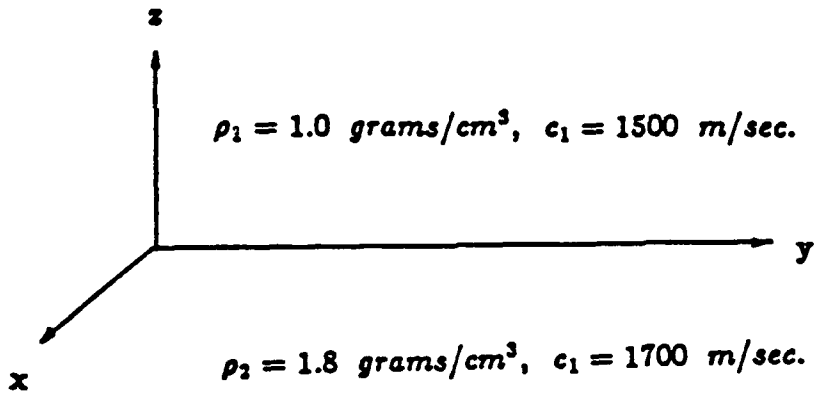

Figure 5.3: Background acoustic parameters

and calculate the plane wave scattering intensity from roughness by Eq.(5.22); also, we can keep the interface flat, but perturb the bottom sound speed in a finite layer immediately beneath the flat interface, to calculate the plane wave scattering intensity from volume inhomogeneities by Eq.(4.9). By comparing the two results, we will be able to get some quantitative understanding of scattering from the rough interface versus scattering due to volume inhomogeneities. Fig.5.4 shows the comparison of scattered pressure magnitudes *vs.* frequency; two of the four curves correspond to interface scattering, the other two curves correspond to volume scattering. In these examples, the rms roughness heights are 0.1 and 0.2 meters, and the rms variations of sound speed are 5 and 7 per cent. In these cases, volume scattering dominates for low frequencies, and interface scattering dominates for high frequencies. It is clear from these examples that the roughness is a strong scatterer; however volume scattering cannot be ignored when the interface is relatively smooth, especially for low frequencies. We note that the crossing points between the curves will move to higher or lower frequencies when the roughness

height or the volume randomness size changes; however the shapes of the curves are determined by the correlation functions of the scatterers. This suggests that as long as the roughness and the volume inhomogeneities have different correlation functions, the frequency dependence of the scattered field will be different. Therefore, there is a possibility to distinguish whether volume scattering exists when we know only the roughness spectra by comparing the predicted scattered field due to roughness alone with the total measured field.

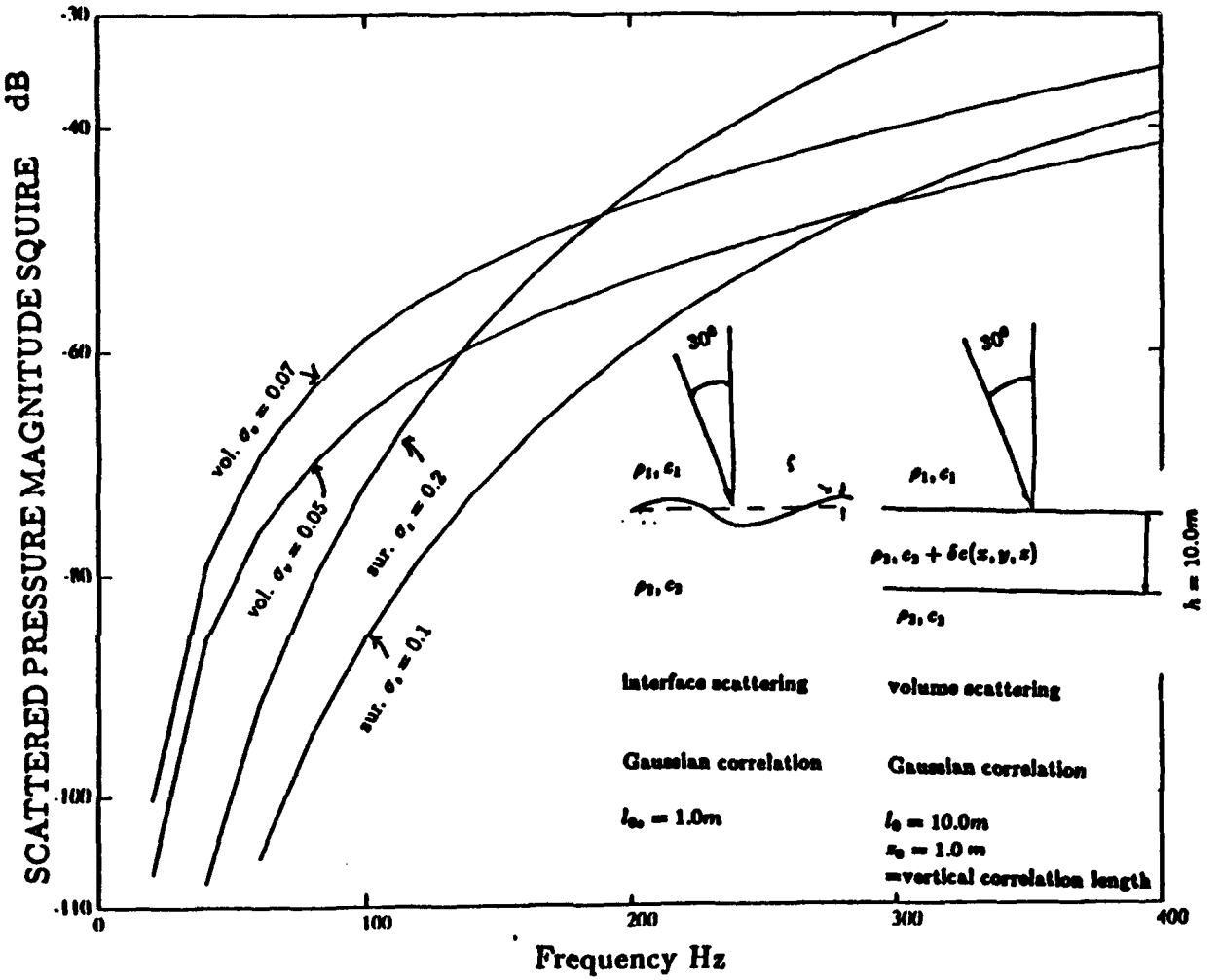

Figure 5.4: Comparison of scattered wave magnitudes

Next, the spatial correlations of scattered fields will be compared. The background profile is the same as in Fig.5.3. Eqs.(5.22) and (4.13) are used to calculate the spatial correlations for rough interface and for volume inhomogeneity scattering, respectively. So far the spatial correlations of scattered field are not normalized. To examine the combined scattering effect of roughness and volume inhomogeneity, we define the normalized spatial correlation:

$$c(\vec{R}_1, \vec{R}_2) = C(\vec{R}_1, \vec{R}_2)/C(\vec{R}_1, \vec{R}_1). \tag{5.26}$$

So the correlation is normalized to unity at zero separation distance.

Figs.5.5 and 5.6 show the case when interface scattering dominates. The spatial correlations in Fig.5.5 is not normalized in order to compare the scattering strength; one of the two curves in Fig.5.5 is the spatial correlation by rough interface; the other curve is the spatial correlation by volume inhomogeneities. Notice that the spatial correlation length for the interface curve is about 5 meters, which equals the correlation length of the rough interface random variable ς; the spatial correlation length for the volume curve is about 15 meters, which equals the correlation length of the volume random variable ϵ. Fig.5.6 is the normalized spatial correlations of scattered field caused by the roughness, by volume inhomogeneities, and by the combined effect. Since the interface scattering is much stronger, the curve for the combined correlation in Fig.5.6 is similar to that of the roughness correlation. Therefore, what we would invert in this case is the roughness correlation length.

Figs.5.7 and 5.8 show the same type of curves as in Figs.5.5 and 5.6 except that neither scattering mechanism dominates. The curves in Fig.5.8 are normalized spatial correlations of the scattered field due to interface, volume and combined effect. We find from the curvature change of the combined correlation that both the 5 meter correlation length from the interface and the 15 meter correlation length

from the volume can be identified. Figs.5.9 and 5.10 are the same as Figs.5.7 and 5.8, except that the correlation function of the random variable ς of the interface is not Gaussian, but exponential. They show similar results.

This suggests that by using a series of receivers to form spatial correlations of the total scattered field, it may be possible to establish whether the scattering process is dominated by one of the scattering mechanisms or by both. When one of the two scattering mechanisms dominates, we will be able to invert its correlation length, and the contribution from the other mechanism will be treated as noise; when neither scattering mechanism dominates, the correlation curve of the scattered will have a turn on its slope.

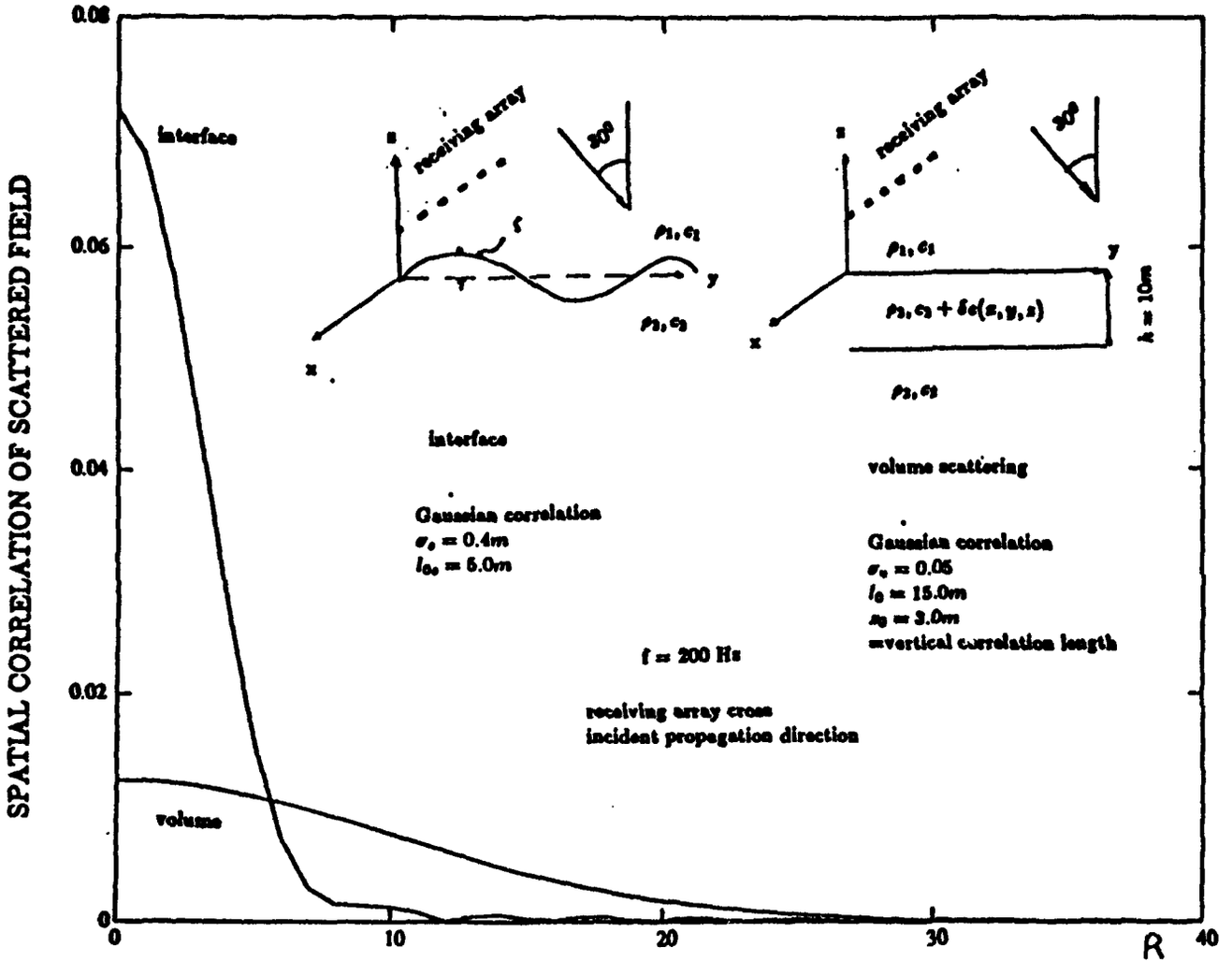

Figure 5.5: Comparison of scattered field correlations; interface roughness dominates; without normalization.

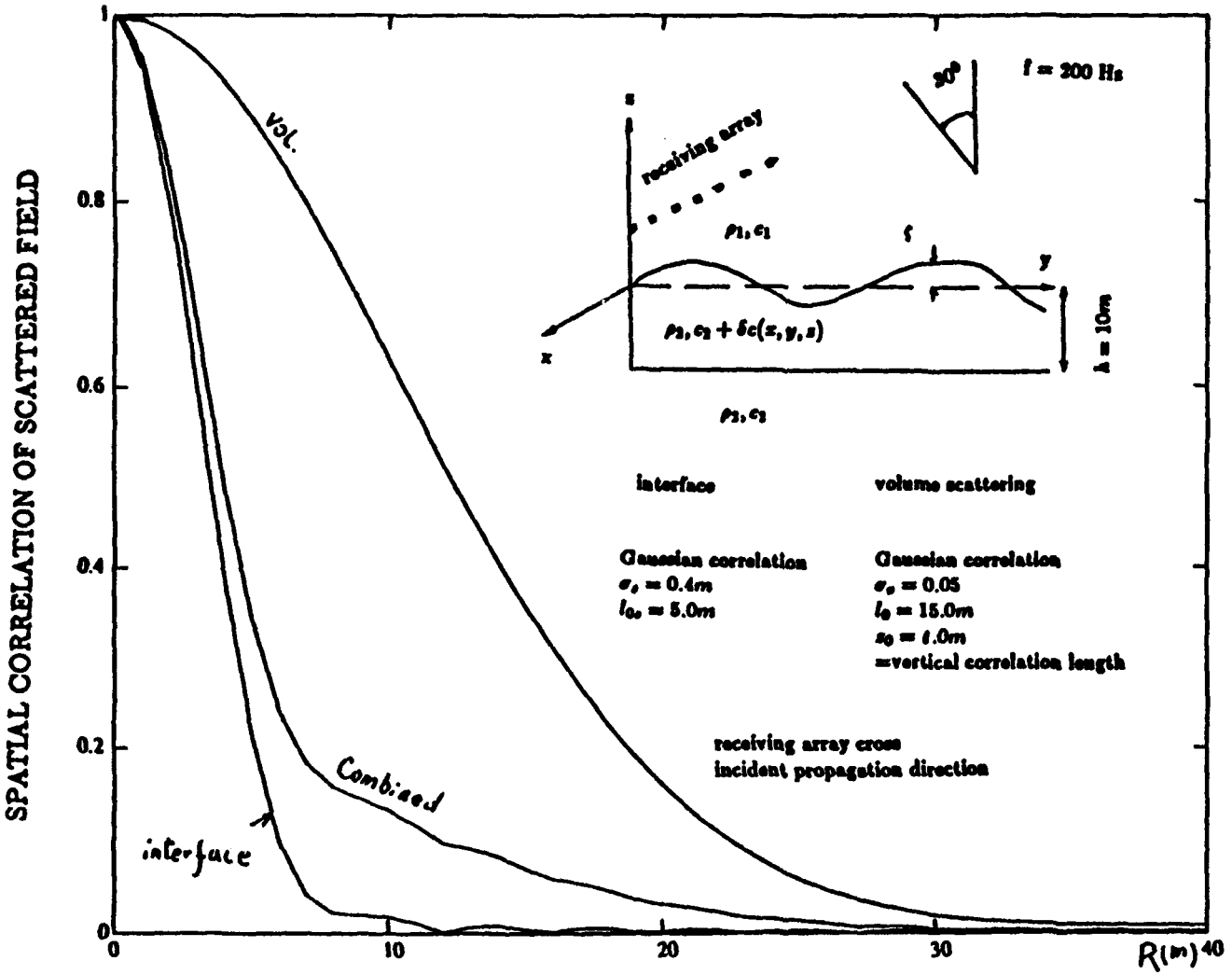

Figure 5.6: Comparison of scattered field correlations, interface roughness dominates; normalized.

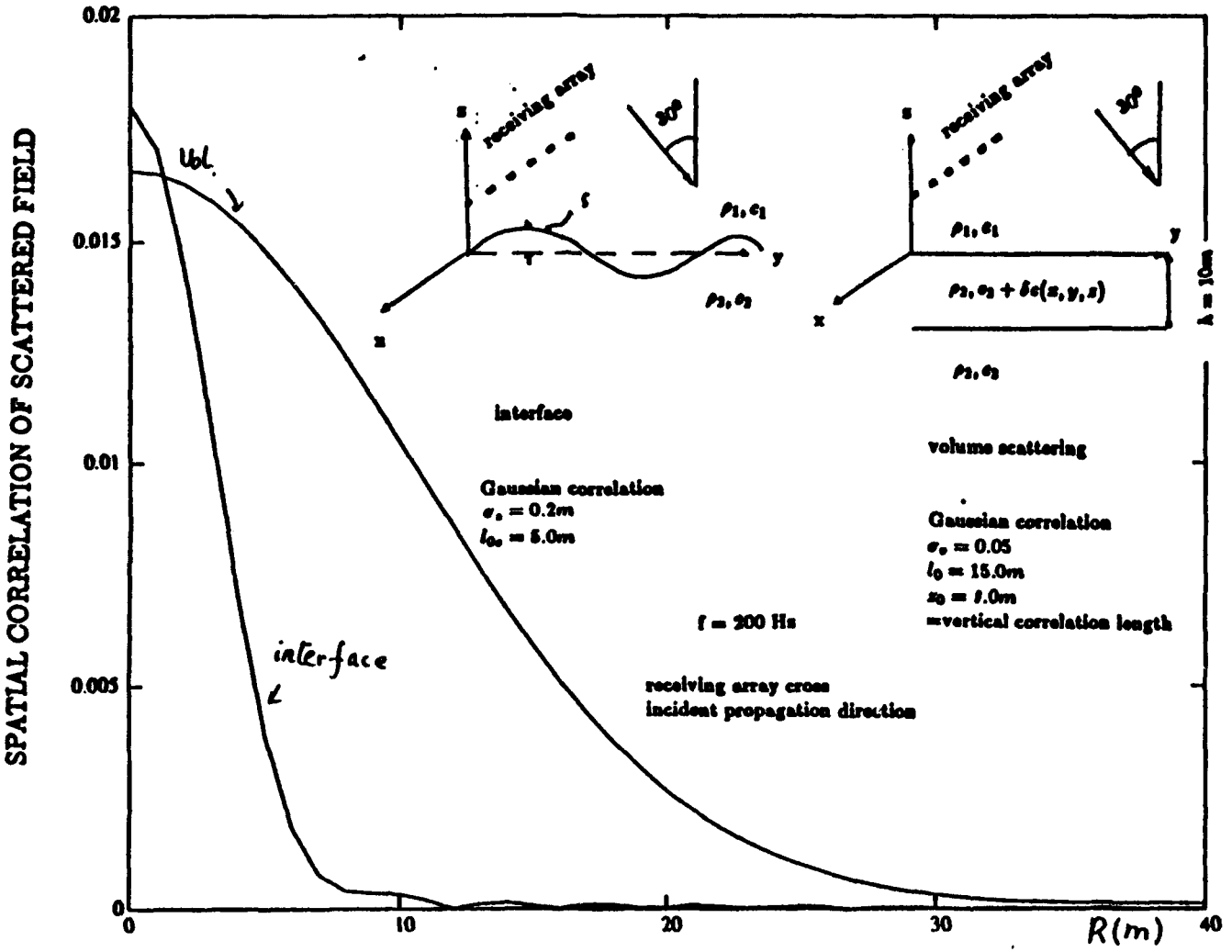

Figure 5.7: Comparison of scattered field correlations; neither interface roughness nor volume dominates; without normalization.

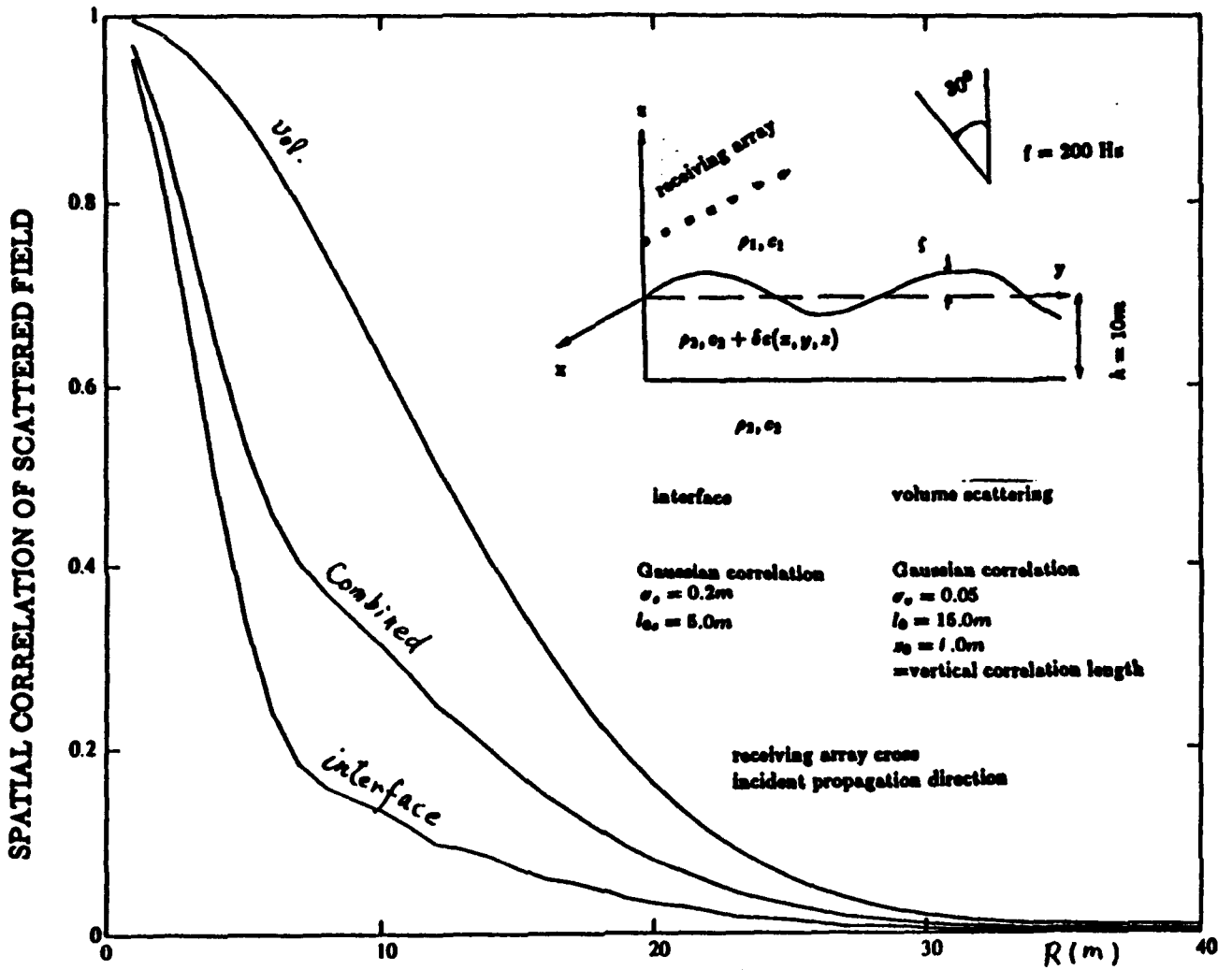

Figure 5.8: Comparison of scattered field correlations, neither interface roughness nor volume dominates; normalized.

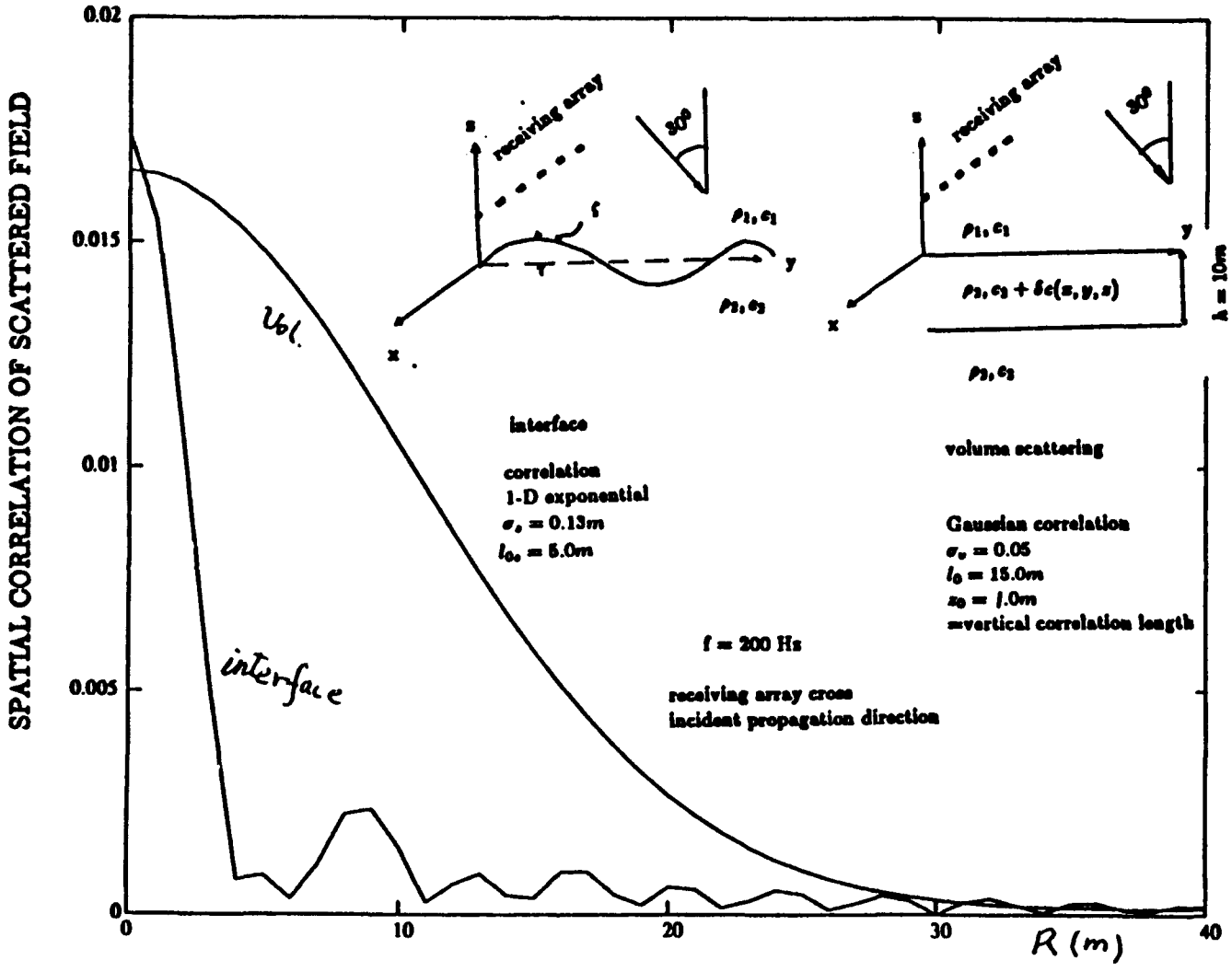

Figure 5.9: Comparison of scattered field correlations; neither interface roughness nor volume dominates; without normalization.

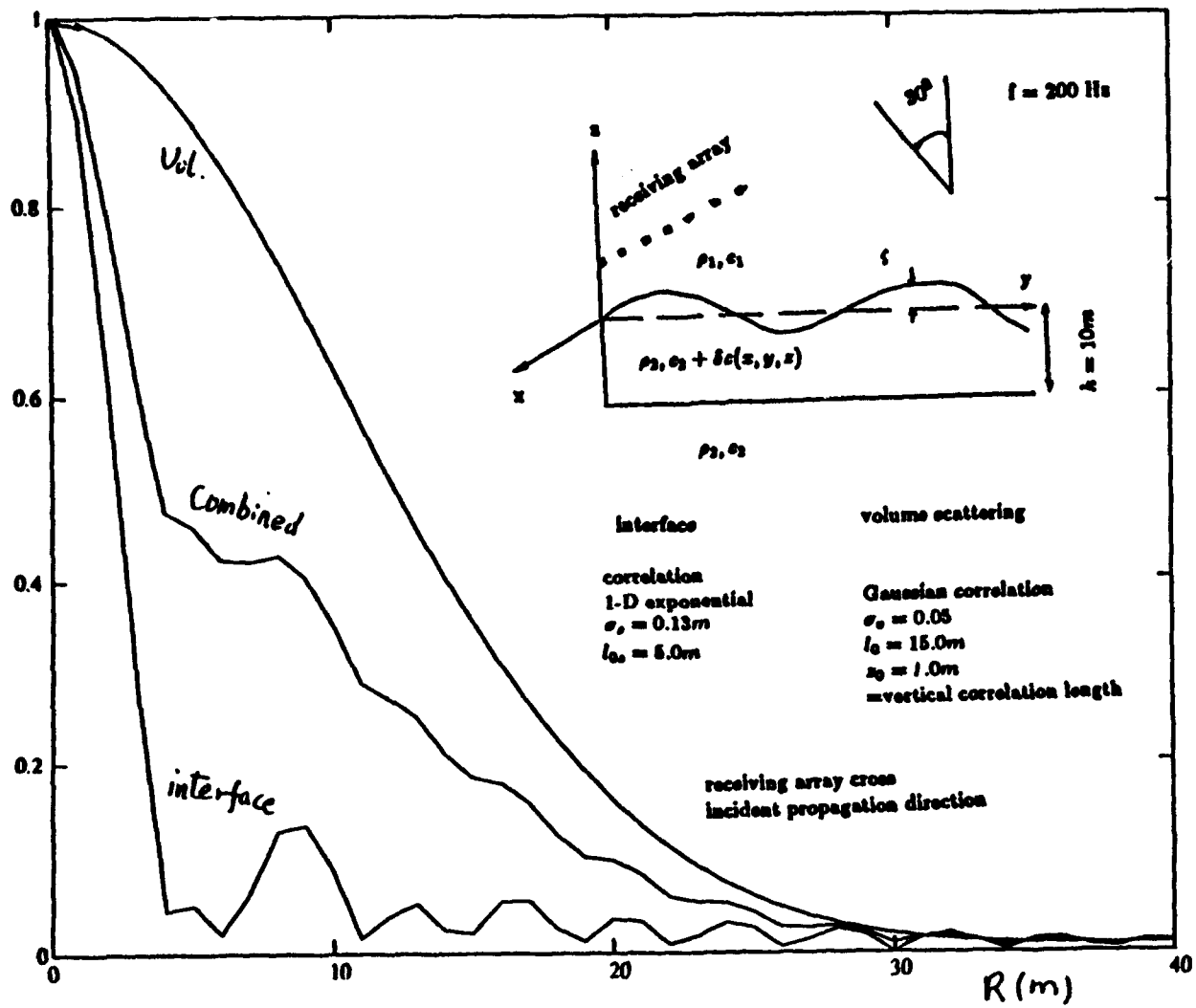

Figure 5.10: Comparison of scattered field correlations, neither interface roughness nor volume dominates; normalized.

Chapter 6

SPECTRAL PARAMETERIZATION OF SCATTERING FROM A RANDOM BOTTOM AND POINT SOURCE CONFIGURATION

The conventional parameter which quantifies scattering from ocean bottoms is the bottom scattering cross section or bottom scattering coefficient. Although this parameter has been widely used, we find it does not have a clear physical meaning. In this chapter, we examine the scattering concept and define a new set of parameters to quantify bottom scattering. In the previous chapters, we examined the plane wave scattering problems; here we will formulate the point source scattering problem in terms of the new parameters.

The physical concept of scattering is developed from the analysis of wave propagation in a medium that is homogeneous except for a small region (the scattering region) where the physical properties, *e.g.* sound speed or density in acoustics, refractive index in electromagnetic (EM) waves, are different from the rest of the medium. However, ocean bottom scattering is different from the classical scattering problem because:

(a) the averaged acoustical parameters of the bottom are not homogeneous and are often layered;

(b) the scattering region is not confined to a finite region.

In order to find a set of parameters to characterize (parameterize) this type of scattering medium, it is necessary to examine the classical definition of scattering cross section which is the parameter characterizing the scattering region.

According to Morse and Feshbach[63] (see Fig.6.1), the total wave function ψ is decomposed into a plane incident wave ψ_i and a scattered wave ψ_s:

$$\psi = \psi_i + \psi_s. \tag{6.1}$$

The incident wave is propagating in the positive z direction:

$$\psi_i = e^{ikz}. \tag{6.2}$$

The scattered wave is evaluated at infinity, which has the asymptotic form:

$$\psi_s \rightarrow f(\theta,\phi)(e^{ikr}/r); \qquad r \rightarrow \infty, \tag{6.3}$$

where r, θ, and ϕ form the spherical coordinates with an origin located in the scattering region. The scattering cross section σ is defined as:

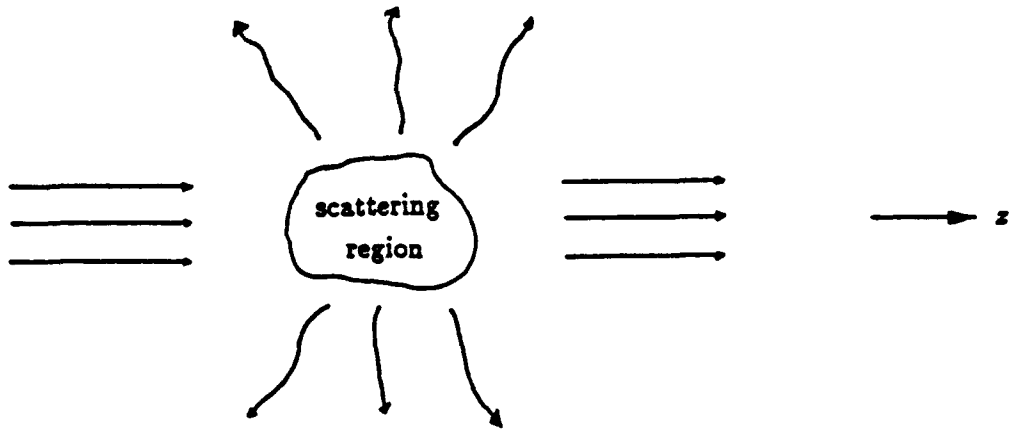

Figure 6.1: Geometry of a classical scattering problem

$$\sigma(\theta,\phi) = |f(\theta,\phi)|^2. \tag{6.4}$$

So, the scattering cross section is a quantity that measures, at infinity, the power scattered into the (θ,ϕ) direction per unit solid angle, per unit incident intensity.

It should be noticed that the definition of σ is independent of source position (plane wave incident), which is necessary for the parameterization; and σ is evaluated at infinity, which means that in the region where σ is measured, the scattered wave has no interaction with the scattering region.

In underwater acoustics, the parameters used to characterize volume scattering and interface scattering are volume and surface scattering coefficients. They are defined, respectively, as

$$\sigma_v = I_s(\theta,\phi)\cdot r^2/[I_0(\theta_0,\phi_0)\cdot dV]; \tag{6.5}$$

and

$$\sigma_s = I_s(\theta,\phi)\cdot r^2/[I_0(\theta_0,\phi_0)\cdot dS]. \tag{6.6}$$

Where, (θ_0, ϕ_0) is the incident plane wave direction, (θ, ϕ) is the scattering direction, I_0 is the incident intensity, I_s is the scattered intensity per unit solid angle measured at a distance r from the scatterer, dV and dS are the insonified volume and area, respectively.

It is clear that the definitions of σ_v and σ_s are transplanted directly from the classical definition of scattering cross section with the following assumptions:

(a) the total scattering volume or surface is divided into many differential elements (small volumes or surfaces), and each of these differential elements is assumed to be an independent scatterer; there are no interactions among the scattering elements. The total scattering is the summation of the contribution of each of the scattering elements.

(b) the incident wavefront should be plane (or locally plane at the scattering element).

(c) compensation by multiplying by the factor r^2 to the scattering strength means that the scattered waves are assumed spherical waves.

Although the scattering coefficients have been used extensively, there are conceptual and practical difficulties when applying them to ocean bottom scattering problems.

First, the division of the scattering volume or surface into differential scattering elements is not justified since interaction among the elements is possible. One could argue that for very high acoustic frequencies, and when the correlation length of the bottom random process is much smaller than the linear dimension of each scattering element, the interaction among the elements can be ignored. However, a proper parameterization should not allow such an assumption.

Secondly, the bottom medium, on average, is not a homogeneous medium. So the incident wavefront at the scattering element may not be planar. Similarly, the scattered wave cannot be assumed spherical, since it can take a curved path to the

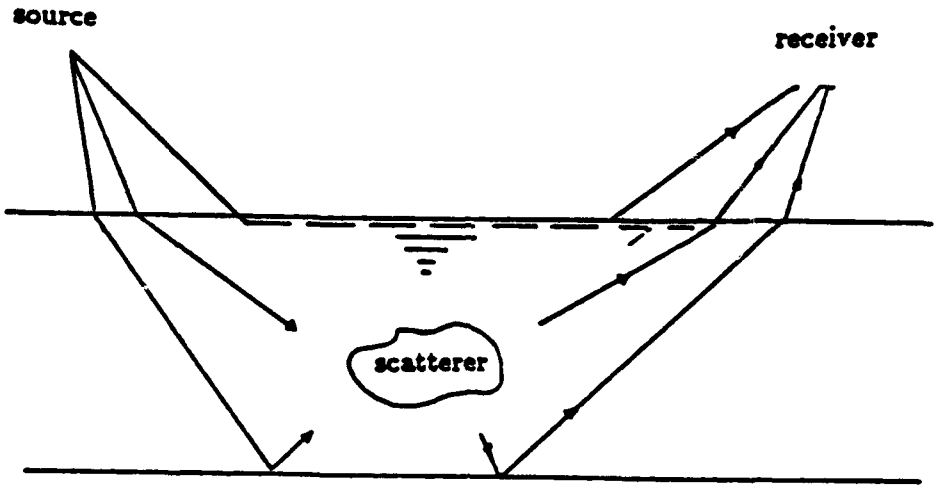

Figure 6.2: Multi-path in a layered structure

observation point via refraction, or divide into more than one wave form via multi-path. Therefore the compensation for spreading loss by the factor r^2 generally is not justified.

As an example, Fig.6.2 shows a case where the scatterer is "sandwiched" in a sub-bottom layer. The figure shows three possible incident paths, i.e refracted by the first interface, refracted first by the first interface and then reflected by the second interface, and a lateral wave path. Also shown are similar scattered paths. In order to find a natural set of parameters to characterize the bottom scattering process, it is helpful to review the parameterization of reflection from layered medium. Broadly speaking, a layered medium itself is a scatterer, because waves will be diffracted away from straight line propagation. Plane wave reflection coefficients[57] are the parameters which fully describe layered media in the sense that, by knowing these parameters, i.e. all the reflection coefficients of incident angles ranging from 0 to 90 degrees and to infinite imaginary angles (inhomogeneous

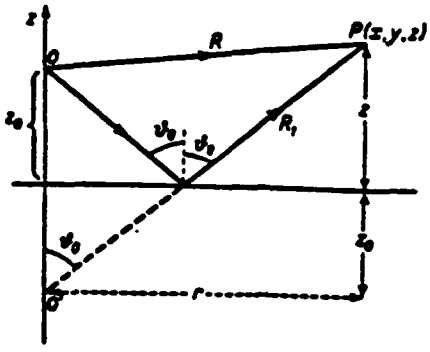

Figure 6.3: Reflection from stratified media. Reproduced from Brekhovskih, *Waves in layered media.*

plane wave) [57], the influence of the layered structure on wave behavior above the layered structure is completely known. For a particular sound source, the response of the layered medium is the linear superposition of the reflection coefficient at all angles. For example, the point source response is given by Brekhovskikh [57](see Fig.6.3):

$$\psi_{refl} = ik \int_0^{(\pi/2)-i\infty} J_0(krsin\theta)exp[ik(z+z_0)cos\theta]V(\theta)sin\theta d\theta. \qquad (6.7)$$

It is clear that in order to obtain a set of parameters that totally characterize the random ocean bottom, one needs to consider the inhomogeneities within the bottom, as well as the layered structure of the averaged background bottom medium as one large scatterer, and to have a plane wave impinging on to the large scatterer. Since the scattering medium is random, the second moments of the randomly scattered field (scattering strength and spatial correlations of scattered field) are concerned; hence the set of parameters will be the cross correlation of the scattering field at the water/bottom interface, induced by two plane waves of unit amplitudes impinging from arbitrary directions, including inhomogeneous plane

waves. This set of parameters will be called Scattering Correlation Coefficients. They form an infinite matrix. The diagonal terms of the matrix are correlations of scattering fields induced by two plane waves impinging from the same direction; the off diagonal terms are correlations induced by two plane waves impinging from different directions. For an arbitrary sound source, the response of the random ocean bottom will be a linear superposition of all the correlation coefficients.

In order to introduce the Scattering Correlation Coefficients, the bottom is modeled as shown in Fig.6.4, and the single scattering approximation (Extended Born approximation) is used. Although the bottom is specific, the Scattering Correlation Coefficients derived therefrom are general.

Assume that a plane wave with horizontal wave vector $\vec{\mu_1}$ and unit amplitude is impinging on to the bottom:

$$P_1^0 = exp(i\vec{\mu_1} \cdot \vec{r} - i\mu_{1z} z), \tag{6.8}$$

where μ_{1z} is the vertical component of the the wave number:

$$\mu_{1z} = \sqrt{k_1^2 - \mu_1^2}. \tag{6.9}$$

The zeroth order solution, i.e. the solution in the absence of the random quantity δc, is the solution of waves in a layered medium, which is available either analytically or numerically[41]. Let the zeroth order solution in the random layer be a complex quantity:

$$P_2^0(\vec{\mu_1}, \vec{r}, z) = T(\vec{\mu_1}, z) e^{i\vec{\mu_1} \cdot \vec{r}}, \tag{6.10}$$

where $e^{i\vec{\mu_1} \cdot \vec{r}}$ results from Snell's law. This quantity is the induced source strength under the Born approximation.

In the random layer, the wave equation governing the scattering field in the Extended Born approximation is:

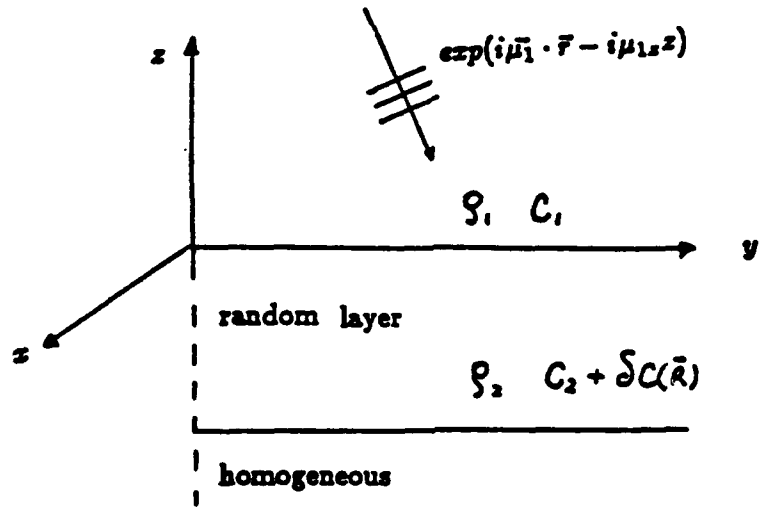

Figure 6.4: Schematic diagram of volume scattering

$$[\nabla^2 + k_2^2]p_2^s \cong 2k_2^2\epsilon(\vec{R})T(\vec{\mu_1}, z)e^{i\vec{\mu_1}\cdot\vec{r}}, \tag{6.11}$$

where $\epsilon = \delta c/c_2$ is the random quantity due to the random sound speed, k_2 is the averaged wave number in the layer.

Since the Green's function for a layered medium can be written as[41]:

$$G(\vec{R}, \vec{R'}) = \frac{1}{2\pi}\int_{-\infty}^{\infty}\int g(\kappa_1, z, z')e^{i\vec{\kappa_1}\cdot(\vec{r}-\vec{r'})}d^2\vec{\kappa_1}, \tag{6.12}$$

where (x, y, z) is the receiver position, and (x', y', z') is the secondary source position, and G obeys

$$[\nabla^2 + k^2]G = \delta(\vec{R} - \vec{R'}), \tag{6.13}$$

the scattered field can be expressed as:

$$\begin{aligned} p_2^s(\vec{R}, \vec{\mu_1}) &= (2k_2^2)\int\int_{v'}\int \epsilon(\vec{R'})T(\vec{\mu_1}, z')e^{i\vec{\mu_1}\cdot\vec{r'}}G(R, R')dv' \\ &= (2k_2^2)\int\int_{v'}\int \epsilon(\vec{R'})T(\vec{\mu_1}, z')e^{i\vec{\mu_1}\cdot\vec{r'}} \\ &\quad (\frac{1}{2\pi})\int_{-\infty}^{\infty}\int g(\kappa_1, z, z')e^{i\vec{\kappa_1}\cdot(\vec{r}-\vec{r'})}d^2\vec{\kappa_1}dv'. \end{aligned} \tag{6.14}$$

Changing the integration order, the above expression becomes:

$$p_2^s(\vec{R},\vec{\mu_1}) = \int_{\infty}^{\infty}\int d^2\vec{\kappa_1}e^{i\vec{\kappa_1}\cdot\vec{r}} \left[(\frac{k_2^2}{\pi})\int\int_{v'}\int dv'\epsilon(\vec{R'})T(\vec{\mu_1},z')g(\kappa_1,z,z')e^{i(\vec{\mu_1}-\vec{\kappa_1})\cdot\vec{r'}}\right]. \quad (6.15)$$

The scattered field in the water column can be written as summation of up-going plane waves:

$$p_1^s(\vec{R},\vec{\mu_1}) = \int_{\infty}^{\infty}\int d^2\vec{\kappa_1}m(\vec{\kappa_1},\vec{\mu_1})e^{i\vec{\kappa_1}\cdot\vec{r}}e^{iz\sqrt{k_1^2-\kappa_1^2}}. \quad (6.16)$$

At the water/bottom interface, $z = 0$, the scattered field is continuous; $p_1^s = p_2^s$. Comparing Eqs.(6.15) and (6.16), we have:

$$m(\vec{\kappa_1},\vec{\mu_1}) = (\frac{k_2^2}{\pi})\int\int_{v'}\int dv'\epsilon(\vec{R'})T(\vec{\mu_1},z')g(\kappa_1,z')e^{i(\vec{\mu_1}-\vec{\kappa_1})\cdot\vec{r'}}. \quad (6.17)$$

Clearly, $m(\vec{\kappa_1},\vec{\mu_1})$ measures the amount of scattering (including amplitude and phase) going to $\vec{\kappa_1}$ direction when a plane wave is impinging upon the random medium from $\vec{\mu_1}$ direction. This quantity is independent of source or receiver position, and it contains all the information about the random bottom necessary for determining the statistics of the scattered field in $\vec{\kappa_1}$ direction.

To measure the second moments of the randomly scattered field p_1^s (the first moment of p_1^s is zero because ϵ is assumed to have zero average value), it is enough to know the cross correlations between the $m(\vec{\kappa_1},\vec{\mu_1})$'s. The Scattering Correlation Coefficients are defined as:

$$D(\vec{\kappa_1},\vec{\kappa_2},\vec{\mu_1},\vec{\mu_2}) = \langle m(\vec{\kappa_1},\vec{\mu_1})\cdot m^*(\vec{\kappa_2},\vec{\mu_2})\rangle. \quad (6.18)$$

Changing variables as before:

$$\vec{l} = \vec{r'} - \vec{r''}, \qquad l = \sqrt{(x'-x'')^2+(y'-y'')^2}, \quad (6.19)$$

and considering the random quantity ϵ to have the same statistics as in the previous chapters:

$$\langle \epsilon(\vec{R}')\epsilon(\vec{R}'')\rangle = \sigma^2 z_0 \delta(z'-z'')N(\vec{l}), \tag{6.20}$$

and

$$S(\vec{s}) = \int\int N(\vec{l})e^{-i\vec{s}\cdot\vec{l}}d^2\vec{l}, \tag{6.21}$$

$D(\vec{\kappa_1},\vec{\kappa_2},\vec{\mu_1},\vec{\mu_2})$ can be evaluated:

$$\begin{aligned} D(\vec{\kappa_1},\vec{\kappa_2},\vec{\mu_1},\vec{\mu_2}) &= z_0\left(\frac{\sigma k_2^2}{\pi}\right)^2 \int dz' g(\kappa_1,z')g^*(\kappa_2,z')T(\vec{\mu_1},z')T(\vec{\mu_2},z') \\ &\quad \int_{-\infty}^{\infty}\int e^{i\vec{r''}\cdot[(\vec{\mu_1}-\vec{\mu_2})-(\vec{\kappa_1}-\vec{\kappa_2})]}d^2r''\int\int N(\vec{l})e^{i(\mu_1-\kappa_1)\cdot\vec{l}}d^2\vec{l} \\ &= z_0(2\sigma k_2^2)^2 S(\vec{\mu_1}-\vec{\kappa_1})\delta[(\vec{\mu_1}-\vec{\mu_2})-(\vec{\kappa_1}-\vec{\kappa_2})] \\ &\quad \int dz' g(\kappa_1,z')g^*(\kappa_2,z')T(\vec{\mu_1},z')T^*(\vec{\mu_2},z'). \end{aligned} \tag{6.22}$$

Among the four vectors in $D(\vec{\kappa_1},\vec{\kappa_2},\vec{\mu_1},\vec{\mu_2})$ only three of them are independent; the fourth one is determined by the Dirac delta in the above expression. This is a consequence of assuming the scatterers are spatially homogeneous.

Knowing the Scattering Correlation Coefficients, we can construct the correlation of the scattered fields, induced by any two incident plane waves, by using Eq.(6.16):

$$\begin{aligned} \langle p_1^s(\vec{R_1},\vec{\mu_1})p_1^{s*}(\vec{R_2},\vec{\mu_2})\rangle &= \int\int d^2\vec{\kappa_1}\int\int d^2\vec{\kappa_2}D(\vec{\kappa_1},\vec{\kappa_2},\vec{\mu_1},\vec{\mu_2}) \\ &\quad e^{i[(\vec{\kappa_1}\cdot\vec{r_1})-(\vec{\kappa_2}\cdot\vec{r_2})]}e^{i[z_1\sqrt{k_1^2-\kappa_1^2}-z_2(\sqrt{k_1^2-\kappa_2^2})^*]}. \end{aligned} \tag{6.23}$$

When a specific acoustic source is used, the spatial correlation of the scattered field can be found by adding up contributions from all incident plane waves with appropriate weighting functions. As an example, a point source can be expressed as superposition of plane waves[57]:

$$e^{ik_1R}/R = \frac{1}{2\pi}\int_{-\infty}^{\infty}\int d^2\vec{\mu_1}W(\mu_1,z_0)e^{i[\vec{\mu_1}\cdot\vec{r}-z\sqrt{k_1^2-\mu_1^2}]}, \tag{6.24}$$

where

$$W(\mu_1, z_0) = \left(\frac{i}{2\pi\sqrt{k_1^2 - \mu_1^2}} \right) e^{iz_0\sqrt{k_1^2-\mu_1^2}} \tag{6.25}$$

is the weighting function of each plane incident wave for point source. Therefore, the spatial correlation of the scattered field from a point source is:

$$\begin{aligned} \langle p_1^s(\vec{R}_1, \vec{R}_0) p_1^{s*}(\vec{R}_2, \vec{R}_0) \rangle &= \int\int d^2\vec{\mu}_1 \int\int d^2\vec{\mu}_2 \\ &[W(\mu_1, z_0) W^*(\mu_2, z_0)] \langle p_1^s(\vec{R}_1, \vec{\mu}_1) p_1^{s*}(\vec{R}_2, \vec{\mu}_2) \rangle \end{aligned} \tag{6.26}$$

Combining Eqs.(6.23) and (6.26), we obtain the expression for spatial correlation of the scattered field due to a point source as a multi-dimensional integral:

$$\begin{aligned} \langle p_1^s(\vec{R}_1, \vec{R}_0) p_1^{s*}(\vec{R}_2, \vec{R}_0) \rangle &= \int\int d^2\vec{\mu}_1 \int\int d^2\vec{\mu}_2 [W(\mu_1, z_0) W^*(\mu_2, z_0)] \\ &\int\int d^2\vec{\kappa}_1 \int\int d^2\vec{\kappa}_2 D(\vec{\kappa}_1, \vec{\kappa}_2, \vec{\mu}_1, \vec{\mu}_2) \\ &e^{i[(\vec{\kappa}_1 \cdot \vec{r}_1) - (\vec{\kappa}_2 \cdot \vec{r}_2)]} e^{i[z_1\sqrt{k_1^2-\kappa_1^2} - z_2(\sqrt{k_1^2-\kappa_2^2})^*]}. \end{aligned} \tag{6.27}$$

When $\vec{R}_1 = \vec{R}_2$, Eq.(6.26) gives the scattering strength; further, if $\vec{R}_1 = \vec{R}_0$, it gives the backscattering strength. It is clear from the general expression of Eq.(6.27) that all the second moments of the scattered field are linear superpositions of the Scattering Correlation Coefficients $D(\vec{\kappa}_1, \vec{\kappa}_2, \vec{\mu}_1, \vec{\mu}_2)$.

There are three points worth mentioning. First, the quantity $T(\vec{\mu}_1, z')T^*(\vec{\mu}_2, z')$ in Eq.(6.22) is the incident strength at the scatterer, which generally is not that of a plane wave; it contains multipath and lateral wave contributions.

Second, Eq.(6.26) shows that the received scattering strength from a point source is the combined result of scattering in all directions. It is valuable to solve Eq.(6.26), and to compare the result with that of the conventional definition of scattering coefficient in Eq.(6.5).

Realizations of the scattered field is possible if we generate a particular random bottom. The statistics of the scatterers can be controled by specifying the spectrum

of the scatterers. By generating realizations over a number of frequencies, we will be able to synthesize scattered time series (reverberation signals).

Chapter 7

CONCLUSIONS AND RECOMMENDATIONS FOR FUTURE RESEARCH

7.1 Conclusions

Ocean bottom scattering is a very complicated problem. This thesis is a theoretical analysis of some aspects of the scattering problem. We emphasize on the scattering from the inhomogeneous volume, but the interface scattering is also extensively covered. The four major accomplishments are:

(1) Detailed study of spatial correlations of scattered field. Spatial correlations of the scattered field carries information which cannot be obtained from the scattering intensity. Conventionally, bottom scattering research has been concentrated on modeling and measuring the scattered intensities. However, the scattering intensity only describes the amount of energy being scattered; it cannot provide information on how the scattered field is spatially related. We found that the spatial correlation

length of the scattered field is related to the statistical properties of the scatterers. By using a wideband acoustic source, and sweeping acoustic frequency, we can invert the correlation length of the scatterers from the measurement of the spatial correlation of the scattered field. In addition, the influence of bottom anisotropy is also investigated.

(2) Introduction of the Scattering Correlation Coefficient. Ocean bottom is a complicated medium, however the scattering cross section, the major parameter quantifying bottom scattering, is transplanted from the much simpler classical scattering problem. In many cases, especially in low frequency scattering problems, the scattering cross section is not a proper parameter. By introducing the Scattering Correlation Coefficient, we have a better understanding of scattering from a random bottom. More importantly, these set of parameters has the potential to be used as a standard quantity in comparing experimental data obtained from different sites.

(3) Comparison of two different scattering mechanisms. When the water/bottom interface is not very rough, it has been speculated that the volume scattering mechanism might be important. We combined the roughness and the inhomogeneity into one model under the assumption that the roughness and the inhomogeneity are uncorrelated, and showed quantitatively in examples that the volume scattering is important, especially for low frequencies.

We also showed that when the scattering is caused by both interface roughness and volume inhomogeneities, it is possible to distinguish the contributions to the scattered field from these two scattering mechanisms by examining the spatial correlation of the scattered field. To do this, we have to assume that the roughness and the volume inhomogeneities have different statistics; in other words, they have

to have different spectra.

(4) Application of the integro-differential equation method. We extended the integro-differential equation method to the problem of weak scattering from a inhomogeneous layer, in which a water/bottom discontinuity is included. By using the coherent field obtained from that integro-differential equation as input to calculate scattered field, we improved upon the Born approximation.

7.2 Recommendations for future research

Theoretically, we recommend the following research in the future:

(a) Develop a fast calculation technique to handle the multifold integration problem.

To evaluate the spatial correlation of the scattered field due to a point source is of practical importance. Although we have formulated that problem in this thesis, we have not been successful in solving it because we do not have an effective method to numerically evaluate that multifold integration involved in that formulation.

(b) Simulate reverberation signals.

Based on the formulation of scattering due to a point source, we can generate Monte Carlo type realizations of a random bottom and calculate the scattered fields over a band of frequencies for each realization. By synthesizing these scattered fields, we will be able to simulate the reverberation signals in time domain due to a realistic finite duration pulsing source. It will help in both designing experiments and processing real data.

(c) Application of the Scattering Correlation Coefficient.

One goal is to express the coefficient through measurable quantities (ex. acoustic pressure) in order to use it as a standard to compare experimental data obtained from different locations. Another goal is to use the Scattering Correlation Coefficient to find the applicable conditions of the classical scattering cross section.

(d) Develop a model which can predict scattered field when the interface roughness and the volume inhomogeneities are correlated.

(e) Investigate the case when the bottom correlation function is not a single parameter form.

Experimentally, the major issue is what geological parameters are necessary to be used as inputs when we apply the theory to experiments. The following are some considerations:

(a) The data supplied by geologists are material properties and they are not *directly* suitable for acousticians. Some of the data are also acoustic properties such as compressional velocity and attenuation coefficient; others are indirectly related to acoustics, such as porosity, water content, grain weight, and grain size. These material properties are especially important to the acoustic scattering process. How the variabilities of these parameters influence acoustic scattering is not clear. There has been some research in this area[63], but they are incomplete. The key question is what dominates volume scattering?

(b) In Chapter 2, we modeled the scatterers as a variation of sound speed within

the seabed; whether the variations of density are also important as scatterers is not clear. So we suggest that in the geological surveys of an experimental site, the correlation between sound speed and density variations be conducted. Ideally, we would like to have the joint distribution of the two random variables, sound speed and density. If the contribution to scattering from density variations is much less than that from sound speed variations, we can directly apply the present theory; if the density is also proved to be important, we will determine how the density variation is correlated with the sound speed variation. If these two quantities are perfectly correlated, as Hines[9] has assumed, the present theory can be easily modified to accommodate the density variation effect; if they are not correlated at all, then the scattered field would be the superposition of the contributions from the two scattering mechanisms. In this case, the theory in this thesis can be improved to account for scattering by the two types of independent scatterers. However, because there are two random processes involved, pin pointing the contribution from each mechanism would be difficult. We find from the available data [53,50] that the likely situation is that the two random variables are partially correlated, but there is no quantitative data to infer the form of the correlation function. Hence it is of great importance to have a detailed exploration of this issue.

(c) What is the horizontal variability of the scatterers? There exists a large amount of drilling data to infer the vertical variability of the sound speed profile in the bottom, but so far there have been few efforts to experimentally determine the horizontal variability of either sound speed or density. Early models assume that the volume scatterers are uncorrelated [14,46], but this assumption not only contradicts intuition, but also disagrees with the drilling data[50]. The theory developed in this thesis is based on the assumption that the sound speed variation is well correlated horizontally, and poorly correlated vertically, because in each sed-

imentation time period, similar material will be deposited in one sediment layer, and the sediment material will be different for different time periods. To get experimental evidence on horizontal variability of the sediment, we need several groups of three to five core samples of sound speed and density. Of primary importance is the rough size of the horizontal correlation length. Since we are interested in low-frequency scattering (below 1 kHz), and we can assume the compressional wave speed is 1500 - 2000 meters/sec., the shortest acoustic wavelength in the sediment will be in the range of 1.5 - 2.0 meters. If the horizontal correlation length is shorter than one meter, we should use the uncorrelated-scatterer model; otherwise, the model developed in the thesis should apply. One key result in the theory is that the spatial correlation length of the scattered field equals the horizontal correlation length of the sound speed variation; therefore knowing the true correlation length of the sound speed variation at the experiment site is crucial in testing the theory in an acoustic scattering experiment. Based on the above argument, if we choose the highest frequency to be 1 kHz, and the lowest frequency to be 50 Hz, the cores should be separated from each other by at least 2 meters, and no more than 40 meters, and they should not be arranged on a straight line in order to find the anisotropy.

(d) Ideally we would like to conduct the experiment in an area where the seafloor is flat. However, the seafloor will always have some roughness, and the roughness is an effective scatterer as shown in Chapter 5. Therefore, measuring the roughness spectrum is necessary to determine the contribution to scattered field from roughness. This could be done with joint registry of a high frequency sidescan sonar and MHz frequency narrow beam bathymeter.

A difficult and also important item to investigate is the geological link between the roughness and the variabilities within the volume. In Chapter 5, we made a

rough comparison of the scattering effects due to roughness and volume inhomogeneity, which is based on the assumption that there is no statistical correlation between the two random quantities. If the two quantities are related statistically, there might be some geological linkage as well. These kinds of information will help in improving the acoustic scattering model. If indeed the two quantities are independent, knowledge of the roughness spectrum will enable us to evaluate the volume scattering contribution by subtracting the roughness contribution from the total scattered field.

Another point worth mentioning concerns the dependence of the roughness spectrum on the probing acoustic frequency. The interface perceived by high-frequency acoustic waves may not necessarily be the same one perceived by low frequency acoustic waves. Therefore, the bottom roughness spectrum should be measured as a function of frequency. How to practically conduct measurements of this kind remains to be investigated.

(e) The background acoustic sound speed profile of the seabed should be included in the geological survey, since the amount of acoustic energy penetrating into the seabed heavily depends on the background acoustic profile, and the amount of acoustic energy penetrating into the seabed is proportional to the energy being scattered by the volume inhomogeneities. The two most important parameters are the average compressional wave speed profile and the average density profile. In this thesis, we have assumed that the average profiles of sound speed and density are constants. If they are not constants, we should modify the theory to accommodate this effect. Ideally, a bi-static acoustic propagation experiment should be part of a scattering experiment in order to collect information on the coherent component of the field.

Bibliography

[1] C. S. Clay and H. Medwin, *Acoustical Oceanography*, John Wiley and Sons, New York (1977).

[2] J. P. Kennett, *Marine Geology*, Prentice-Hall (1982).

[3] C. Eckart, "The scattering of sound from the sea surface," J. Acoust. Soc. Am. **25**, 566 (1953).

[4] H. W. Marsh, "Exact solution of wave scattering by irregular surfaces," J. Acoust. Soc. Am. **33**, 330 (1961).

[5] E. Y. Kuo, "Wave scattering and transmission at irregular surfaces," J. Acoust. Soc. Am. **36**, 2135 (1964).

[6] W. A. Kuperman, "Coherent component of specular reflection and transmission at a randomly rough two-fluid interface", J. Acoust. Soc. Am. **58**, 365 (1975).

[7] W. A. Kuperman and H. Schmidt, "Rough surface elastic wave scattering in a horizontally stratified ocean," J. Acoust. Soc. Am. **79**, 1767 (1986).

[8] P. A. Crowther, "Some statistics of the sea-bed and acoustic scattering therefrom", in *Acoustics and the Sea-Bed*, ed. N. G. Pace, Bath Univ., Bath, England (1983).

[9] P. C. Hines, "Examination of acoustic backscattering from an inhomogeneous volume beneath a planar interface," *Ph.D* thesis, University of Bath, School of Physics, England, 1988.

[10] A. N. Ivakin and Yu. P. Lysanov, "Theory of underwater sound scattering by random inhomogeneities of the bottom," Sov. Phys. Acoust. **27**, Jan-Feb. (1981).

[11] H. M. Merklinger, "Bottom reverberation measured with explosive charges fired deep in the ocean", J. Acoust. Soc. Am. **44**, 508 (1968).

[12] D. R. Jackson, D. P. Winebrenner, and A. Ishimaru, "Application of the composite roughness model to high-frequency bottom backscattering," J. Acoust. Soc. Am. **79** (1986).

[13] P. C. Hines, "Theoretical model of acoustic backscatter from a smooth seabed," J. Acoust. Soc. Am. **88**, 324 (1990).

[14] J. H. Stockhausen, "Scattering from the volume of an inhomogeneous half-space", NRE report, 63/9, (1963).

[15] A. N. Ivakin, "Sound scattering by random inhomogeneities of stratified ocean sediments", Soviet Physics Acoust. **32**, 492 (1986).

[16] L. A. Chernov, *Wave Propagation in a Random Medium*, (McGraw-Hill, NY, 1975), Translated from Russian by R. A. Silverman.

[17] A. N. Ivakin and Yu. P. Lysanov, "Underwater sound scattering by volume inhomogeneities of a bottom bounded by a rough surface", Soviet Physics Acoust. **27**, 212-215 (1981).

[18] G. V. Frisk, Private communications (1989).

[19] F. G. Bass and I. M. Fuks, *Wave Scattering from Statistically Rough Surfaces*, Pergamon, Oxford (1979).

[20] V. I. Tatarskii, *The Effects of the Turbulent Atmosphere on Wave Propagation*, Israel program for scientific translations, Jerusalem, Israel (1971).

[21] K. Aki and P. G. Richards, *Quantitative Seismology*, W. H. Freeman and Company, San Francisco (1980).

[22] A. Ishimaru, *Wave Propagation and Scattering in Random Media*, Academic Press, New York (1978).

[23] S. M. Flatté, "Wave propagation through random media: contributions from ocean acoustics," Proc. IEEE, Vol. 71, pp 1267 (1983).

[24] S. M. Flatté, R. Dashen, W. H. Munk, K. M. Watson, and F. Zachariasen, *Sound Transmission Through a Fluctuating Ocean*. New York, Cambridge Univ. Press (1979).

[25] A. N. Ivakin and Yu. P. Lysanov, "Backscattering of sound from an inhomogeneous bottom at small grazing angles", Soviet Physics Acoust. **31**, 236-237 (1985).

[26] R. C. Bourret, "Propagation in randomly perturbed fields," Can. J. Phys. **40**, 782 (1962).

[27] J. B. Keller, "Stochastic equations and wave propagation in random media," Proc. Symp. Appl. Math. **16**, 145 (1964).

[28] S. Rosenbaum, "On the coherent wave motion in bounded randomly fluctuating regions" Radio Science, 4(8), 709-719, August (1969).

[29] I. Kupiec, L. B. Felsen, S. Rosenbaum, J. B. Keller and P. Chow, "Reflection and transmission by a random medium" Radio Science 4(11), 1067, Nov. (1969).

[30] V. M. Kurtepov, "Influence of internal waves on sound propagation in the ocean", Sov. Phys. Acoust., **22**, No. 2, March-April (1976).

[31] L. Fortuin, "Survey of literature on reflection and scattering of sound waves at sea surface", J. Acoust. Soc. Am. **47**, No. 5 (part 2), 1209 (1970).

[32] F. G. Bass, "Izv. Vyssh. Uchebn. Zaved Radiofitz.", **4**, 476 (1961); (JPRS:10223).

[33] S. R. Brown, "A note on the description of surface roughness using fractal dimension", Geophys. Res. Lett., **14**, 1095-1098 (1987).

[34] C. G. Fox, "Empirically derived relationships between fractal dimension and power law from frequency spectra", Pure Appl. Geophys., **131**, 211-239 (1989).

[35] C. G. Fox and D. E. Hayes, "Quantitative methods for analyzing the roughness of the seafloor", Rev. Geopgys., **23**, 1-48 (1985).

[36] J. A. Goff and T. H. Jordan, "Stochastic modeling of seafloor morphology: Inversion of Sea Beam data for second order statistics", J. Geophys. Res., **93**, 13 589-13 608 (1988).

[37] J. A. Goff, T. H. Jordan, M. H. Edwards, and D. J. Fornari, "Comparison of a stochastic seafloor model with SeaMARC II bathymetry and Sea Beam data near the East Pacific Rise 13° – 15° N", J. Geophys. Res., in press (1991).

[38] A. Ishimaru, "Theory and application of wave propagation and scattering in random media," Proc. IEEE, Vol. **65**, 1030 (1977).

[39] S. T. McDaniel and A. D. Gorman, "An examination of the composite-roughness scattering model", J. Acoust. Soc. Am. 73, 1476 (1982).

[40] Yu. N. Barabanenkov, Yu. A. Kravtsov, S. M. Rytov, and V. I. Tatarskii, "Status of the theory of propagation of waves in a randomly inhomogeneous medium", Soviet Physics, *Uspekhi*, (A translation of Uspeki Fizicheskikh), Vol. 13, No. 5, pp 551- 680, (Russian original Vol. 102, Nos. 1 and 2), March - April (1971).

[41] H. Schmidt, *SAFARI Seismo-Acoustic Fast Field Algorithm for Range Independent Environments–User' Guide*, SACLANT ASW Research Center, I-19100 La Spezia, Italy (1987).

[42] C. S. Clay and H. Medwin, "Dependence of spatial and temporal correlation of forward-scattered underwater sound on the surface statistics. I. Theory," J. Acoust. Soc. Am. 47, 1412-1418 (1970).

[43] H. Medwin and C. S. Clay, "Dependence of spatial and temporal correlation of forward-scattered underwater sound on the surface statistics. II. Experiment," J. Acoust. Soc. Am. 47, 1419-1429 (1970).

[44] W. A. Kinney and C. S. Clay, "The spatial coherence of sound scattered from a wind-driven surface: Comparison between experiment, Eckart theory, and the facet-ensemble method", J. Acoust. Soc. Am. 75, 145-148 (1984).

[45] W. A. Kinney and C. S. Clay, "Insufficiency of surface spatial power spectrum for estimating scattering strength and coherence: Numerical studies", J. Acoust. Soc. Am. 78, 1777-1784 (1985).

[46] A. W. Nolle, W. A. Hoyer, J. F. Mifsud, W. R. Runyan, M. B. Ward, "Acoustic properties of water-filled sands", J. Acoust. Soc. Am. 35, 1394-1408, (1963).

[47] Yu. Yu. Zhitkovskii, "The scattering of sound by inhomogeneities of the top layer of the ocean bottom," Izvest. Atmos. Ocean. Phys. 4, (1968).

[48] V. I. Volvov, Yu. Yu. Zhitkovskii, "Reflection and scattering of sound by the ocean bottom", page 395 in *Ocean Acoustics*, Part 6, (in Russian),ed. L. Brekhovskikh, Moscow (1974).

[49] M. E. Dougherty, "Ocean bottom seismic scattering," *Ph.D.* thesis, MIT/WHOI Joint Program, 1989.

[50] T. Yamamoto, "Geoacoustic properties of the seabed sediment critical to acoustic reverberation at 50 to 500 Hz: a preliminary data set" J. Acoust. Soc. Am. Suppl. 1, 85, Spring, s86 (1989).

[51] T. Yamamoto, A. Turget, M. Schikin and R. Bennett, "Geoacoustic properties of the seabed sediment critical to acoustic reverberation at 50 to 500 Hz: a preliminary data set" RSMAS TR-91-001, G.A.L. Report No.1014, Univ. of Miami.

[52] R. H. Bennett, D. N. Lambert, M. H. Hulbert, T. J. Burns, W. B. Sawyer, and G. L. Freland, "Electrical Resistivity/Conductivity in Seabed Sediments", pp 333-375, in Handbook of Geophysical Exploration at Sea, Ed. R. A. Geyer, CRC Press, Boca Raton, FL (1983).

[53] R. H. Bennett, G. H. Keller, and R. F. Busby, "Mass property variability in three closely spaced deep-sea sediment cores", J. Sed. Petrology, 40, pp 1038-1043 (1970).

[54] G. V. Frisk, A. V. Oppenheim and D. R. Martinez, "A technique for measuring the plane-wave reflection coefficient of the ocean bottom", J. Acoust. Soc. Am. *68* (2), Aug. (1980).

[55] I. S. Gradshteyn and I. M. Ryzhik, *Table of Integrals, Series, and Products*, page 718 (Academic Press 1980).

[56] L. Brekhovskikh and Yu. Lysanov, *Fundamentals of Ocean Acoustics*, (Springer-Verlag, 1982).

[57] L. Brekhovskikh, *Waves in Layered Media*, Translated from the Russian by D. Lieberman, Academic Press NY (1960).

[58] A. Wenzel, "A method for distinguishing between the attenuation due to scattering and the attenuation due to absorption for waves propagating in a dissipative, randomly inhomogeneous medium," J. Acoust. Soc. Am. 80, suppl.1, Fall, s90 (1986).

[59] S. H. Gray, J. K. Cohen, and N. Bleistein, "Velocity inversion in a stratified medium with separated source and receiver", J. Acoust. Soc. Am. 68, 234-240 (1980).

[60] J. K. Cohen, and N. Bleistein, "An inverse method for determining small variations in propagation speed", SIAM J. Appl. Math. 32, 784-799 (1977).

[61] J. K. Cohen, and N. Bleistein, "Velocity inversion for acoustic waves," Geophysics, 44, 1077-1087 (1979).

[62] N. Bleistein and J. K. Cohen, "Direct inversion procedure for Claerbout's Equations," Geophysics, 44, 1034-1040 (1979).

[63] E. L. Hamilton, "Geoacoustic modeling of the sea floor", J. Acoust. Soc. Am. 68, 1313-1340 (1980).

[64] P. M. Morse and H. Feshbach, *Methods of Theoretical Physics, Ch. 9*, McGraw-Hill, NY (1953).

[65] A. Papoulis, *Probability, Random Variables, and Stochastic Processes*, McGraw-Hill, NY (1965).

DOCUMENT LIBRARY

March 11, 1991

Distribution List for Technical Report Exchange

Attn: Stella Sanchez-Wade
Documents Section
Scripps Institution of Oceanography
Library, Mail Code C-075C
La Jolla, CA 92093

Hancock Library of Biology &
Oceanography
Alan Hancock Laboratory
University of Southern California
University Park
Los Angeles, CA 90089-0371

Gifts & Exchanges
Library
Bedford Institute of Oceanography
P.O. Box 1006
Dartmouth, NS, B2Y 4A2, CANADA

Office of the International
Ice Patrol
c/o Coast Guard R & D Center
Avery Point
Groton, CT 06340

NOAA/EDIS Miami Library Center
4301 Rickenbacker Causeway
Miami, FL 33149

Library
Skidaway Institute of Oceanography
P.O. Box 13687
Savannah, GA 31416

Institute of Geophysics
University of Hawaii
Library Room 252
2525 Correa Road
Honolulu, HI 96822

Marine Resources Information Center
Building E38-320
MIT
Cambridge, MA 02139

Library
Lamont-Doherty Geological
Observatory
Columbia University
Palisades, NY 10964

Library
Serials Department
Oregon State University
Corvallis, OR 97331

Pell Marine Science Library
University of Rhode Island
Narragansett Bay Campus
Narragansett, RI 02882

Working Collection
Texas A&M University
Dept. of Oceanography
College Station, TX 77843

Library
Virginia Institute of Marine Science
Gloucester Point, VA 23062

Fisheries-Oceanography Library
151 Oceanography Teaching Bldg.
University of Washington
Seattle, WA 98195

Library
R.S.M.A.S.
University of Miami
4600 Rickenbacker Causeway
Miami, FL 33149

Maury Oceanographic Library
Naval Oceanographic Office
Stennis Space Center
NSTL, MS 39522-5001

Marine Sciences Collection
Mayaguez Campus Library
University of Puerto Rico
Mayaguez, Puerto Rico 00708

Library
Institute of Oceanographic Sciences
Deacon Laboratory
Wormley, Godalming
Surrey GU8 5UB
UNITED KINGDOM

The Librarian
CSIRO Marine Laboratories
G.P.O. Box 1538
Hobart, Tasmania
AUSTRALIA 7001

Library
Proudman Oceanographic Laboratory
Bidston Observatory
Birkenhead
Merseyside L43 7 RA
UNITED KINGDOM

50272-101

REPORT DOCUMENTATION PAGE	1. REPORT NO. WHOI-91-25	2.	3. Recipient's Accession No.

4. Title and Subtitle
Acoustic Wave Scattering from a Random Ocean Bottom

5. Report Date
June 1991

6.

7. Author(s)
Dajun Tang

8. Performing Organization Rept. No.

9. Performing Organization Name and Address
Woods Hole Oceanographic Institution
Woods Hole, Massachusetts 02543

10. Project/Task/Work Unit No.
WHOI-91-25

11. Contract(C) or Grant(G) No.
(C) N00014-86-C-0338
(G)

12. Sponsoring Organization Name and Address
Office of Naval Research

13. Type of Report & Period Covered
Ph.D. Thesis

14.

15. Supplementary Notes
This thesis should be cited as: Dajun Tang, 1991. Acoustic Wave Scattering from a Random Ocean Bottom. Ph.D. Thesis. MIT/WHOI, WHOI-91-25.

16. Abstract (Limit: 200 words)

This thesis investigates low frequency acoustic wave scattering from the ocean bottom. It is divided into four parts. The first part models the ocean bottom as a fluid medium where sound speed and density are constants except a layer in which the density is still a constant, but the sound speed is composed of a large constant and superimposed with a small random component. It is assumed that the random sound speed is horizontally well correlated and vertically poorly correlated.

In the second part, an integro-differential equation method is used to calculate the scattering from that random layer. Emphasis is put on the study of the spatial correlation of the scattered field. It is found that the spatial correlation length of the scattered field is related to the correlation length of the scatterer, therefore it is possible to invert the bottom correlation length by measuring the spatial correlation of the scattered field using multiple receivers. Also included in this part are an estimation of energy loss in the coherent field, a discussion on the influence of bottom anisotropy, and a comparison between the integro-differential equation method and the Born approximation.

The third part concerns the influence of the bottom roughness. A small roughness is added to the water/bottom interface and perturbation method is used to calculate the scattering from the roughness. Under the assumption that the roughness and the volume inhomogeneity are uncorrelated, comparisons are made on the scattering strengths between roughness scattering and volume scattering, and the spatial correlation of the total scattered field is evaluated. It is found that at low frequencies, volume scattering cannot be ignored when the seafloor is not very rough, and it is possible to distinghish the two scattering mechanisms by measuring spatial correlations of the scattered field.

In the fourth part, the classical definition of the bottom scattering cross section is questioned, and a new set of parameters, the Scattering Correlation Coefficient, is introduced, which does not have the ambiguities associated with the conventional notion of the scattering cross section.

17. Document Analysis a. Descriptors

ocean bottom scattering
wave propagation in random media
acoustic reverberation

b. Identifiers/Open-Ended Terms

c. COSATI Field/Group

18. Availability Statement	19. Security Class (This Report)	21. No. of Pages
Approved for publication; distribution unlimited.	UNCLASSIFIED	133
	20. Security Class (This Page)	22. Price

(See ANSI-Z39.18) *See Instructions on Reverse* OPTIONAL FORM 272 (4-77)
(Formerly NTIS-35)
Department of Commerce